

หน่วยแปรรูปเชื้อเพลิงเพื่อการผลิตไฮโดรเจนผ่านการเปลี่ยนรูปเมทานอลด้วยไอน้ำบนตัวเร่งปฏิกิริยา

ฐานทองแดง



นายยุทธพันธุ์ พงศ์บุญชู

จุฬาลงกรณ์มหาวิทยาลัย

CHULALONGKORN UNIVERSITY

บทคัดย่อและแฟ้มข้อมูลฉบับเต็มของวิทยานิพนธ์ตั้งแต่ปีการศึกษา 2554 ที่ให้บริการในคลังปัญญาจุฬาฯ (CUIR)

เป็นแฟ้มข้อมูลของนิสิตเจ้าของวิทยานิพนธ์ ที่ส่งผ่านทางบัณฑิตวิทยาลัย

The abstract and full text of theses from the academic year 2011 in Chulalongkorn University Intellectual Repository (CUIR) are the thesis authors' files submitted through the University Graduate School.

วิทยานิพนธ์นี้เป็นส่วนหนึ่งของการศึกษาตามหลักสูตรปริญญาวิทยาศาสตรดุษฎีบัณฑิต

สาขาวิชาเคมีเทคนิค ภาควิชาเคมีเทคนิค

คณะวิทยาศาสตร์ จุฬาลงกรณ์มหาวิทยาลัย

ปีการศึกษา 2559

ลิขสิทธิ์ของจุฬาลงกรณ์มหาวิทยาลัย

FUEL PROCESSOR FOR HYDROGEN PRODUCTION VIA METHANOL STEAM REFORMING
OVER COPPER-BASED CATALYSTS

Mr. Yuththaphan Phongboonchoo



A Dissertation Submitted in Partial Fulfillment of the Requirements
for the Degree of Doctor of Philosophy Program in Chemical Technology

Department of Chemical Technology

Faculty of Science

Chulalongkorn University

Academic Year 2016

Copyright of Chulalongkorn University

Thesis Title	FUEL PROCESSOR FOR HYDROGEN PRODUCTION VIA METHANOL STEAM REFORMING OVER COPPER- BASED CATALYSTS
By	Mr. Yuththaphan Phongboonchoo
Field of Study	Chemical Technology
Thesis Advisor	Professor Nattaya Pongstabodee, Ph.D.
Thesis Co-Advisor	Professor Apanee Luengnaruemitchai, Ph.D.

Accepted by the Faculty of Science, Chulalongkorn University in Partial
Fulfillment of the Requirements for the Doctoral Degree

.....Dean of the Faculty of Science
(Associate Professor Polkit Sangvanich, Ph.D.)

THESIS COMMITTEE

.....Chairman
(Professor Tharapong Vitidsant, Ph.D.)

.....Thesis Advisor
(Professor Nattaya Pongstabodee, Ph.D.)

.....Thesis Co-Advisor
(Professor Apanee Luengnaruemitchai, Ph.D.)

.....Examiner
(Professor Pattarapan Prasassarakich, Ph.D.)

.....Examiner
(Associate Professor Prasert Reubroycharoen, Ph.D.)

.....External Examiner
(Siriphong Rojluechai, Ph.D.)

ยุทธพันธ์ พงศ์บุญชู : หน่วยแปรรูปเชื้อเพลิงเพื่อการผลิตไฮโดรเจนผ่านการเปลี่ยนรูปเมทานอลด้วยไอน้ำบนตัวเร่งปฏิกิริยาฐานทองแดง (FUEL PROCESSOR FOR HYDROGEN PRODUCTION VIA METHANOL STEAM REFORMING OVER COPPER-BASED CATALYSTS) อ.ที่ปรึกษาวิทยานิพนธ์หลัก: ศ. ดร.ณัฐชยาน์ พงศ์สถาปตี, อ.ที่ปรึกษาวิทยานิพนธ์ร่วม: ศ. ดร.อาภาณี เหลืองนฤมิตชัย, 162 หน้า.

งานวิจัยนี้มีวัตถุประสงค์เพื่อผลิตแก๊สไฮโดรเจนความบริสุทธิ์สูงจากเมทานอลโดยใช้หน่วยแปรรูปเชื้อเพลิงที่ประกอบด้วยหน่วยเปลี่ยนรูปเมทานอลและหน่วยการจัดแก๊สคาร์บอนมอนอกไซด์แบบเลือกเกิด เริ่มจากศึกษาความว่องไวของตัวเร่งปฏิกิริยาทองแดงบนตัวรองรับอลูมิเนียมออกไซด์ที่ใช้แมกนีเซียมและซีเรียมเป็นโปรโมเตอร์สำหรับหน่วยเปลี่ยนรูปเมทานอลด้วยไอน้ำ โดยพิจารณาจากการเปลี่ยนของเมทานอล การเลือกเกิดแก๊สคาร์บอนมอนอกไซด์ และผลได้แก๊สไฮโดรเจน จากผลการทดลองพบว่าตัวเร่งปฏิกิริยาที่ใช้แมกนีเซียมและซีเรียมเป็นโปรโมเตอร์ร่วมกันมีความว่องไวสูงกว่าตัวเร่งปฏิกิริยาชนิดอื่นเนื่องจากการแทรกสอดของแมกนีเซียมเข้าสู่โครงสร้างของซีเรียมก่อให้เกิดตำหนิที่ว่างของออกซิเจนบนซีเรีย จากนั้นหาภาวะที่เหมาะสมโดยใช้การออกแบบการทดลองเชิงสถิติที่ระดับความเชื่อมั่นร้อยละ 95 พบว่าภาวะที่เหมาะสมคือการใช้ตัวเร่งปฏิกิริยาที่มีปริมาณทองแดงร้อยละ 46-50 โดยมวล และอัตราส่วนแมกนีเซียมต่อผลรวมของแมกนีเซียมและซีเรียมในช่วงร้อยละ 16.2-18.0 โดยมวล ณ อุณหภูมิ 245-250 องศาเซลเซียส และอัตราส่วนไอน้ำต่อคาร์บอน 1.74-1.80 ต่อมาได้ศึกษาความว่องไวของตัวเร่งปฏิกิริยาฐานทองแดงบนตัวรองรับดัดแปรซีเรียมสำหรับหน่วยกำจัดแก๊สคาร์บอนมอนอกไซด์แบบเลือกเกิด โดยพิจารณาจากการเปลี่ยนคาร์บอนมอนอกไซด์ และการเลือกเกิดแก๊สคาร์บอนไดออกไซด์ จากผลการทดลองพบว่า ตัวเร่งปฏิกิริยาทองแดงบนตัวรองรับซีเรียมที่ดัดแปรด้วยแมกนีเซียมมีความว่องไวสูงกว่าตัวเร่งปฏิกิริยาชนิดอื่นเนื่องจากแมกนีเซียมส่งเสริมให้เกิดปฏิกิริยาออกเตอร์แก๊สซิฟต์ได้ดียิ่งขึ้น อีกทั้งยังช่วยปรับปรุงการจัดเรียงตัวของแท่งนาโนบนตัวรองรับอีกทางหนึ่ง จากนั้นหาภาวะที่เหมาะสมโดยใช้การออกแบบการทดลองเชิงสถิติที่ระดับความเชื่อมั่นร้อยละ 95 พบว่าภาวะที่เหมาะสมคือการใช้สารป้อนที่มีระดับความเข้มข้นของคาร์บอนมอนอกไซด์อยู่ในช่วงร้อยละ 0.65-0.75 ระดับความเข้มข้นของออกซิเจนอยู่ในช่วงร้อยละ 0.80-0.90 ณ อุณหภูมิ 130-140 องศาเซลเซียส เมื่อทำการผลิตแก๊สไฮโดรเจนความบริสุทธิ์สูงจากหน่วยแปรรูปเชื้อเพลิงพบว่ามีผลได้แก๊สไฮโดรเจนร้อยละ 45-47 โดยไม่พบแก๊สคาร์บอนมอนอกไซด์ในแก๊สผลิตภัณฑ์ที่อัตราการผลิต 120 ลิตรต่อวันต่อกรัมตัวเร่งปฏิกิริยา

ภาควิชา	เคมีเทคนิค	ลายมือชื่อนิสิต
สาขาวิชา	เคมีเทคนิค	ลายมือชื่อ อ.ที่ปรึกษาหลัก
ปีการศึกษา	2559	ลายมือชื่อ อ.ที่ปรึกษาร่วม

5572866923 : MAJOR CHEMICAL TECHNOLOGY

KEYWORDS: METHANOL STEAM REFORMING / PREFERENTIAL OXIDATION OF CO / FUEL PROCESSOR / HYDROGEN PRODUCTION / OPTIMIZATION / COPPER-BASED CATALYSTS / CERIA / MAGNESIUM OXIDE

YUTHTHAPHAN PHONGBOONCHOO: FUEL PROCESSOR FOR HYDROGEN PRODUCTION VIA METHANOL STEAM REFORMING OVER COPPER-BASED CATALYSTS. ADVISOR: PROF. NATTAYA PONGSTABODEE, Ph.D., CO-ADVISOR: PROF. APANEE LUENGNARUEMITCHAI, Ph.D., 162 pp.

The purpose of this work is to produce high purity hydrogen stream from methanol by an integration of steam reformer and preferential oxidation of CO unit. For methanol steam reformer (MSR), Catalytic activities of Ce-Mg promoted Cu/Al₂O₃ catalysts was investigated in terms of the methanol conversion level, carbon monoxide (CO) selectivity and hydrogen (H₂) yield. It was found that the Ce-Mg bi-promoter catalysts gave a higher performance due to magnesium penetration into the cerium structure causing oxygen vacancy defects on the ceria. A face-centered central composite design response surface model was then designed to optimize the condition at a 95% confidence interval revealed an optimal copper level of 46–50 wt%, Mg/(Ce+Mg) of 16.2–18.0%, temperature of 245–250 °C and S/C ratio of 1.74–1.80. In case of preferential oxidation of CO unit, catalytic activities of copper based catalysts over a series of modified ceria support was investigated in terms of the CO conversion level and carbon dioxide (CO₂) selectivity. The results revealed that the Ce-Mg support gave a higher performance due to magnesium promoted water-gas shift reaction and improved nanorods arrangement. Box-Behnken design response surface model was then designed to optimize the condition at a 95% confidence interval revealed an optimal CO level of 0.65-0.75%, O₂ level of 0.80-0.90% and temperature of 130–140 °C. When integrating both MSR and PROX unit, high purity hydrogen was yielded around 45-47% without CO detected at a rate of ~120 L d⁻¹ g.cat⁻¹.

Department: Chemical Technology Student's Signature

Field of Study: Chemical Technology Advisor's Signature

Academic Year: 2016 Co-Advisor's Signature

ACKNOWLEDGEMENTS

The completion of this dissertation would not have been possible without the assistance of the following people and organizations:

I would like to express my deepest sense of gratitude to my dissertation advisors, Professor Nuttaya Pongstabodee, Ph.D. and Professor Apanee Luengnaruemitchai, Ph.D., for their valuable guidance and encouragement to this research. Moreover, I especially extend my appreciation to Professor Tharapong Vitidsant, Ph.D., Professor Pattarapan Prasassarakich, Ph.D., Associate Professor Prasert Reubroycharoen, Ph.D., and Mr. Siriphong Rojluechai, Ph.D. for their participation on the dissertation chairman and committees.

Secondly, I sincerely appreciate to the 90th Anniversary of Chulalongkorn University Fund (Ratchadaphiseksomphot Endowment Fund) and Center for Excellence on Petrochemical and Materials Technology for their financial support throughout this research.

The last, I would like to thank all members and staff whose names may not all be enumerated. Their contributions are sincerely appreciated and gratefully acknowledge, especially Mr. Nutthavich Thouchprasitchai, Ph.D., for his assistance and encouragement.

CONTENTS

	Page
THAI ABSTRACT	iv
ENGLISH ABSTRACT	v
ACKNOWLEDGEMENTS	vi
CONTENTS	vii
LIST OF TABLES	xi
LIST OF FIGURES	xii
CHAPTER I	1
1.1 Rationale	1
1.2 Research objective.....	3
1.3 Scope of the dissertation.....	4
1.4 Research Procedure.....	5
1.5 Expected beneficial outcome(s) from the dissertation.....	6
CHAPTER II	7
2.1 Energy demand	7
2.2 Fuel cells and hydrogen energy	11
2.3 Hydrogen production process.....	14
2.3.1 Conventional process.....	16
2.3.2 Alternative approaches for small scale fuel processor.....	21
2.4 Hydrogen purification process	22
2.5 Fuel processor for PEMFCs	24
2.5.1 Methanol steam reforming (MSR).....	25
2.5.2 Preferential oxidation (PROX) of CO	28

	Page
2.6 Catalyst preparation method.....	30
2.6.1 Impregnation method	31
2.6.2 Precipitation method.....	33
2.6.3 Hydrothermal method	34
2.7 Catalyst characterization	35
2.8 Literature reviews.....	38
2.8.1 Methanol steam reforming.....	38
2.8.2 Preferential oxidation of CO	41
2.8.3 Fuel processor for hydrogen production.....	45
CHAPTER III	48
3.1 Materials.....	48
3.1.1 Chemicals	48
3.1.2 Gases	49
3.2 Equipment and apparatus	49
3.2.1 Equipment.....	49
3.2.2 Apparatus set-up	50
3.3 Experiment procedure	50
3.3.1 Methanol steam reforming unit (MSR).....	50
3.3.1.1 Catalysts preparation	50
3.3.1.2 Catalysts characterization	52
3.3.1.3 Catalytic activity measurement	54
3.3.1.4 Statistical design of experiments for optimization.....	55
3.3.2 Preferential oxidation (PROX) of CO unit	59

	Page
3.3.2.1 Catalyst preparation	59
3.3.2.2 Catalysts characterization	60
3.3.2.3 Catalytic activity measurement	62
3.3.2.4 Statistical design of experiments for optimization.....	63
3.3.3 Integration of MSR unit and PROX unit	67
CHAPTER IV.....	68
4.1 Catalyst characterization	68
4.2 Catalytic activities test	77
4.2.1 Level of copper content	77
4.2.2 Mono- and bi-promoter catalysts with various Mg/(Ce+Mg) wt%	81
4.2.3 S/C ratio	85
4.3 Statistical designs for optimization	87
4.4 Stability test	99
CHAPTER V	101
5.1 Catalyst characterization	101
5.2 Catalytic activity test.....	111
5.2.1 type of ceria support.....	111
5.2.2 Level of copper content	117
5.2.3 O ₂ /CO molar ratio.....	118
5.3 Statistical design for optimization	119
5.4 Stability test	128
CHAPTER VI.....	133
6.1 Stability test	133

	Page
CHAPTER VII.....	138
7.1 Methanol steam reformer unit.....	138
7.2 Preferential oxidation of CO unit.....	140
7.3 Integration of MSR and PROX unit.....	141
7.4 Recommendation.....	141
REFERENCES.....	142
APPENDIX.....	150
VITA.....	162



LIST OF TABLES

	Page
Table 3.1 Experimental variable over $\text{Cu}_x\text{Ce}_y\text{Mg}_z/\text{Al}$ in coded and actual unit for a full 2^4 design with five central points in the standard order from 1 to 21	57
Table 3.2 Experimental variable for FCCCD-RSM.....	58
Table 3.3 Experimental variable over 5wt% $\text{CuO}/\text{Ce}_{0.95}\text{Mg}_{0.05}$ in coded and actual unit for a full 2^4 design with five central points in the standard order from 1 to 21 ..	65
Table 3.4 Experimental variable for Box–Behnken design	66
Table 4.1 Textural properties of the copper-based catalysts.	71
Table 4.2 Independent factors and the FCCCD-RSM experimental design.	88
Table 4.3 ANOVA results for the methanol conversion level, CO selectivity and H_2 yield from FCCCD-RSM.....	91
Table 4.4 Variation of the RSM.....	98
Table 5.1 Textural properties of ceria support and CuO/CeO_2 catalysts.....	105
Table 5.2 Independent factors and the Box Behnken-RSM experimental design.	119
Table 5.3 ANOVA results for the CO conversion level and CO_2 selectivity from Box Behnken-RSM.....	123

LIST OF FIGURES

	Page
Figure 1.1 Schematic outline of fuel processor for hydrogen production via methanol steam reforming	3
Figure 2.1 Energy-related CO ₂ emissions growth by region	8
Figure 2.2 World primary energy consumption	8
Figure 2.3 Thailand energy consumption in 2015.....	10
Figure 2.4 Phenomena in a PEM fuel cell: two-dimensional sectional view.....	12
Figure 2.5 Fuel processing of gaseous, liquid, and solid fuels for hydrogen production.....	16
Figure 2.6 Flow scheme of methanol fuel processor and heat exchanger network... 24	
Figure 2.7 Phenomena of transport involved in (a) wet impregnation and (b) dry impregnation.....	32
Figure 2.8 LaMer and Dinegar model for the generation of atoms, nucleation, and subsequent growth of homogeneous precipitation.	33
Figure 2.9 Schematic of a Teflon® lined stainless steel autoclave typically used for hydrothermal synthesis.	35
Figure 3.1 Experimental set-up for fuel processor	51
Figure 4.1 Representative (of 10 samples) XRD patterns of the copper-based catalysts after H ₂ pretreatment at 300 °C for 1 h. Shown are the fresh (a) Cu _{0.3} /Al, (b) Cu _{0.3} Mg _{0.3} /Al, (c) Cu _{0.2} Ce _{0.15} Mg _{0.15} /Al, (d) Cu _{0.3} Ce _{0.15} Mg _{0.15} /Al, (e) Cu _{0.4} Ce _{0.15} Mg _{0.15} /Al, (f) Cu _{0.5} Ce _{0.15} Mg _{0.15} /Al, (g) Cu _{0.3} Ce _{0.2} Mg _{0.1} /Al, (h) Cu _{0.3} Ce _{0.25} Mg _{0.05} /Al and (i) Cu _{0.3} Ce _{0.3} /Al catalysts, plus (j) the spent Cu _{0.5} Ce _{0.25} Mg _{0.05} /Al catalyst after MSR at 250 °C for 72 h.	68
Figure 4.2 Representative (of 9 samples) H ₂ -TPR profiles of the copper-based catalysts: (a) Cu _{0.3} /Al, (b) Cu _{0.3} Mg _{0.3} /Al, (c) Cu _{0.2} Ce _{0.15} Mg _{0.15} /Al, (d)	

Cu_{0.3}Ce_{0.15}Mg_{0.15}/Al, (e) Cu_{0.4}Ce_{0.15}Mg_{0.15}/Al, (f) Cu_{0.5}Ce_{0.15}Mg_{0.15}/Al, (g) Cu_{0.3}Ce_{0.2}Mg_{0.1}/Al, (h) Cu_{0.3}Ce_{0.25}Mg_{0.05}/Al and (i) Cu_{0.3}Ce_{0.3}/Al. 75

Figure 4.3 Representative FESEM images (20 k magnification; scale bar = 1 μm) of (a) Cu_{0.30}/Al, (b) Cu_{0.30}Ce_{0.30}/Al, (c) Cu_{0.30}Mg_{0.30}/Al, (d) Cu_{0.30}Ce_{0.25}Mg_{0.05}/Al, (e) Cu_{0.30}Ce_{0.20}Mg_{0.10}/Al and (f) Cu_{0.30}Ce_{0.15}Mg_{0.15}/Al catalysts. 76

Figure 4.4 The MSR catalytic performances in terms of the (a) methanol conversion level, (b) CO selectivity and (c) H₂ yield for the copper based catalysts with different copper loading levels; Cu_{0.2}Ce_{0.15}Mg_{0.15}/Al (◆), Cu_{0.3}Ce_{0.15}Mg_{0.15}/Al (■), Cu_{0.4}Ce_{0.15}Mg_{0.15}/Al (▲) and Cu_{0.5}Ce_{0.15}Mg_{0.15}/Al (×). All reactions had an S/C of 1.5, feed rate of 1 mL h⁻¹ and 0.1 g of catalyst. Data are shown as the mean, derived from three replicates. 79

Figure 4.5 The MSR catalytic performances in terms of the (a) methanol conversion level, (b) CO selectivity and (c) H₂ yield for the copper based catalysts with different promoter ratios; Cu_{0.3}/Al (◆), Cu_{0.3}Mg_{0.3}/Al (▲), Cu_{0.3}Ce_{0.15}Mg_{0.15}/Al (■), Cu_{0.3}Ce_{0.2}Mg_{0.1}/Al (×), Cu_{0.3}Ce_{0.25}Mg_{0.05}/Al (+) and Cu_{0.3}Ce_{0.3}/Al (●). All reactions had an S/C of 1.5, feed rate of 1 mL h⁻¹ and 0.1 g of catalyst. Data are shown as the mean, derived from three replicates. 82

Figure 4.6 The MSR catalytic performances in terms of the (a) methanol conversion level, (b) CO selectivity and (c) H₂ yield of Cu_{0.3}Ce_{0.25}Mg_{0.05}/Al with S/C ratios of 1.5 (+) and S/C = 2 (▲) at a feed rate of 1 mL h⁻¹ and 0.1 g of catalyst. Data are shown as the mean, derived from three replicates. 86

Figure 4.7 Normal probability plots of the residues for each response (a–c) and plots of residues and each evaluated response (d–f): (a and d) MeOH conversion; (b and e) CO selectivity; and (c and f) H₂ yield. 96

Figure 4.8 Contour plots for the optimal conditions for the (a) methanol conversion level; (b) CO selectivity; and (c) H₂ yield. 97

Figure 4.9 Catalyst stability test in the MSR reaction in terms of the methanol conversion level (◆), CO selectivity (■) and H₂ yield (▲) over 0.1 g of Cu_{0.5}Ce_{0.25}Mg_{0.05}/Al catalyst at 250 °C and a S/C ratio of 1.75. 100

Figure 5.1 FESEM images of ceria support shown are the fresh (a) commercial CeO_2 , (b) synthesized CeO_2 prepared with 5M NaOH, (c) synthesized CeO_2 prepared with 15M NaOH, (d) synthesized $\text{Ce}_{0.95}\text{Mg}_{0.05}$ and (e) synthesized $\text{Ce}_{0.80}\text{Mg}_{0.20}$ 102

Figure 5.2 Representative (of 13 samples) XRD patterns of the ceria support and CuO/ CeO_2 catalysts: (a) com- CeO_2^a , (b) 5.0wt%CuO/com- CeO_2^a , (c) CeO_2^b , (d) 5.0wt% CuO/ CeO_2^b , (e) CeO_2^c (f) 5.0wt% CuO/ CeO_2^c , (g) $\text{Ce}_{0.80}\text{Mg}_{0.20}^c$, (h) 5.0wt% CuO/ $\text{Ce}_{0.80}\text{Mg}_{0.20}^c$, (i) $\text{Ce}_{0.95}\text{Mg}_{0.05}^c$, (j) 2.5wt% CuO/ $\text{Ce}_{0.95}\text{Mg}_{0.05}^c$, (k) 5.0wt% CuO/ $\text{Ce}_{0.95}\text{Mg}_{0.05}^c$, (l) 7.5wt% CuO/ $\text{Ce}_{0.95}\text{Mg}_{0.05}^c$ and (m) 10.0wt% CuO/ $\text{Ce}_{0.95}\text{Mg}_{0.05}^c$; ^a commercial CeO_2 , ^b ceria support prepared in NaOH 5M and ^c ceria support prepared in NaOH 15M..... 106

Figure 5.3 Representative (of 8 samples) H_2 -TPR profiles of the CuO/ CeO_2 catalysts: (a) 5.0wt% CuO/com- CeO_2^a , (b) 5.0wt% CuO/ CeO_2^b , (c) 5.0wt% CuO/ CeO_2^c , (d) 5.0wt% CuO/ $\text{Ce}_{0.80}\text{Mg}_{0.20}^c$, (e) 2.5wt% CuO/ $\text{Ce}_{0.95}\text{Mg}_{0.05}^c$, (f) 5.0wt% CuO/ $\text{Ce}_{0.95}\text{Mg}_{0.05}^c$, (g) 7.5wt% CuO/ $\text{Ce}_{0.95}\text{Mg}_{0.05}^c$ and (h) 10.0wt% CuO/ $\text{Ce}_{0.95}\text{Mg}_{0.05}^c$; ^a commercial CeO_2 , ^b ceria support prepared in NaOH 5M and ^c ceria support prepared in NaOH 15M..... 109

Figure 5.4 The PROX catalytic performances in terms of the (A) CO conversion level and (B) CO_2 selectivity for the 5wt%CuO/ CeO_2 catalysts with different supports. All reactions had oxygen excess factor of 2, feed rate of 100 mL h^{-1} and 0.1 g of catalyst. Data are shown as the mean, derived from three replicates. 113

Figure 5.5 The PROX catalytic performances in terms of the (A) CO conversion level and (B) CO_2 selectivity for the CuO/ $\text{Ce}_{0.95}\text{Mg}_{0.05}$ catalysts with different level of copper oxide. All reactions had oxygen excess factor of 2, feed rate of 100 mL h^{-1} and 0.1 g of catalyst. Data are shown as the mean, derived from three replicates. 115

Figure 5.6 The PROX catalytic performances in terms of the (A) CO conversion level and (B) CO_2 selectivity for the 10wt%CuO/ $\text{Ce}_{0.95}\text{Mg}_{0.05}$ catalysts with different

level of oxygen excess factor. All reactions had feed rate of 100 mL h^{-1} and 0.1 g of catalyst. Data are shown as the mean, derived from three replicates. 116

Figure 5.7 Normal probability plots of the residues for each response (a–b) and plots of residues and each evaluated response (c-d): (a and c) CO conversion and (b and d) CO₂ selectivity. 126

Figure 5.8 Contour plots for the optimal conditions for the 10wt%CuO/Ce_{0.95}Mg_{0.05} catalyst (a) CO conversion level and (b) CO₂ selectivity. 127

Figure 5.9 Catalyst stability test in the PROX reaction in terms of the CO conversion level (◆) and CO₂ selectivity (■) over 0.13 g of 10wt%CuO/Ce_{0.95}Mg_{0.05} catalyst at $130 \text{ }^\circ\text{C}$ and oxygen excess factor of 2; (A) without CO₂ and H₂O, (B) CO₂ 20%, (C) H₂O 15% and (D) CO₂ 20% and H₂O 15%. 131

Figure 5.10 Catalyst stability test in sequence via PROX reaction in terms of the CO conversion level (◆) and CO₂ selectivity (■) over 0.13 g of 10wt%CuO/Ce_{0.95}Mg_{0.05} catalyst at $130 \text{ }^\circ\text{C}$ and oxygen excess factor of 2; (A) without CO₂ and H₂O, (B) CO₂ 20%, (C) CO₂ 20% and H₂O 15% and (D) without CO₂ and H₂O. 132

Figure 6.1 Catalyst stability test for fuel processor at the optimum conditions in terms of the methanol conversion level (◆), CO selectivity (■) and H₂ yield (▲) over 0.1 g of Cu_{0.5}Ce_{0.25}Mg_{0.05}/Al catalyst in MSR unit at $250 \text{ }^\circ\text{C}$ and a S/C ratio of 1.75 and 0.13 g of 10wt%CuO/Ce_{0.95}Mg_{0.05} catalyst in PROX unit at $130 \text{ }^\circ\text{C}$ and oxygen excess factor=2. 135

Figure 6.2 Product composition for fuel processor at the optimum conditions over 0.1 g of Cu_{0.5}Ce_{0.25}Mg_{0.05}/Al catalyst in MSR unit at $250 \text{ }^\circ\text{C}$ and a S/C ratio of 1.75 and 0.13 g of 10wt%CuO/Ce_{0.95}Mg_{0.05} catalyst in PROX unit at $130 \text{ }^\circ\text{C}$ and oxygen excess factor=2. H₂ (▲), CO (■) and CO₂ (◆). 136

Figure 6.3 Hydrogen production rate for fuel processor at the optimum conditions over 0.1 g of Cu_{0.5}Ce_{0.25}Mg_{0.05}/Al catalyst in MSR unit at $250 \text{ }^\circ\text{C}$ and a S/C ratio of 1.75 and 0.13 g of 10wt%CuO/Ce_{0.95}Mg_{0.05} catalyst in PROX unit at $130 \text{ }^\circ\text{C}$ and oxygen excess factor=2. 137

CHAPTER I

INTRODUCTION

1.1 Rationale

Global warming has widely effect on both environment and human's way of life. Most scientists agree that the main cause of these phenomena is due to greenhouse effect which traps heat radiation from Earth toward space [1, 2]. The extent of climate change effect in each region depends on its geographical and weather condition but it's certainly has effects on human lifestyle [3-6]. Carbon dioxide (CO₂) is well known as a main element of greenhouse gases which is released through human activities such as deforestation, transportation, industrial and burning fossil fuels. Furthermore, the development of global economy and industrial to keep up with the growth rate of human population required great inputs of natural resources and energy. Human activities which mostly rely on fossil fuel is driving a rapid growth in energy consumption, yet the global primary fuel supply is, in contrast, decreasing leading towards a shortfall in the future. The requirement of the sustainable energy and the rise of global warming are the major force to drive many researches to seek new energy resource to reduce the effect of these problems.

Hydrogen (H_2) has been proposed as a promising energy carrier [7-12]. It can be produced from various hydrocarbon and can effectively use as fuel through fuel cell. The effluent contains only steam and heat which will not pollute environment. Hydrogen can be applied to modified internal combustion engine as well. However, the major problem which suppress the use of hydrogen as an alternative fuel is due to a technical limitation from its low energy densities per volume which required high standard storage both on capacity and quality. Therefore, hydrogen will likely be generated on site by reforming available resources. Methanol is a suggested fuel resource for hydrogen production to solve this problem on account of its high density which allowing it to be stored, transporting and applying to conventional infrastructure [13-15]. Moreover, methanol could be produced from biomass which makes it suitable for further development in Thailand and does not required pre-reforming or desulfurization processes. Copper-based catalysts have been used for methanol steam reforming (MSR) due to its high activity and low carbon monoxide selectivity which is favor to PEM fuel cell. However, the hydrogen stream produced by conventional catalysts, $CuO/ZnO/Al_2O_3$, still has high CO concentration which will affect the performance of platinum catalysts in PEM fuel cell. Further improvement of potential catalysts for hydrogen production with minimal of CO selectivity via methanol steam reforming still needed. The CO content is needed to be reduced to less than 100 ppm in a CO clean-up. Among the CO removal units, the preferential oxidation (PROX) of CO is the most promising one both in terms of technical and economic feasibility due

to its high selectivity toward CO oxidation in H₂ rich stream and low energy required [16, 17].

This research focuses on improving copper-based catalyst performance by using various promoters such as ceria and magnesium oxide. These promoters have an advantage of oxygen vacancies which can release oxygen to oxidize CO to CO₂. Furthermore, CO in the reformat was then reduced to less than 100 ppm via preferential oxidation of CO. The principal concept of a fuel processor for hydrogen production via methanol steam reforming is shown in Fig 1.1

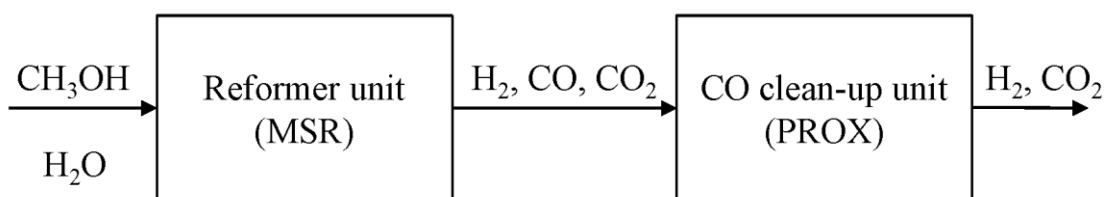


Figure 1.1 Schematic outline of fuel processor for hydrogen production via methanol steam reforming

1.2 Research objective

To study hydrogen production via methanol steam reforming over copper-based catalysts and hydrogen purification process via preferential oxidation of carbon monoxides

1.3 Scope of the dissertation

1. Investigation of the synthesized copper-based catalysts for MSR unit and optimization condition of effective catalysts

The copper-based catalysts prepared via co-precipitation method was used to find the effective catalysts for MSR unit at constant condition of steam to carbon ratio (S/C) = 1.5, liquid feed rate = 1 mL h^{-1} and catalysts weight to He flow rate = 0.15 g s mL^{-1} in temperature range from $200 \text{ }^{\circ}\text{C}$ to $300 \text{ }^{\circ}\text{C}$. The optimal condition for MSR was obtained by 2^k experimental design. Four independent factors selected were operating temperature, ratios of steam to carbon (S/C ratio), Mg/(Ce+Mg) weight percent (wt%), and amount of Cu loading. The methanol conversion, CO selectivity and H_2 yields were carried out as response.

2. Investigation of the synthesized catalysts for PROX unit and optimization condition of effective catalysts

The synthesized catalysts which consist of CuO, MgO and CeO_2 was used to find the effective catalysts for PROX unit under simulated gas which consist of 1% CO, 1% O_2 , 40% H_2 in He balance at constant feed rate = 100 mL min^{-1} in temperature range from $40 \text{ }^{\circ}\text{C}$ to $300 \text{ }^{\circ}\text{C}$. The optimal condition for PROX was obtained by 2^k experimental design. Four independent factors selected were operating temperature, level of CO in simulated gas, level of O_2 in simulated gas and catalyst weight. The CO conversion and CO_2 selectivity were carried out as response.

3. Integration of MSR and PROX unit

The combination of MSR unit and PROX unit was used to produce high purity hydrogen stream for PEM fuel cell applications.

4. Catalysts characterization

The synthesized catalysts are characterized by analytical instrument such as

- Field emission scanning electron microscopy (FESEM) is employed to determine the morphology of the catalysts.

- X-ray diffractometer (XRD) is used to examine the crystalline structure of the catalysts.

- The Brunauer-Emmett-Teller (BET) method is used to determine the specific area, pore volume and pore size of the catalysts by N₂ adsorption/desorption.

- Temperature programmed reduction (TPR) is used to investigate reduction of copper phase on catalysts.

จุฬาลงกรณ์มหาวิทยาลัย
CHULALONGKORN UNIVERSITY

1.4 Research Procedure

1. Survey literature related to hydrogen production

2. Synthesis copper-based catalysts via co-precipitation method for methanol steam reforming

3. Characterize morphology and others properties of copper-based catalysts with FESEM, XRD, BET and TPR technique

4. Study the factors which affect to methanol conversion and carbon monoxide selectivity such as reaction temperature, Cu-loading, type of additive and additive-loading.

5. Survey literature related to PROX

6. Synthesis copper-based catalysts via co-precipitation method for PROX

7. Characterize morphology and others properties of copper-based catalysts with FESEM, XRD, BET and TPR technique

8. Study the factors which affect to carbon monoxide conversion, carbon dioxide yield and product composition such as Cu-loading, type of additive and additive-loading, reaction temperature, CO/O₂ ratio, water additive and CO₂ additive

9. Write publication and dissertation

1.5 Expected beneficial outcome(s) from the dissertation

To produce hydrogen-rich stream with CO content less than 100 ppm via methanol steam reforming and PROX over copper-based catalysts

CHAPTER II

THEORY AND LITERATURE REVIEWS

2.1 Energy demand

There were many evidences of increased carbon dioxide (CO₂) and related greenhouse gases (GHGs) in the atmosphere [3, 4]. It had been acknowledged that the GHGs had effects on climate variation in each region depended on its geographical and weather condition which expected to have influence on human civilization [3-6]. Carbon dioxide is well known as a main element of GHGs released through human activities such as deforestation, transportation, industrial and burning fossil fuels. In 2015, carbon dioxide emissions from fossil fuels burning alone reached 33.5 billion tons as shown in Fig. 2.1 which expressed energy-related CO₂ emissions growth by region [18]. Regardless of the development of industrial and transportation or the raising of world population, energy demand is bound to increase while the supply must be provided in a way that not have effect on the other needs for human activities such as food production or human habitat with the excessive impact on the environment must also be avoided.

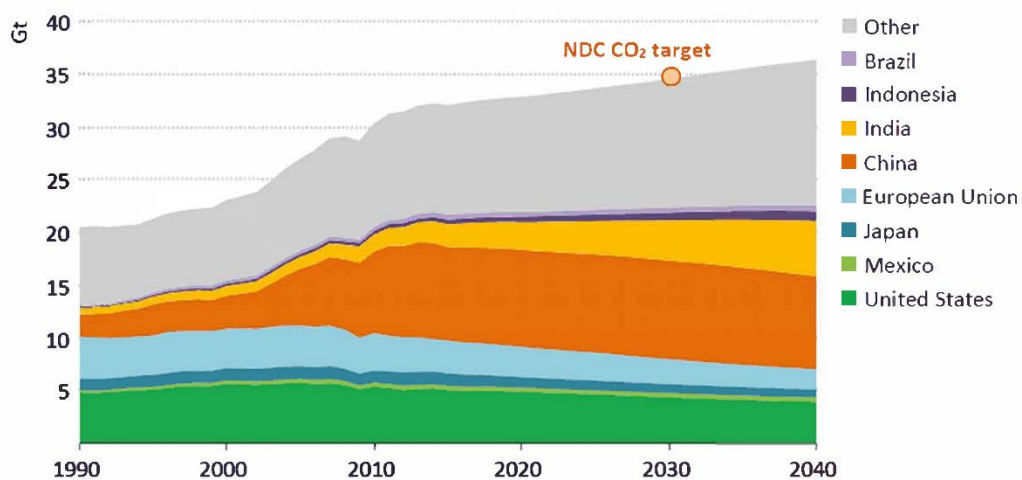


Figure 2.1 Energy-related CO₂ emissions growth by region [18]

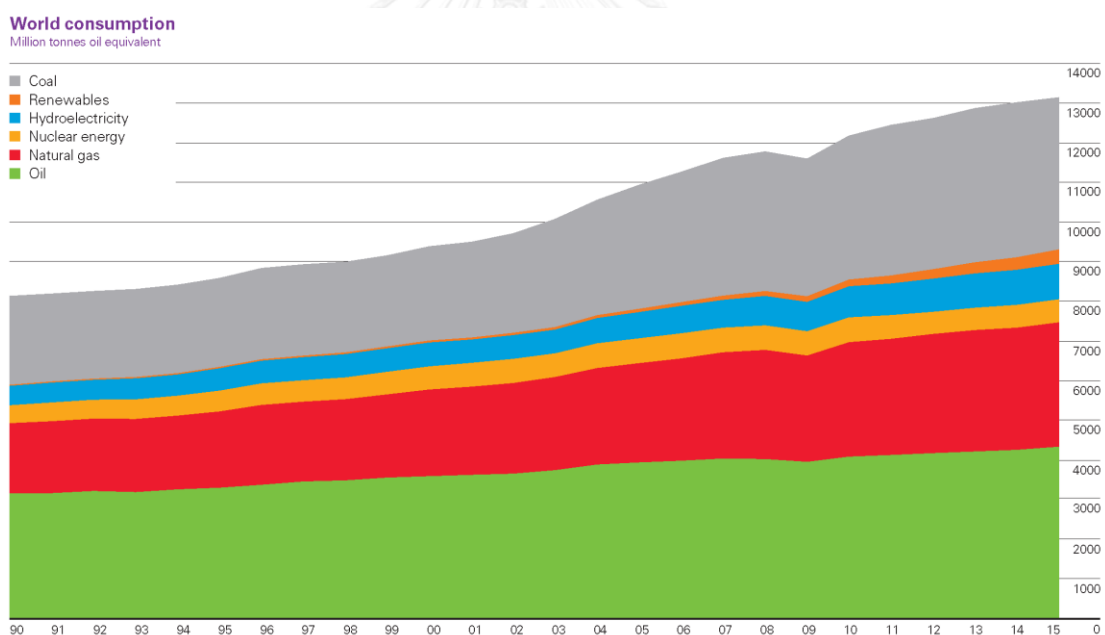


Figure 2.2 World primary energy consumption [19]

According to BP's Statistical Review of World Energy [19], global energy consumption gradual decelerated and grew by just 1.0% in 2015 which is much lower than the growth over the past decade (1.9%) due to weakness in global economy (Fig.

2.2). World primary energy consumption reached 13,147 million tons of oil equivalent in the same year. The demand for oil remains the highest consumption at 4,331 million tons, accounting for 32.9 percent of the world energy consumption. Even though global proved oil reserves increased to 1,697.6 billion barrels, or 24%, over the past decade and sufficient to meet 50.7 years of global production, it's still remains the fact that oil will be depleted in the near future. In Thailand, the energy consumption reached 79.9 million tons of oil equivalent which grew at an average annual rate of 2.6% [20]. Thailand energy consumption in 2015 shown in Fig. 2.3 revealed that oil still remained the leading fuel at 49.0% followed by electricity, renewable energy, natural gas and coal at 19.9%, 9.7%, 7.7% and 5.2%, respectively. While Thailand energy consumption continued to increase, Thailand energy production was decreased and needed to be imported from other countries. Even though global oil production was rapidly increased more than consumption rate due to an increase in OPEC production. The requirement of sustainable energy and the rise of global warming were the major force to drive many researches to seek new energy resources to reduce the effect of these problems.

Renewable energy, mostly came from the sun either directly or indirectly which could be replenished and will never run out, had become major areas of research due to the challenge to supply more clean fuels with the high-energy demand. In 2015, renewable energy sources in power generation continued to increase and reached 2.8% of global energy consumption [19]. In recent years, Thai government had a policy

to promote the use of renewable energy in the country, as well as to increase energy efficiency. Thailand renewable energy consumption reached 11.5 million tons of oil equivalent which grew at average annual rate of 9.7% [21]. Wind and solar electricity, which has plenty source in local, had been in attention to reduce the impact from coal power plant but constrained by their intermittency and the growing difficulties to incorporate them into the electric grid in the long run.

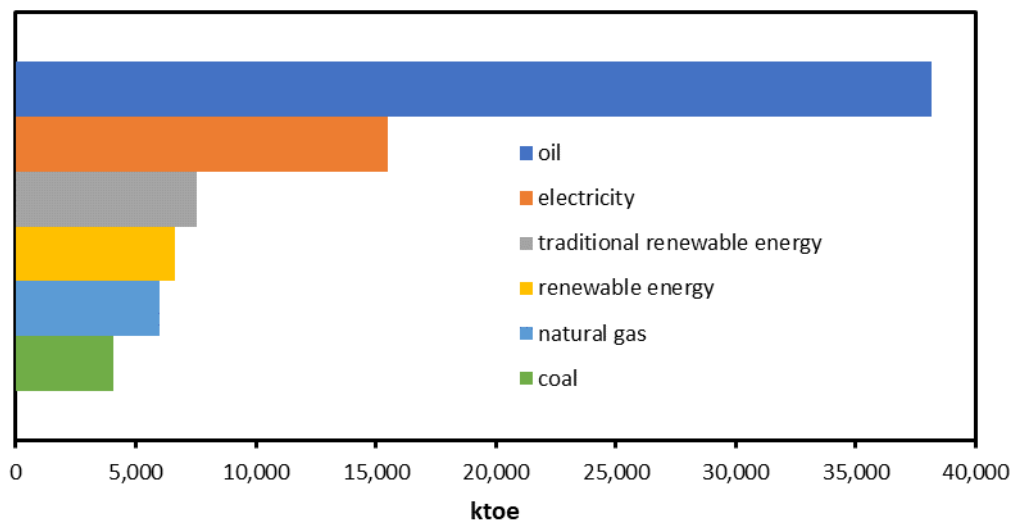


Figure 2.3 Thailand energy consumption in 2015 [20]

The development of new technologies to reduce energy consumption while improve efficiently of energy production process has been taken an interest in the past decade since the energy demand cannot be reduced and fossil fuel reserves is steady depleted. In agreement with the call for sustainable development and environmental concerns, fuel cells have been recognized to be the cornerstone of energy conversion and power generation technologies since it has more efficiency than internal

combustion engine and compatible with alternative fuels and renewable energy source.

2.2 Fuel cells and hydrogen energy

Fuel cell is an electrochemical energy conversion device, which continuously converts the chemical energy from a fuel into electricity through a chemical reaction of hydrogen ions (H^+) with oxygen (O_2) or another oxidizing agent. The efficiency of fuel cell can reach as high as 60% in electrical energy conversion and overall 80% in co-generation of electrical and thermal energies. Fuel cells are different from batteries since fuel cells can produce electricity continuously as long as the continuous source of fuel and oxygen or air to sustain the chemical reaction are supplied [22, 23].

Generally, fuel cells could be distinguished into five types on the basis of the electrolyte employed since electrolyte has an essential role which only allows the appropriate ions to pass between the anode and cathode. If other ions were allowed to flow between the anode and cathode, the chemical reactions within the cell would be disrupted. They differ in the composition of the electrolytes and in operating temperature ranges and are in different stages of development. They are alkaline fuel cells (AFCs), phosphoric acid fuel cells (PAFCs), proton exchange membrane fuel cells (PEMFCs), molten-carbonate fuel cells (MCFCs), and solid-oxide fuel cells (SOFCs).

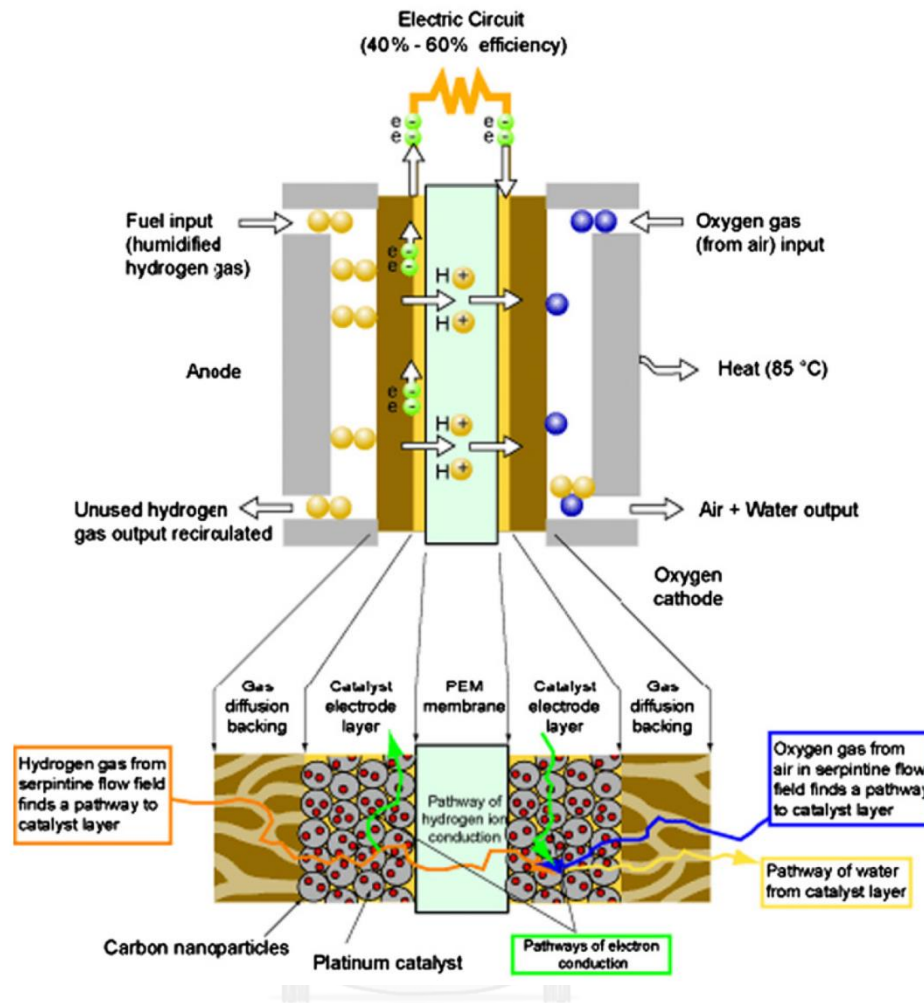
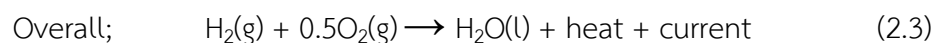
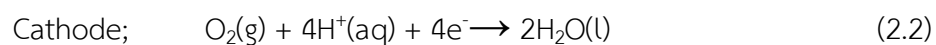


Figure 2.4 Phenomena in a PEM fuel cell: two-dimensional sectional view [22].

CHULALONGKORN UNIVERSITY

The majority of the world's leading automotive manufacturers now have publicly stated their aim to launch the prototype of PEMFCs vehicles and some companies are in the way of commercialization. At present, the proton exchange membrane fuel cell is the most promising energy system used in commercialized electric vehicles due to their features include low-temperature operation (80 °C) to make them suitable for home applications and vehicles, high power density (40%–60%), nearly zero pollutants compactness, quick start-up, silent operation and

suitability for discontinuous operations. Phenomena in a PEM fuel cell was summarized in Fig. 2.4. PEMFCs are constructed using polymer electrolyte membranes as proton conductor and Platinum (Pt)-based materials as catalyst. It has two electrodes where the reactions take place and an electrolyte which carries the charged particles from one electrode to the other. The hydrogen will diffuse into the porous electrode at the anode where Pt-catalyst is located. A chemical reaction strips the hydrogen molecules of their electrons and the atoms become ionized to form H^+ . The electrons travel through external circuit to provide a current to do work. The oxygen, usually from the air, enters at the cathode where the oxidant reduction occurs. The oxygen picks up the electrons that have completed their circuit and then combines with the ionized hydrogen atoms (H^+). Water (H_2O) is formed as the waste product and then exits the fuel cell. The reaction in PEMFCs were shown in Eq. (2.1) - (2.3).



One of the main component for PEMFCs is the catalysts which provides hydrogen dissociation to proton and electron in anode. Platinum is the most widely used catalysts due to its highly active and stable. However, it can be deteriorated by

CO poisoning that contaminated in feed stream. CO will compete with H₂ to adsorb on the active site and prevent molecules of H₂ to be dissociate, resulted in the drop of fuel cell performance. One idea to solve this problem is using CO-tolerant catalysts and another is using pure H₂ as fuel for fuel cell. This research will focus on the latter method. Nevertheless, H₂ has low energy density by volume which needs high pressure to condense into liquid or large storage capacity which is not suitable for transportation. Thus, H₂ is favor to be produced on-board from hydrocarbons or liquid fuels.

2.3 Hydrogen production process

Hydrogen is well known as an important feedstock in chemical industries and in refineries as well as a promising energy carrier [24]. It has a very high energy density at 142.0 MJ/kg which is 2.6 times when compare with natural gas (55.5 MJ/kg), revealing the potential applications as a fuel. Hydrogen can be produced from various hydrocarbon include fossil resource such as natural gas and coal, together with renewable resource such as biomass and water (electrolysis with input from renewable resources). The global hydrogen production has reached around 55 billion kg per year [25]. Most of them were consumed on-site in refineries for upgrading crude oils, and in the production of ammonia and methanol. Pure H₂ streams have also been used in a number of hydrogenation reactions for the production of other daily products such as

vitamins, cosmetics, and lubricants. The global demand for H₂ in refineries is still growing due to the need to process heavier and dirtier feedstocks, combined with the desire to produce much cleaner transportation fuels, especially the interest in using H₂ as a future energy carrier will result in a large demand for H₂.

Hydrogen can be produced from a variety of process technologies, including thermochemical, chemical, biological, electrolytic and photolytic [9]. H₂ production from fossil fuels and biomass involves conversion technologies such as reforming, gasification, and pyrolysis, while electrolysis and photolysis are used when the source of H₂ is water. Each technology is in a different stage of development, and each offers unique opportunities, benefits and challenge. In the near term, water electrolysis and small-scale natural gas reformers were recommended due to their proven technology that can be used in the early phases for building a hydrogen infrastructure for transportation. Hydrogen production based on renewable source production with CO₂ capture and storage is more feasible in the long term even though it needs additional focus on local availability of feedstock and the maturity of technology.

The most outstanding technology for direct hydrogen production is steam reforming from hydrocarbon. Steam reforming of natural gas or steam methane reforming is widely practiced technology for hydrogen production since the efficiency of this process is among the highest of current commercial technology about 65% - 75%. Natural gas is a mixture of hydrocarbon and nonhydrocarbon gases which the main constituent is methane (CH₄) and its composition is varied from each region.

Hydrogen production from natural gas is attractive since natural gas is an easy to handle feedstock with a high hydrogen to carbon ratio (H/C) and the well-developed infrastructure already widely available around the world.

2.3.1 Conventional process

Full-scale hydrogen production via steam reforming of hydrocarbons includes six different catalytic processes consisting of desulfurization, primary and secondary steam reforming, high and low temperature water-gas shift reaction and methanation [24]. The first three steps involve syngas production while the latter three are purification steps. The process flow diagram is shown in Fig. 2.5 while the reactions and typical catalysts for these 6 steps are discussed below.

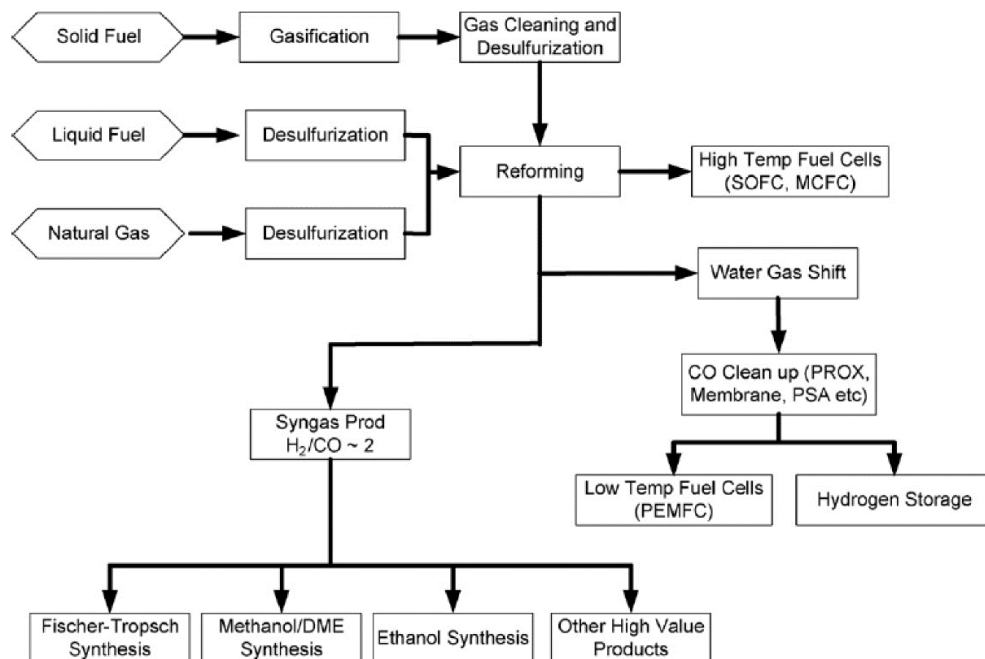
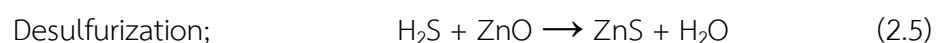
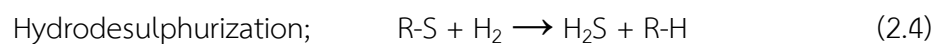


Figure 2.5 Fuel processing of gaseous, liquid, and solid fuels for hydrogen production [9].

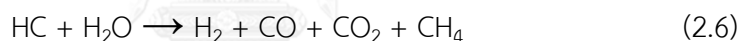
Most hydrocarbon resources whether is petroleum, natural gas or coal contained sulfur which needed to be removed or desulfurized before applied for fuel cell applications. Sulfur in the fuel, even trace amounts, can poison the catalysts in the process including reforming, water-gas shift and anode catalysts in fuel cells. Therefore, sulfur must be removed to below 1 ppm for most fuel cells, preferably below 60 ppb. There are many methods for the sulfur removal including dry desulfurization, wet desulfurization, and catalytic adsorption. For dry desulfurization, activated carbon (AC), zeolites, and molecular sieves, are used. Wet desulfurization method is liquid-phase chemical/physical solvent absorption systems which usually used for scrubbing H₂S. For large-scale hydrogen production from natural gas, hydrodesulphurization (HDS) which mixed natural gas with hydrogen is preferred. The catalyst is either CoMo/Al₂O₃ or NiMo/Al₂O₃. The sulfur-contained hydrocarbons are reduced to H₂S at 200 °C and pressures up to 20 bars. H₂S will then absorbed on ZnO by the following equation which decrease sulfur levels to 20 ppb.



After sulfur removal, the feed will be fed to primary steam reforming and continuously reacted with steam in secondary steam reforming. In case of

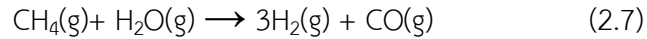
hydrocarbons that heavier than methane, the primary steam reforming or pre-reformer may be required to prevent steam cracking [26]. Pre-reforming can be an advantageous step for hydrogen plants because it increased feedstock flexibility while improve energy efficiency. The pre-reforming stage is an adiabatic hydrocarbon feedstock pre-treatment which takes place at around 400 °C to 550 °C and pressures up to 70 bars depending on the feedstock. The heavy hydrocarbons are steam reformed to syngas and then reacted with hydrogen over Ni-based catalyst such as Ni/MgO. The effluent contains methane, hydrogen, carbon monoxide, carbon dioxide and steam.

Primary steam reforming;



Methane from primary reforming enter secondary reforming unit and reacted with steam to produce hydrogen and carbon monoxide. The steam reforming of natural gas is highly endothermic (+205.9 kJ/mol) and requires high energy input. In practice, steam reforming of natural gas has been performed at high temperatures over Ni-based catalysts (Ni/Al₂O₃) due to its sufficient activity and low cost. The steam methane reforming is widely practiced technology and involves several catalyzed reactions such as water-gas shift, reverse water-gas shift, Boudouard reaction and methane decomposition reactions with the overall reaction described below:

Steam methane reforming;

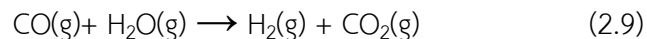


Secondary steam reforming;

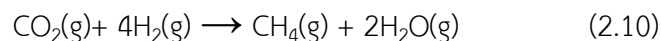
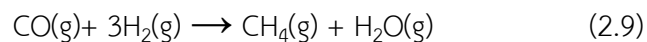


The reformat after secondary reforming, contained 10-20% CO, is fed to a high temperature water-gas shift reactor (350-400 °C) which typically used $\text{Fe}_3\text{O}_4/\text{Cr}_2\text{O}_3$ catalyst to decrease CO concentration to ~2% and further increase hydrogen content. The effluent is then fed to a low temperature water-gas shift reactor (200 °C) which typically contain $\text{Cu}/\text{ZnO}/\text{Al}_2\text{O}_3$ catalyst to further decreased CO to less than ~1% with additional hydrogen. The remaining CO, which could poison Pt catalysts in fuel cell, is commonly removed by pressure swing adsorption by using activated carbon or zeolites as an adsorbent. In some case, methanation over a Ni-based catalyst is used.

Water-gas shift;



Methanation;



Large scale H₂ plants typically operate at steady-state for a long period with few shutdowns and need experienced operators and engineers. While small scale hydrogen fuel processor, for on-board production, often operated with frequent startup-shutdowns and need much more critical concern for size, weight, pressure drop, mechanical integrity and safety when compare to large scale H₂ plants.

As vehicle will often start and stop, frequent startup-shutdowns of hydrogen production unit will be necessary depending on the duty cycle. Mechanical integrity or attrition resistance of particulate beds are also important for the vehicle design. Pressure drop occurred from methane flow through bed can limit residential applications where the line pressure in building is only slightly above atmospheric. For the Ni-based catalyst used in reformer, it must be well reduced to be active. If the reduced catalyst is exposed to the air, Ni will spontaneously ignite with oxygen and released heat which is unacceptable safety issue. Ni can form a highly toxic nickel tetracarbonyl (Ni(CO)₄) when exposed to high CO partial pressure. Moreover, Ni catalysts rapidly deactivated in a presence of sulfur and sulfur removal unit is required. Hydrodesulphurization used on commercial steam reforming plant required high H₂ pressure which in not suitable for residential applications. For water-gas shift catalyst, Cu-based catalyst or Fe/Cr-based catalyst required slow reduction procedure to avoid sintering which is not likely to be feasible. Although pressure swing adsorption is commonly used for hydrogen purification step to remove CO, CO₂, H₂O and any hydrocarbons remained in traditional plants, this process is not practicable for small

scale fuel processor since high pressure is not readily available. Methanation to remove CO is probably not feasible for small scale fuel processor since a vast amount of hydrogen will be consumed.

Given that conventional catalyst and technologies has serious limitations to applying for small scale fuel processor, new catalyst and technologies for hydrogen production is developed to meet these demands especially for cost effective fuel processor.

2.3.2 Alternative approaches for small scale fuel processor

Various types of catalyst and reactor technologies for hydrogen production have been developed for transportation applications. The major problem which suppress the use of hydrogen as an alternative fuel is due to technical limitations such as low energy densities per volume which required high standard storage or the lack of infrastructure [27]. One of the most favorable way to solve this problem is using liquid fuels that has high energy densities and convert them to hydrogen-rich stream via on board fuel processor. Methanol is a suggested fuel resource for hydrogen production on account of its high density which allowing it to be stored, transporting and applying to conventional infrastructure. Moreover, methanol can be produced from biomass which makes it suitable for further development in Thailand and does not require pre-reforming or desulfurization processes since it is free from sulfur. It has high hydrogen to carbon ratio ($H/C=4$) with no C-C bonds, minimizing the chance for

coke or soot formation. In addition, methanol can be reformed at low reaction temperature around 300 °C and atmospheric pressure to produce 3 moles of H₂ and 1 mole of CO₂ per 1 mole of methanol. This low temperature reforming makes rapid startup possible and prevents the chance to form other pollutants such as NO_x and SO_x. Even though 1% of CO is produced as by-product that must be removed, CO level is low enough to be cleaned by preferential oxidation (PROX). This makes the fuel processing relatively simple and less complicated since water-gas shift reactor is not necessary.

2.4 Hydrogen purification process

There are several processes to remove trace contaminants from reformat. They can be categorizing as adsorption, membranes, scrubbers, and selective reaction [24]. Powder activated carbon (PAC) or pressure swing adsorption (PSA) is typically employed for adsorption process to physically condense or trap the contaminant. These 2 processes are the most mature conventional adsorption technologies for CO removal from the reformat but they need high pressure to achieve high removal efficiencies and required special design to support the system. Membrane separation is another technology with high efficiency to remove CO. Membranes is widely used for chemical purification and have been applied to purified reformat as well. It allows hydrogen to pass while retaining other gases. Membranes are constructed by either

inorganic ceramics or precious metal alloys and usually operate at temperatures up to about 200 ° C. Another separation technique is the scrubber. Scrubbers are the most mature technology that developed from the chemical separation industry and can achieve 99.99% removal efficiency. Liquid-gas interaction is employed for contaminant removal. It need large stationary scrubber which is suitable for large scale plants. It's hard to scale-down and not feasible for small scale fuel processor.

Selective oxidation or preferential oxidation (PROX) is a purification technology to remove trace amounts of CO (1% mole or less) from a reformat stream. The reformat from methanol steam reforming usually contains 20% CO₂, 15% H₂O, 1% CO, 40% H₂ in inert balance. PROX has the ability to selective convert the small amount of CO in the presence of large quantities of H₂. and can be operated on continuous basis at low temperature and atmospheric pressure. Unlike other technologies, PROX can convert CO into CO₂, so regeneration or bed replacement is not necessary. Moreover, the reactor size is much smaller than WGS reactor. However, there are some concerns about durability of the catalyst. The contaminants in the reformat may render the catalyst completely inactive. In addition, unexpected over-temperature, which cause sintering on catalyst, can affect the performance or durability of the catalyst too.

2.5 Fuel processor for PEMFCs

Fuel processor for hydrogen production via methanol steam reforming is developed for PEMFCs consists of the following process: a methanol steam reformer, burner which provides heat for reformer and a gas cleaning unit to reduce CO level in effluent before fed into PEMFCs. A gas storage system may also integrate in the fuel cell system to provide feed during startup [23]. The process flow diagram was shown in Fig. 2.6.

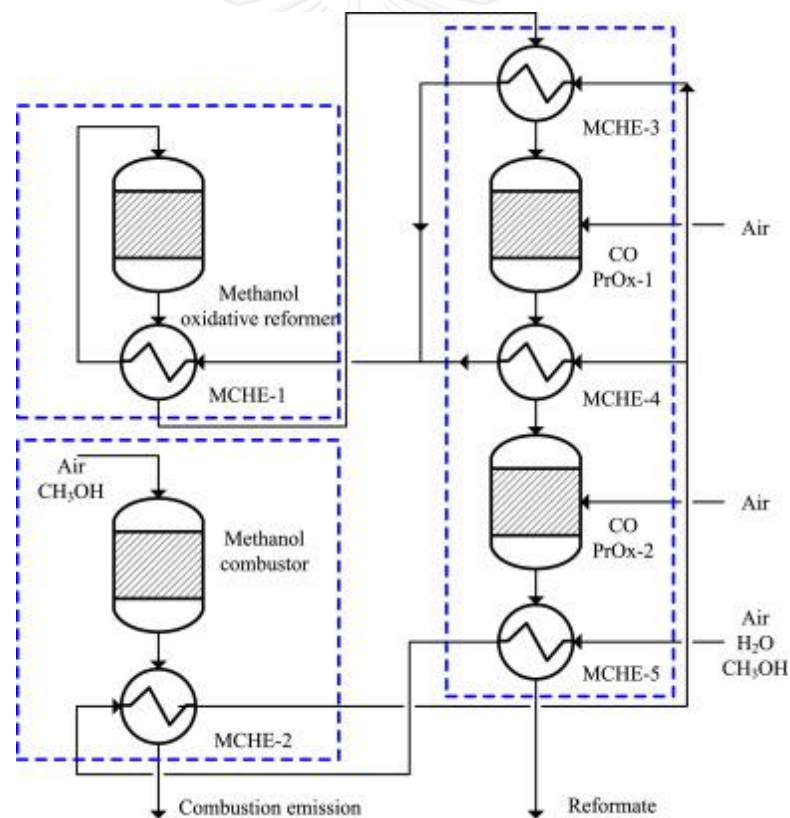


Figure 2.6 Flow scheme of methanol fuel processor and heat exchanger network [28].

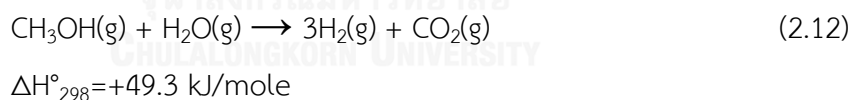
2.5.1 Methanol steam reforming (MSR)

Hydrogen can be produced from methanol by various processes such as decomposition, steam reforming, partial oxidation, and oxidative steam reforming as shown in equations 2.11-2.14, respectively. Among these processes, methanol steam reforming is considered to be the most attractive one for fuel cell applications because of the ability to produce high hydrogen concentration (ideally, 75%) with high selectivity for CO₂. The effluent mainly contains hydrogen and carbon dioxide with a low level of CO.

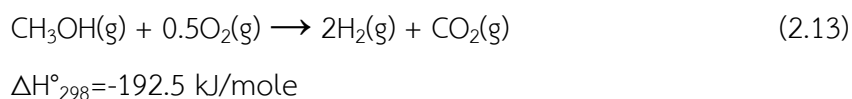
Decomposition of methanol;



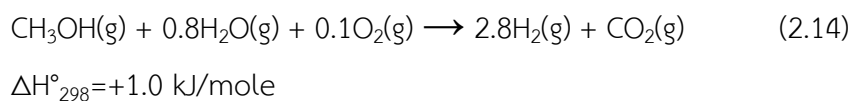
Methanol steam reforming;



Partial oxidation of methanol;



Oxidative steam reforming;



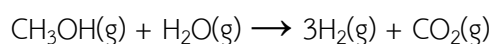
Methanol steam reforming has major developed for the past 20-30 years. The reaction is generally performed over Cu-based catalysts such as Cu/ZnO/Al₂O₃, methanol synthesis catalyst, in the temperature range from 200 °C to 300 °C and atmospheric pressure. Steam to carbon (S/C) ratio is one of the essential factor for methanol steam reforming and typically used between 1 and 2. Higher S/C ratio could favor the WGS, which lower CO concentration in the reformat and suppress carbon formation on the catalyst surface. The obstacle for this process is that the reaction is highly endothermic and need external heat supply.

Two reaction pathways for methanol steam reforming have been suggested in the literature. The mechanism of CO formation during the process also received high attention. The first one suggested that methanol decomposed and then followed by WGS reaction to form H₂ and CO₂. The other is methanol dehydrogenation to formaldehyde/methylformate to formic acid followed by decomposition to H₂ and CO₂. Nevertheless, the WGS reaction is reversible. Therefore, CO can form via either methanol decomposition or reverse water-gas shift.

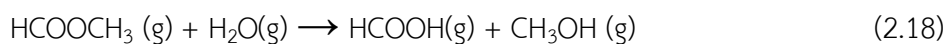
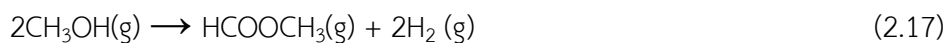
Pathway I;



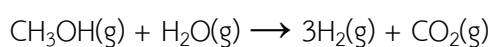
Overall;



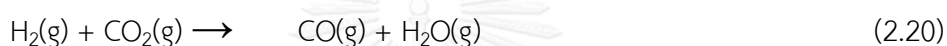
Pathway II;



Overall;



Reverse water-gas shift



The MSR catalysts can be classified into 2 main groups: Cu-based catalysts and noble metal-based catalysts. Copper-based catalysts have been widely used since the MSR reaction is the reverse of the methanol synthesis reaction. The commercial Cu/ZnO/Al₂O₃, which commonly used for methanol synthesis and WGS, has high catalytic activity for MSR as well. Since metallic copper is the active site in these reactions, highly dispersed Cu become the one of the most essential part in preparation. ZnO acts as a textural support to improve copper dispersion since copper is highly sensitive for sintering. Al₂O₃ serves as a high surface area support to improve Cu dispersion and decreases the risk of copper sintering. Catalyst preparation method plays an essential role to further improve catalytic performance of MSR catalysts by improving CuO reducibility and Cu metal dispersions. Some suggested that

Cu/ZnO/Al₂O₃ catalysts prepared via hydrotalcite precursors by coprecipitation is highly active for MSR. The high activity of the catalyst is attributed to highly dispersed Cu particles which improve accessibility to methanol and steam.

Substitution of Al₂O₃ in the Cu/ZnO/Al₂O₃ catalysts by some metal oxide such as ZrO₂, CeO₂ and La₂O₃ has been found to improve the catalytic performance in MSR. The results reveal that the substitution of Al can improve the CuO reducibility, Cu metal surface area, and dispersion which also improve methanol conversion, hydrogen yields and lower CO selectivity. Although the noble metal-based catalysts such as Pd/ZnO catalyst are more stable compared with Cu-based catalysts, it's not feasible for large-scale applications since the catalyst require high Pd loading. Thus, Cu-based catalysts with modified metal oxide which improve the thermal stability of Cu-based catalysts may be promising catalyst candidates for large-scale applications.

2.5.2 Preferential oxidation (PROX) of CO

Since trace amount of CO in reformat can deteriorate the efficiency of Pt catalyst in PEMFCs via CO poisoning, CO become the target to be removed and should be eliminated to less than 100 ppm. The overall reaction for preferential oxidation of CO is the oxidation of CO via a carefully controlled oxygen to carbon (O₂/C) ratio. Although PROX is the most cost-effective process and has high selectivity toward CO oxidation, it should be noted that the side reactions also occur, especially in the presence of H₂. The undesired reaction is the oxidation of hydrogen, reverse water-gas

shift and methanation. Hydrogen oxidation not only consume hydrogen, the desired product in reformate, but also consume oxygen which leaving less oxygen for CO oxidation. Moreover, Oxidation of hydrogen can release excess heat which raise the probability of unexpected over-temperature and need to be avoided. Most PROX catalysts was carried out at low temperature around 25-200 °C. At higher range, the oxidation may be accompanied by reverse water-gas shift and methanation reaction which could promote CO or consume more H₂.



In general, reaction in PROX system begin with CO adsorbed on the surface of catalyst. Thus, temperature of the system has significant role on CO oxidation. As the temperature increased, the level of CO adsorbed on the surface decreases and reveal the sites for oxygen adsorption and CO oxidation. Further increasing temperature, hydrogen would compete with CO to adsorb and react on the surface, reducing the selectivity toward CO oxidation. Therefore, the catalysts for PROX should operate at a

temperature sufficient for CO oxidation but below the level that consume hydrogen. Supported noble metal catalysts such as Ru, Rh, Pt and Au have highly selective for the PROX of CO especially Pt. Initially, CO is adsorbed on a Pt surface site, while an oxygen molecule adsorbs either on nearby site or on the support in order for CO to react with O atoms to produce CO₂. An optimum O₂/C ratio is also required in order to balance the amount of CO and oxygen. CuO-CeO₂ catalysts and Cu/CeO₂ catalysts were also studied and revealed the high selectivity and conversion of CO oxidation, with an operating temperature of 140 °C. The advantage of the Cu-Ce catalyst is that it can inhibit reverse water-gas shift reaction.

2.6 Catalyst preparation method

Solid catalysts are derived from chemicals by means of several procedures. Properties of catalysts are strongly affected by both preparation method and quality of the raw materials. Most manufacturer target is to develop stable, active, and selective catalyst, results in several preparation methods are developed to achieve catalyst with high surface area, good porosity, and suitable mechanical strength. Three methods are discussed below [29, 30].

2.6.1 Impregnation method

Impregnation method is a method to mount the dissolved aqueous precursors on oxide supports while the solution is drawn into the pores by capillary suction. There are 3 main steps for impregnation method which involves contacting the support with the impregnating solution, drying the support to remove liquid and activating the catalyst. The method for contacting the support with the impregnating solution can be classified into 2 categories, according to the volume of solution added. The first method is executed by using excess of solution and is also called “wet impregnation”. The support is dipped into an excess quantity of solution and then drained and dried. These 2 steps play significant roles to control the amount of the precursor mounted onto the porous support and its concentration profile within the pore. The amount of the precursor introduced into the porous support also depends on the equilibrium concentration of the impregnating solution, the porous volume of the carrier, and the adsorption isotherm. In case of nonequilibrium conditions, the distribution of the impregnated component is mainly dependent on sorption-diffusion mechanism and is only slightly affected during drying.

The other method is using more precise control which is called “dry impregnation” or “incipient wetness impregnation”. The support is contacted with no excess of solution remain outside the pore space. Incipient wetness impregnation is often used when the interaction strength between the active precursor and the support is weak. The drawback of this method is that the maximum loading is limited

by the precursor solubility in the solution. In addition, severe redistribution of the impregnated species may occur during drying step due to the absence of sufficiently strong interactions.

The Phenomena of transport involved for both techniques shown in Fig.2.7, the penetration of the solution required the elimination of air from the pores. Heat is generally released when solid/liquid interface replaces solid/gas interface. Thus, the main operating variable is the temperature which affects both the solubility and viscosity of the solution. After impregnation, the solvent need to be remove which typically heat in an oven up to boiling point of the solvent. When the solution is removed from the pore, the concentration of precursor is increase up to saturation and crystallization. Hydrate salts like nitrate melt at moderate temperature can be removed by calcination at higher temperature.

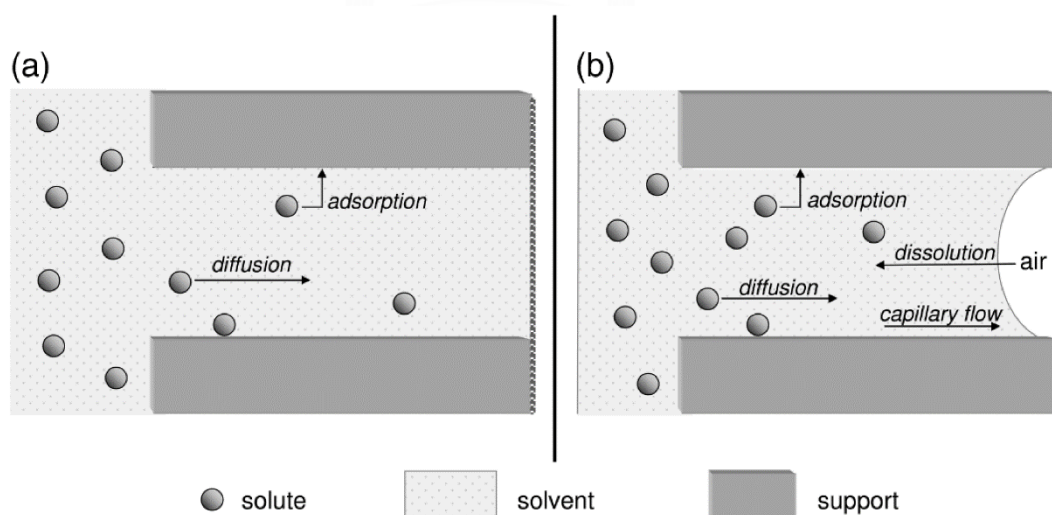


Figure 2.7 Phenomena of transport involved in (a) wet impregnation and (b) dry impregnation [31].

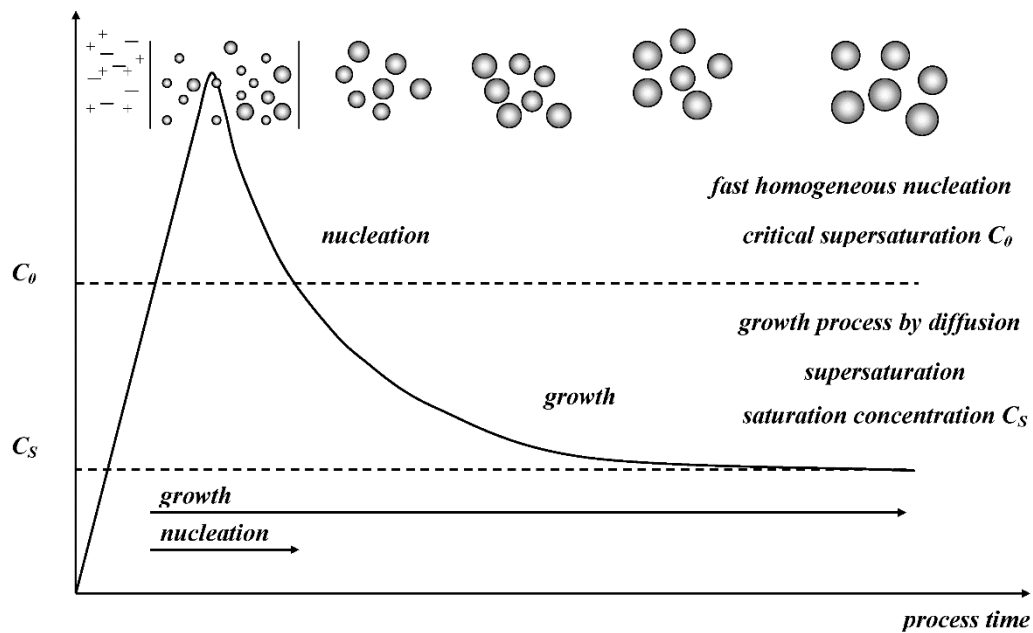


Figure 2.8 LaMer and Dinegar model for the generation of atoms, nucleation, and subsequent growth of homogeneous precipitation [32].

2.6.2 Precipitation method

Precipitation method is the process which solid metal is formed after supersaturation and then precipitate from the homogeneous solution. Precipitation usually involves three steps: supersaturation, nucleation and growth. Plot of La Mer and Dinegar model for the generation of precipitate was shown in Fig. 2.8. In most case, the system in supersaturation region is unstable and precipitation easily occurs with any small perturbation. Supersaturation can be achieved by increasing solvent concentration, decreasing the temperatures or increasing the pH. After the supersaturation region is achieved, the precipitate is then developed by nucleation and growth. Nucleation may proceed spontaneously or be initiated with seed materials

such as the dust or the rough edges of the vessel surface. While the growth of precipitate depends on concentration, temperature and pH. Most precipitates are crystalline solid but it is also possible to obtain amorphous solids if the supersaturation is very high. It should be note that particles with strong affinity to water can form hydrophilic colloids which is difficult to flocculate and difficult to filter. Typically, Hydroxides and carbonates salts are the preferred precursor because they can easily decompose by heat.

Precipitation procedures can be used to prepare either single metal or mixed metal catalysts. The latter is very suitable for intimate mixing of the catalyst components since it can achieve homogeneous distribution of catalyst component. However, the pH should be adjusted and kept constant during the operation to avoid independent or consecutive precipitations due to differences in solubility between the components. While rapid nucleation and growth in the bulk solution must be avoided, since it produces a deposition only outside the support porosity. Subsequent to formation of the coprecipitate, hydrothermal treatments may be carried to transform amorphous precipitates to crystalline materials while improved thermal stability and surface acidity.

2.6.3 Hydrothermal method

Hydrothermal is a method to obtain nanocrystalline materials but is usually consider as the modification of precipitates, gels or flocculates by inducing

temperature, under aging in the presence of the solution which it's typically use water. Hydrothermal treatment (see Fig. 2.9) is usually carried out at low temperatures (<300°C) to modify textural or structural of the solid such as increasing crystal size or particles, increasing crystallinity. Most transformations usually occur in liquid phase. There are many variables that has influence during the treatment such as pH, temperature, pressure, time and concentration. It's also possible to modify the initial properties of hydrothermal solution by employ some additives such as CO₂ to widen the range of applications.

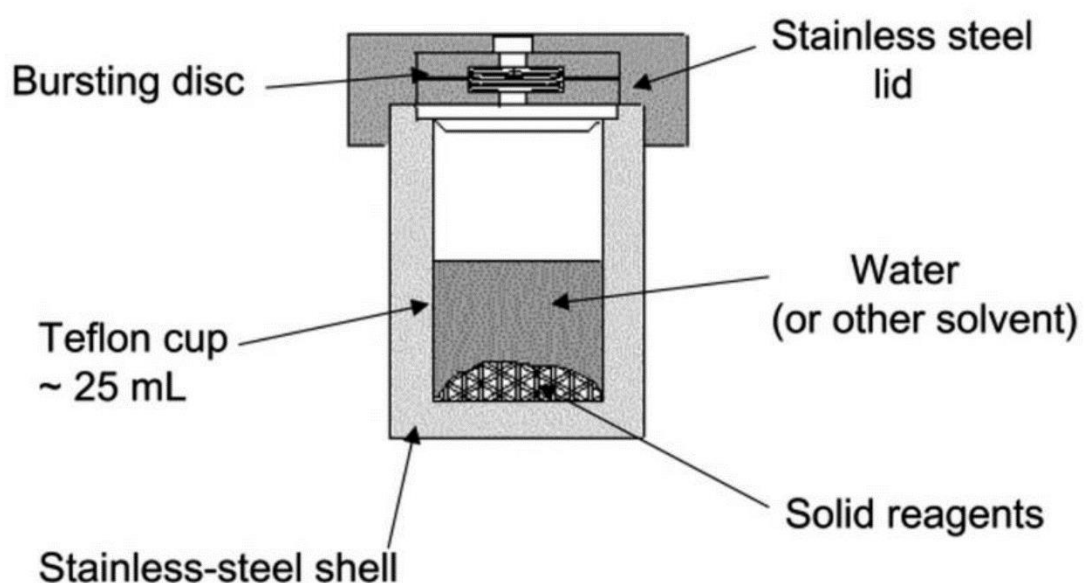


Figure 2.9 Schematic of a Teflon® lined stainless steel autoclave typically used for hydrothermal synthesis [33].

2.7 Catalyst characterization

Characterization of a heterogeneous catalyst is a procedure to measure its characteristic both physical and chemical properties which presumably to be responsible for its catalytic performance. Many characteristics of catalyst involve morphology, physical properties, surface properties, bulk properties, particle size distribution and mechanical properties [34].

BET or Brunauer–Emmett–Teller Method: Most heterogeneous catalysts are porous materials. The porosity of catalyst usually depends on preparation methods. The porous structure enables the catalyst to achieve much higher surface area and improves catalytic performance. Thus, morphological parameters are very important to understand for catalyst development. BET is a method which is widely accepted for analyzing multi-layer physisorption isotherm of inert gas to determine the specific surface area of materials and pore distribution in the structure. Nitrogen adsorption at boiling temperature (77 K) is used to determine catalyst morphology by analyzing the adsorption isotherm (nitrogen volume adsorbed vs. its relative pressure).

XRD or X-ray diffraction: XRD becomes a fundamental technique since most catalysts are crystalline materials. XRD is used to characterize bulk crystal structure and chemical phase composition by plot the intensity of diffraction of X-ray beam as a function of the angle of incident beam. It's often used to follow solid evolution during thermal treatment and analyze nature of crystalline phases and crystallite size.

TPR or Temperature-programmed reduction: TPR is used to identify different species of the same element by measure the rate of reduction as a function of

temperature which enable the study of oxidation state on catalyst surface. TPR let the reducing gas mixture (typically 3% to 17% hydrogen diluted in argon or nitrogen) flows over the sample and then measure changes in the thermal conductivity of the gas stream by using thermal conductivity detector (TCD).

FESEM or Field emission scanning electron microscopy: Microscopy is a technique that give a direct view of the material with increasing resolution power up to Angstroms and frequently use to study catalysts, particularly to obtain various data such as shape, size, homogeneity and crystalline faces. FESEM provides topographical and elemental information at magnifications of 10x to 300,000x with depth of field. It's also provide clearer and less electrostatically distorted images when compare with conventional SEM due to the field-emission cathode in the electron gun provide narrow probing beams. In addition, FESEM can examine contaminant spots by apply with energy dispersive spectroscopy (EDS).

FTIR or Fourier transform infrared spectroscopy: Although the catalytic activity occurs on the surface, only some part is utilized for reaction. Thus, the knowledge on the nature of active sites is indispensable to understand how a catalyst works. Spectroscopy is widely used for bulk characterization to determine both local and structural characteristics. IR spectroscopy provide spectra of solids which working both in transmission and reflectance. FTIR is used to analyze the structure of adsorbed molecules on a catalyst surface under controlled atmosphere.

2.8 Literature reviews

2.8.1 Methanol steam reforming

M. Mrad et al. [13] studied the effect of Zn addition on the performances of Cu/Ce and Cu/Ce–Al catalysts for methanol steam reforming. Alumina support was prepared by sol-gel method and then impregnated by $\text{Ce}(\text{NO}_3)_3$ and $\text{Cu}(\text{NO}_3)_2$ aqueous solution, respectively. The operating temperature were hold constant at 350 °C with a GHSV of 15,500 h^{-1} and a S/C=2. The results revealed that catalytic performance of catalysts is depend on both copper species and the support. The addition of ZnO up to 5 wt% on 5Cu10Ce catalyst promotes interaction between Cu-Ce-O which improve reduction ability of copper species, the active species in methanol steam reforming as shown in TPR results. Only peak of Cu^0 for Cu/Ce catalyst with ZnO while Cu_2O and Cu^0 were observed over other catalysts. In case of Cu/Ce–Al catalysts, the CuAl_2O_4 spinel was observed to improve catalytic performance by enhanced copper dispersion.

A.A. Pechenkin et al. [35] studied steam reforming of dimetoxymethane (DMM) to hydrogen-rich gas by using $\text{CuO-CeO}_2/\gamma\text{-Al}_2\text{O}_3$ catalysts prepared by incipient wetness co-impregnation method. The optimum conditions to achieved complete DMM conversion with CO content were obtained at 300 °C, GHSV=10,000 h^{-1} and $\text{H}_2\text{O}/\text{DMM} = 5 \text{ mol/mol}$. Acid sites of $\gamma\text{-Al}_2\text{O}_3$ enhanced DMM hydration to methanol and formaldehyde and then copper-cerium oxide species steam reformed methanol and formaldehyde to hydrogen with low CO level (<1 vol.%). The catalytic

performance of CeO₂-promoted Cu-based catalysts is high due to the highly dispersed copper species, resulted from strong Cu and CeO₂ interactions as seen in TPR results. Moreover, the H₂ uptake analysis revealed that copper species over CuO/ γ -Al₂O₃ catalysts could complete reduce from CuO to Cu₀ while only 90% reduction of copper species was observed over CuO-CeO₂/ γ -Al₂O₃ indicated that the CuO and CeO₂ interact on the support to produce a solid solution of copper and cerium oxides

D. Das et al. [15] prepared a series of Cu/CeO₂-ZrO₂ catalysts to study the behavior of catalyst for methanol steam reforming. Various ratio of ceria-zirconia solid solutions was prepared by surfactant assisted coprecipitation method and then impregnated by copper solution. None of the pure CeO₂-ZrO₂ could exhibit MSR activity during studied period of temperature (200-330°C) but complete methanol conversion at 300 °C was achieved after loading copper up to 10 wt% on Ce_{0.6}Zr_{0.4}O₂. The TPR and XPS results revealed that 3 copper species on the ceria-zirconia matrix which are Cu²⁺, Cu⁺ and Cu⁰. The Ce 3d spectra revealed that the redox property of ceria prevent copper from complete reduction to Cu⁰, Cu species subsequently stabilized by zirconia structure and maintain at +1 states. Cu⁺/Cu⁰ ratio played significant role for CO formation from reverse water-gas shift. The higher Cu⁺ species on the catalyst surface would enhance the CO to react with the available surface oxygen to form CO₂ and lower CO selectivity.

X. Wang et al. [36] studied the catalytic activity of dimethyl ether steam reforming by using Cu-Ni/ γ -Al₂O₃ catalysts prepared by deposition-precipitation

method. The maximum DME conversion was achieved at 350 °C and total gas flow rate was 3,240 ml g⁻¹ h⁻¹. The TPR results reveal that addition of nickel improved the copper dispersion and increased the interaction between copper and γ -Al₂O₃. This strong interaction would inhibit copper from sintering. Moreover, the acid amount and acid strength of Cu-Ni/ γ -Al₂O₃ catalyst were decreased after increase metal loading as shown in NH₃-TPD. This fact indicate that metal particles could occupy the acid sites and suppress steam reforming reaction since γ -Al₂O₃ is a vital component of steam reforming.

R. Zhang et al. [37] studied the catalytic reforming of toluene by using Ce and Ce-Mg promoted Ni/olivine catalysts prepared by impregnation method. The results reveal that addition of Ce on Ni/olivine catalysts improve toluene conversion from 59% to 88% and reduce coke formation as observed by TG. Further addition of Mg to the catalysts increases toluene conversion to 93%, prevents coke deposition and is resistant to H₂S poison up to 10 ppm by improved metal dispersion and reduced energy for coke combustion from 165 to 12k kJ mol⁻¹.

B. Malleshram et al. [38] developed Cu/Mg catalysts for selective hydrogenation of bioglycerol to 1,2-propanediol. A series of Ce-promoted Cu/Mg catalysts was prepared by coprecipitation method. The results expressed that addition of ceria to Cu/Mg catalysts improved glycerol conversion from 30.9% to 56.4%. Addition of ceria on Cu/Mg catalysts promoted catalytic activity by increased specific surface area from 119 to 209 m² g⁻¹ by inhibits the crystal growth of CuO as seen in XRD and BET results.

The XPS results showed that Cu 2p core level features shifted to high binding energy, revealed the improvement of charge transfer from Cu to the CeO₂ and MgO. Moreover, it's also revealed that Cu/Ce₃/Mg catalysts has the highest Ce³⁺ concentration which is proportional to the amount of oxygen vacancy defect sites. These oxygen vacancy defects had a significant role in the reaction by improve reducibility of Ce⁴⁺ to Ce³⁺.

2.8.2 Preferential oxidation of CO

F. Marino et al. [39] investigated supported base metal catalysts for the preferential oxidation of CO. The catalysts were prepared by impregnation method with a wide range of transition metals (Co, Cr, Cu, Ni and Zn) supported on various metal oxides (MgO, La₂O₃, SiO₂-Al₂O₃ and CeO₂). The results revealed that only ceria supported copper catalyst was comparable with the performance of Pt/Al₂O₃, noble catalyst. Moreover, CuO/CeO₂ catalysts also expressed constant and high selectivity towards CO oxidation in the temperature range of 50-150 °C. Only small amount of copper (0.3-3 wt%) was necessary to get an active catalyst due to strong synergetic effect between copper and ceria. The excess copper would lead to the formation of bulk CuO which is inactive for the PROX reaction. This work also proposed some theories about the synergism between copper and cerium. First, CO and H₂ adsorbed on the copper sites while oxygen source was provided by ceria. Thus, the oxidation reactions were mainly occurred proceed at the Cu-Ce interface.

J. Li et al. [40] studied hydrogen purification process by using modified mesoporous CuO-CeO₂ catalysts prepared by hydrothermal method. The catalysts were doped by transition metals, such as Mn, Fe, Co and Cr, to enhanced selective oxidation of CO in H₂-rich for fuel cell application. The results showed that the addition of Mn and Fe to CuO-CeO₂ catalysts could promote catalytic performance at low temperature (<100 °C) by enhanced interaction between copper and ceria which increased the formation of Cu⁺ and oxygen vacancies on the catalysts. While addition of Cr and Co dopant achieved maximum conversion at higher temperature (>130 °C) due to the nature of dopants which the dopant substitute with Cu in ceria lattice as seen in XPS analysis and weaken Cu-Ce interaction and inhibits the Cu⁺ formation.

J. Li et al. [41] also studied the effect of preparation method for selective CO oxidation by using CuO-MnO_x-CeO₂ catalysts. The catalysts were inscribed as hydrothermal (CuMC-HY), co-precipitation (CuMC-CP), impregnation (CuMC-IM) and citrate sol-gel (CuMC-SG) methods, respectively. The results reveal that CuMC-HY catalyst exhibit the best catalytic performance among the prepared samples by achieved low temperature of 50% CO conversion (T50) at 74 °C and wide temperature window of CO conversions (>99.0%) from 110 to 140 °C. The XRD and XPS analysis revealed the formation of Mn-Cu-Ce-O solid solution on the CuMC-HY catalysts with the existence of more Cu⁺ and Mn⁴⁺ species as well as oxygen vacancies. CuMC-IM expressed good catalytic performance as well (T50 at 85°C), as the existence of Mn-Cu-Ce-O solid solution was also found. While CuMC-CP achieved temperature of 50%

CO conversion (T50) higher range at 145 °C which presumably due to the existence of independent CuO_x and MnO_x oxides weaken interaction of Cu and Mn with ceria in the catalyst.

C. G. Maciel et al. [42] studied the influence of ceria support in CuO/CeO_2 catalysts for preferential oxidation of CO reaction. The CuO/CeO_2 catalyst were prepared by 2 different methods; hydrothermal ($\text{CeO}_2\text{-HT}$) and precipitation ($\text{CeO}_2\text{-PP}$) methods. The CuO/CeO_2 catalyst supported on $\text{CeO}_2\text{-HT}$ expressed high catalytic performance by achieved high CO conversion (>90%) with temperature window from 100-250 °C and 100 % selectivity toward CO oxidation throughout studied temperature range. While the catalysts supported on $\text{CeO}_2\text{-PP}$ achieved high CO conversion in the narrow temperature from 150-200 °C with the selectivity decreased to 90%. The BET and XRD result revealed that CuO was highly dispersed on the $\text{CuO}/\text{CeO}_2\text{-HT}$ surface when compared with $\text{CuO}/\text{CeO}_2\text{-PP}$ due to higher surface area and smaller crystallite size. The morphology of ceria has effect role on the metal-support interaction which affects CuO dispersion, enhanced redox properties and lower reduction temperature.

D. G. Araiza et al. [43] was used 5 wt% Cu supported on various type of ceria nanomaterials such as nanopolyhedra, nanorods and nanocubes to investigate the catalytic performance for hydrogen production via partial oxidation of methanol. The ceria supports were prepared by hydrothermal method and then impregnated by copper solution. The reaction was carried out at $\text{O}_2/\text{CH}_3\text{OH}$ molar ratio of 0.3 and temperature in the range of 160-280°C. The results reveal that ceria morphology had significant

influenced on structural, textural and chemical properties of support. Copper was highly dispersed on ceria nanorods and nanopolyhedra due to the interaction of copper with the crystal planes of each ceria structures which led to incorporation of Cu^{2+} ion into ceria lattice. XRD analysis showed the ceria cell parameter trends as followed: Cu/Ce-nanorods (5.4200\AA) > Cu/Ce- nanopolyhedra (5.4143\AA) > Cu/Ce-nanocubes (5.4110\AA). This shrinkage of ceria lattice suggested that incorporation of copper in the ceria lattice as substitution of Ce^{4+} (0.092 nm) ion by Cu^{2+} (0.072 nm) ion. Nanorods and nanopolyhedra-shaped materials also has higher surface area in the range $75\text{--}85\text{ m}^2\text{ g}^{-1}$ while for surface area of nanocubes samples was much lower at $18\text{ m}^2\text{ g}^{-1}$.

L. Yan et al. [44] prepared Pr-doped ceria nanorods via high-temperature precipitation and low-temperature aging route. From XRD and TEM analysis, a uniform cubic fluorite structure was observed with a size of 30 nm in diameter and 400 nm in length. The morphologies, surface area and crystallization of the nanorods were improved after doped ceria with praseodymium at an appropriate molar ratio. The surface area of ceria support was increased from $84.55\text{ m}^2\text{ g}^{-1}$ to $152.9\text{ m}^2\text{ g}^{-1}$ when increased Pr content from 5 wt\% to 30 wt\% . The Ce 3d XPS spectra reveal the main cerium species in the nanorods was Ce^{+4} . Ce^{3+} species were decreased after increased Pr content as observed in XPS analysis that the binding energy of Ce^{3+} decreases.

D. Gamarra and A. Martinez-Arias [45] studied the deactivating effect of CO_2 and H_2O on preferential oxidation of CO over CuO/CeO₂ catalyst. The CuO/CeO₂ catalyst

was prepared by incipient wetness impregnation of a copper nitrate aqueous solutions on ceria nanostructured support. The deactivating effects induced by CO_2 and H_2O were observed by the mean of operando-DRIFTS experiments. The presence of CO_2 or H_2O in the reactant stream interrupted the formation of Cu^+ -carbonyls which led to the reduction of CuO-CeO_2 interfacial redox activity. Carbonates was formed on interfacial ceria sites in the presence of CO_2 which limited the capability redox property of ceria and prevented the generation of partial reduced CuO_x , the active species for CO oxidation. However, H_2 oxidation was also decreased in the presence of CO_2 which can be related to limited reduction of CuO species. While the presence of H_2O mainly related to blocking effect which limited the access of the reactant to the active sites.

2.8.3 Fuel processor for hydrogen production

G. Park et al. [46] developed 2 types of microchannel methanol steam reformer small scale fuel cell application with different dimension. The system was integrated fuel vaporizer, heat exchanger, catalytic combustor and steam reformer to evaluate hydrogen production performance. $\text{Cu/ZnO/Al}_2\text{O}_3$ catalyst was coated inside the microchannel reactor to steam reform methanol while $\text{Pt/Al}_2\text{O}_3$ pellets was used at the catalytic combust. Type B fuel processor used single microchannel patterned sheet 500 mm thick to replace the four patterned sheets for reactor A. The catalytic performance revealed that fuel processor type B expressed higher methanol conversion at 99% when compare with fuel processor type A (85%). At the optimum

condition, Type B fuel processor produce power output of 59 W with the reformat at a rate of 450 ml/min at 250 °C and the composition as followed: 73.3% H₂, 24.5% CO₂ and 2.2% CO. The superior catalytic performance is mainly due to the difference in homogeneous flow distribution and the efficient heat balance.

H.H.F. Wang et al. [47] studied the effect of the heat transfer area and the thermal conductivity on compact methanol steam reformer by using three different reactor materials with differ in their thermal conductivity: aluminum alloy (AL-6161, 180 W/M-K), brass-34 (110 W/M-K) and stainless steel-316 (15 W/M-K). The results revealed that the higher thermal conductivity of the reactor material improve heat flux and decreased heat lost to the surrounding, led to a higher thermal efficiency and smaller temperature differentials. Therefore, the compact reactor made of aluminum alloy of Al-6061, which achieved 84.7% thermal efficiency with low CO content (0.53 mol%) at 230 °C was an effective steam reformer to hydrogen.

M. Yang et al. [28] developed a self-sustained, complete and miniaturized methanol fuel processor which comprised of methanol oxidative reformer, methanol combustor and two-stage CO preferential oxidation unit by integrated the unit with microchannel heat exchanger. Microchannel heat exchanger was employed to improve energy utilization efficiency by recover heat from hot stream and miniaturize system size. The results revealed that both methanol combustor exhaust gas and H₂-rich product could maintain at 53 °C, suggested that the heat was recovered. The thermal

efficiency was achieved at 86% by optimized CH_3OH to O_2 molar ratio at reformer, amount of methanol at combustor and split ratio of O_2 at PROX unit. A self-sustained state was achieved with H_2 production rate of $0.99 \text{ Nm}^3 \text{ h}^{-1}$ and low CO content (<25 ppm), sufficient to supply a 1 kW_e PEMFCs. Moreover, the fuel processor could start up in 10 min at room temperature without external heating.



CHAPTER III

EXPERIMENTAL

3.1 Materials

3.1.1 Chemicals

- Copper(II) nitrate trihydrate ($\text{Cu}(\text{NO}_3)_2 \cdot 3\text{H}_2\text{O}$), M.W. = $241.60 \text{ g mol}^{-1}$
from Qrec
- Aluminium(III) nitrate nonahydrate ($\text{Al}(\text{NO}_3)_3 \cdot 9\text{H}_2\text{O}$) M.W. = $375.13 \text{ g mol}^{-1}$ from Merck
- Cerium(III) nitrate hexahydrate ($\text{Ce}(\text{NO}_3)_3 \cdot 6\text{H}_2\text{O}$), M.W. = $434.23 \text{ g mol}^{-1}$
from Merck
- Magnesium(II) nitrate hexahydrate ($\text{Mg}(\text{NO}_3)_2 \cdot 6\text{H}_2\text{O}$), M.W. = $256.40 \text{ g mol}^{-1}$ from Merck
- Praseodymium(III) nitrate hexahydrate ($\text{Pr}(\text{NO}_3)_3 \cdot 6\text{H}_2\text{O}$), M.W. = $435.01 \text{ g mol}^{-1}$ from Sigma-Aldrich
- Cerium(IV) oxide (CeO_2) M.W. = $172.11 \text{ g mol}^{-1}$ from Merck
- Sodium carbonate anhydrous (Na_2CO_3), M.W. = $105.99 \text{ g mol}^{-1}$ from Ajax
Finechem
- Sodium hydroxide anhydrous (NaOH), M.W. = 40.00 g mol^{-1} from Merck
- Methanol (CH_3OH), M.W. = 32.04 from Merck

3.1.2 Gases

- High purity (99.99%) H₂ from Thai Industrial Gases Public CO., Ltd.
- High purity (99.99%) CO from Thai Industrial Gases Public CO., Ltd.
- 5% O₂ in He from Thai Industrial Gases Public CO., Ltd.
- Ultra high purity (99.999%) He from Praxair (Thailand) Co., Ltd.
- 30% CO₂ in He from Praxair (Thailand) Co., Ltd.

3.2 Equipment and apparatus

3.2.1 Equipment

- Mass flow controller (AALBORG, model: GFC 1715)
- Temperature controller equipped with thermocouple and solenoid electric furnace (PID temperature)
- Syringe pump
- Tube, fitting and valve (Stainless steel 316) from Swagelok
- Gas chromatography (GC, model: GC-2014; Shimadzu Scientific Instruments equipped with a TCD detector)

- Quartz tube reactor (I.D. = 1/4 in)
- Heating tape
- Glass water trap
- Electric oven
- Static air muffle furnace
- Regulator

3.2.2 Apparatus set-up

Fuel processor for hydrogen production consists of 2 main parts, hydrogen production unit and CO purification unit. Hydrogen is produced from methanol steam reforming reaction (MSR) and CO is eliminated by preferential oxidation (PROX) of CO. The experiment schematic is shown in Fig. 3.1

3.3 Experiment procedure

3.3.1 Methanol steam reforming unit (MSR)

In MSR unit, the procedure is presented as the following topics: catalysts preparation, catalysts characterization and catalytic activity measurement. After that, statistical design of the experiments was then mentioned in order to evaluate the importance of chosen factors. Finally, the optimum conditions for MSR were determined by using response surface methodology (RSM)

3.3.1.1 Catalysts preparation

Copper-based catalysts supported on alumina with mono- or bi-promoters were prepared by co-precipitation. The level of copper was varied from 20–50 wt%, maintaining the total weight of mono- and bi-promoters at 30 wt%. The Ce:Mg weight ratios were designed at 30:0, 25:5, 20:10, 15:15 and 0:30, respectively, to obtain a Mg/(Ce+Mg) wt% of 0, 16.67, 33.33, 50 and 100, respectively.

To fabricate the catalysts, the desired mixture of $\text{Cu}(\text{NO}_3)_2 \cdot 3\text{H}_2\text{O}$, $\text{Mg}(\text{NO}_3)_2 \cdot 6\text{H}_2\text{O}$, $\text{Ce}(\text{NO}_3)_3 \cdot 6\text{H}_2\text{O}$ and $\text{Al}(\text{NO}_3)_3 \cdot 9\text{H}_2\text{O}$ were first dissolved in 50 mL of

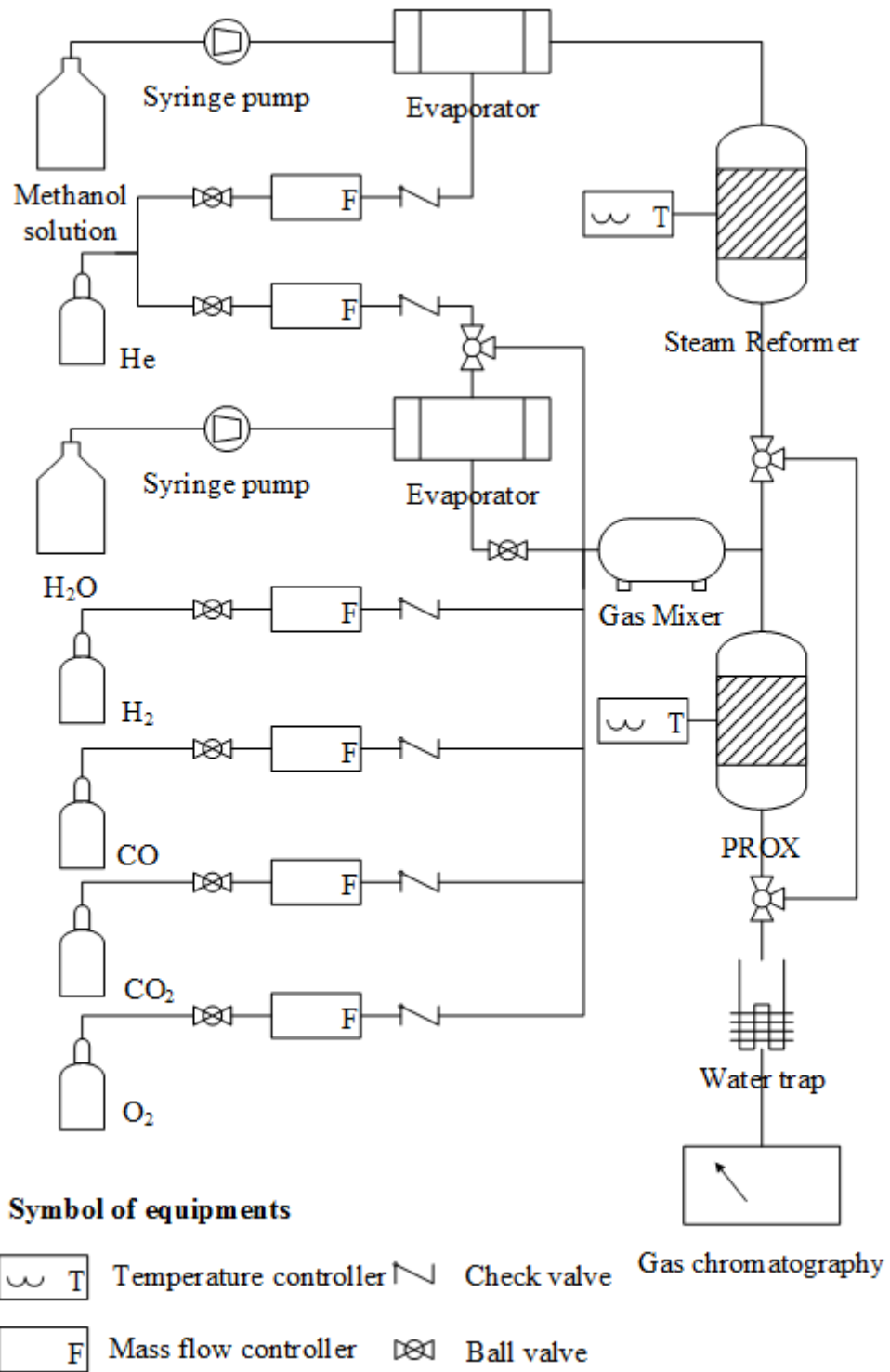


Figure 3.1 Experimental set-up for fuel processor

deionized water (DW) with stirring gently at 60 °C for 0.5 h. Next, 1.0 M Na₂CO₃ aqueous alkaline solution, as a precipitating agent, was added drop wise slowly into the metal nitrate solution with vigorous stirring until at a constant pH 10. The slightly viscous blue suspension was aged by stirring continuously for 12 h at 60 °C, and then cooled down to room temperature. The blue precipitate was harvested by filtration, washed with DW until the filtrate pH was 7, dried at 110 °C overnight and then calcined at 500 °C for 5 h at a heating rate of 10 °C min⁻¹ under a static air atmosphere to remove the remaining impurities. The catalyst was noted as Cu_xCe_yMg_z/Al, where x, y and z are the loading levels (wt%) of Cu, Ce and Mg, respectively. For example, the Cu_{0.3}Ce_{0.25}Mg_{0.05}/Al catalyst was composed of 30 wt% Cu, 25 wt% Ce and 5 wt% Mg.

3.3.1.2 Catalysts characterization

- *Field Emission Scanning Electron Microscopy (FESEM)*: the particle morphology of catalysts was carried out in a JSM-7610F instrument, an ultra-high resolution Schottky Field Emission Scanning Electron Microscope, equipped with an energy dispersive X-ray analyzer (EDX). The FESEM with 2 Secondary electrons (upper and lower) and 1 backscattered electrons detectors provide high resolution at 15 kV and high magnification x20,000 to x100,000. The catalysts were dried overnight and coated with gold before analyze.

- *X-ray diffraction (XRD)*: The XRD patterns of the samples were taken with a Bruker D8 Advance X-Ray diffractometer, operated at 40 kV and 40 mA using

monochromatic Cu $K\alpha$ radiation with a wavelength of 0.154 nm. The XRD patterns were recorded over a scanning angle (2θ) range from 5–80° at a rate of 5° min⁻¹. The analysis was performed to examine the crystalline structure and average copper particle size. The particle sizes were calculated by the Debye-Scherrer equation at the diffraction peak of Cu (111).

- *Brunauer-Emmett-Teller (BET)*: the BET method was used to determine the specific surface area, pore volume and pore diameter of the catalysts. Nitrogen (N₂) adsorption-desorption isotherms were measured at -196 °C using Micromeritics ASAP 2020 equipment. Prior to analysis, the samples were degassed at 250 °C for 1 h and increased to 300 °C for 1 h. The specific surface area of the samples was determined according to the BET method.

- *Temperature-programmed reduction (TPR)*: The reduction temperature of the catalysts was evaluated by H₂-TPR analysis. The catalysts were pretreated in a U-shaped quartz reactor under an argon (Ar) flow rate of 40 mL min⁻¹ at 500 °C for 1 h at a heating rate of 10 °C min⁻¹. After this pretreatment, the catalysts were cooled to room temperature. A reducing gas of 10% (v/v) H₂ in Ar was then switched to the reactor at a flow rate of 40 mL min⁻¹ and the catalysts were heated up to 500 °C at a rate of 10 °C min⁻¹. A thermal conductivity detector (TCD) was employed to determine the amount of H₂ uptake.

3.3.1.3 Catalytic activity measurement

Catalytic tests were performed by sandwich-packing 0.1 g of sample between two layers of quartz wool in a 0.6 cm internal diameter tubular quartz reactor. Prior to measurement of the catalytic performance, the catalyst was reduced in situ with 40 mL min⁻¹ of pure H₂ at 300 °C for 1 h to reduce Cu species to the metallic Cu⁰ form. Methanol and water were pre-mixed at a given water: methanol mole ratio and stored in a reservoir. The water/methanol mixture was pumped into a vaporizer at a rate of 1 mL h⁻¹ by a syringe pump, while helium (He) was also fed into the vaporizer at 40 mL min⁻¹ as the carrier gas, and was used as the carrier gas throughout the experiments. The final methanol and steam composition was nominally set at S/C ratios of 1.5, 1.75 and 2, respectively. This mixture with a desired mole ratio of water to methanol was then routed into the reactor at reaction temperatures between 200–300 °C. The reaction temperature was controlled by a temperature controller and was measured by a thermocouple placed in the center of the catalyst bed. The gaseous influent and effluent were passed through a water-trapping unit and then analyzed by on-line gas chromatography (GC-2014; Shimadzu Scientific Instruments) equipped with a TCD and using He as the carrier gas.

The catalytic performances were expressed in terms of the methanol conversion level (%), CO selectivity (%) and H₂ yield (%), respectively, calculated from Eqs. (3.1) – (3.3), respectively:

$$\text{Methanol conversion (\%)} = \{([\text{CO}]_{\text{out}} + [\text{CO}_2]_{\text{out}}) \times 100 / [\text{CH}_3\text{OH}]_{\text{in}}\} \quad (3.1)$$

$$\text{CO selectivity (\%)} = ([\text{CO}]_{\text{out}} \times 100) / ([\text{H}_2]_{\text{out}} + [\text{CO}]_{\text{out}} + [\text{CO}_2]_{\text{out}}) \quad (3.2)$$

$$\text{H}_2 \text{ yield (\%)} = ([\text{H}_2]_{\text{out}} \times 100 / (3 \times [\text{CH}_3\text{OH}]_{\text{in}})) \quad (3.3)$$

where $[\text{CH}_3\text{OH}]_{\text{in}}$ is the molar flow rate of methanol in the feed stream (mol min^{-1}), and $[\text{H}_2]_{\text{out}}$, $[\text{CO}]_{\text{out}}$ and $[\text{CO}_2]_{\text{out}}$ are the molar flow rate of H_2 , CO and CO_2 in the effluent, respectively.

To study the catalyst stability, the catalyst that expressed the highest performance at the optimal condition was selected to test its stability over a 72-h reaction period.

3.3.1.4 Statistical design of experiments for optimization

Since univariate analysis informs only a behavior of the catalytic performance when changing one factor at a time, neither any crucial factors on the performance nor optimal conditions are identified. Therefore, a full 2^4 factorial design with complete randomization was adopted in order to optimize the conditions for complete methanol conversion to yield a H_2 -rich stream with a low CO content. The four main factors chosen were the operating temperature ($^{\circ}\text{C}$), S/C ratio, $\text{Mg}/(\text{Ce}+\text{Mg})$ (wt%) and level of Cu content (wt%), noted as factors *A*, *B*, *C* and *D*, respectively. Three responses, in terms of the methanol conversion level, CO selectivity and H_2 yield, respectively, were considered to optimize the condition for the MSR catalytic

performance. A matrix of the four factors was then fabricated by varying each factor within the level of the other factors (Table 3.1). The natural measurements were encoded in dimensionless co-ordinates as -1, 0 and +1 for the minimum, median and maximum level, respectively. Other factors that might affect the responses, such as the amount of catalyst and the reactor volume, were kept constant throughout the experiments. All tests were run in triplicate and the data is shown as the mean value. The experiments were run completely in random mode in order to minimize any errors. The Design-Expert 7.0 software package (Stat Ease Inc. Minneapolis, USA) was used to analyze the results at a 95% confidence interval, using analysis of variance (ANOVA) and percentage of contribution of each important factor to the responses. Statistical significance of the differences in means was accepted at the $p < 0.05$ level.

After screening the 4 factors for any significant effect upon each response with the factorial design, a face-centered central composite design (FCCCD-RSM) was design as shown in Table 3.2. This model was adopted in order to optimize the conditions for methanol conversion with a minimal CO selectivity and high H₂ yield in MSR unit. To elucidate the adequacy of the RSM results, normal probability plots of residues and the residues with estimated responses were then employed. To verify the models, four more experiments were randomly run, reporting the concurrence between the experimental data and the estimated one in terms of the error percentage. Additionally, to test the sensitivity of the models, two more experiments, which were outside the given level range, were performed.

Table 3.1 Experimental variable over $\text{Cu}_x\text{Ce}_y\text{Mg}_z/\text{Al}$ in coded and actual unit for a full 2^4 design with five central points in the standard order from 1 to 21

Factors	Variables	Unit	Low (-1)	Medium (0)	High (1)
A	Temperature	°C	200	225	250
B	S/C ratio	-	1.50	1.75	2.00
C	Mg/(Ce+Mg)	wt%	0.00	16.67	33.33
D	Cu content	wt%	30	40	50

Standard order	Run order	A	B	C	D
1	3	-1	-1	-1	-1
2	10	+1	-1	-1	-1
3	12	-1	+1	-1	-1
4	2	+1	+1	-1	-1
5	16	-1	-1	+1	-1
6	11	+1	-1	+1	-1
7	18	-1	+1	+1	-1
8	7	+1	+1	+1	-1
9	1	-1	-1	-1	+1
10	17	+1	-1	-1	+1
11	8	-1	+1	-1	+1
12	13	+1	+1	-1	+1
13	6	-1	-1	+1	+1
14	14	+1	-1	+1	+1
15	15	-1	+1	+1	+1
16	9	+1	+1	+1	+1
17	19	0	0	0	0
18	21	0	0	0	0
19	5	0	0	0	0
20	4	0	0	0	0
21	20	0	0	0	0

Table 3.2 Experimental variable for FCCCD-RSM

Factors	Variables	Unit	Low (-1)	Medium (0)	High (1)
A	Temperature	°C	200	225	250
B	S/C ratio	-	1.50	1.75	2.00
C	Mg/(Ce+Mg)	wt%	0.00	16.67	33.33
D	Cu content	wt%	30	40	50

Standard order	Run order	A	B	C	D
1	25	-1	-1	-1	-1
2	2	+1	-1	-1	-1
3	15	-1	+1	-1	-1
4	29	+1	+1	-1	-1
5	22	-1	-1	+1	-1
6	10	+1	-1	+1	-1
7	6	-1	+1	+1	-1
8	13	+1	+1	+1	-1
9	14	-1	-1	-1	+1
10	21	+1	-1	-1	+1
11	12	-1	+1	-1	+1
12	9	+1	+1	-1	+1
13	5	-1	-1	+1	+1
14	11	+1	-1	+1	+1
15	4	-1	+1	+1	+1
16	7	+1	+1	+1	+1
17	27	-1	0	0	0
18	3	+1	0	0	0
19	19	0	-1	0	0
20	1	0	+1	0	0
21	17	0	0	-1	0
22	18	0	0	+1	0

Table 3.2 (cont.)

Standard order	Run order	A	B	C	D
23	24	0	0	0	-1
24	26	0	0	0	+1
25	20	0	0	0	0
26	23	0	0	0	0
27	8	0	0	0	0
28	16	0	0	0	0
29	28	0	0	0	0

3.3.2 Preferential oxidation (PROX) of CO unit

In PROX unit, the procedures are presented as the following topics: catalysts preparation, catalysts characterization and catalytic activity measurement. After that, statistical design of the experiments over the effective catalysts was then mentioned in order to evaluate the importance of chosen factors. Finally, the optimum conditions for PROX over the effective catalysts were determined by using response surface methodology (RSM)

3.3.2.1 Catalyst preparation

- Support preparation

Synthesized ceria support was prepared by hydrothermal method. The support was obtained by dissolved 1.2 g of $\text{Ce}(\text{NO}_3)_3 \cdot 6\text{H}_2\text{O}$ in 80 mL of 15M NaOH solution in 100 mL glass vial with stirring vigorously at 70 °C for 1 h. Next, the viscous solution was aged in oven at 70 °C for 25 h and then cooled down to room temperature. After that, the white suspension was removed by filtration, washed with

deionized water until the filtrate pH was 7 and dried at 110 °C overnight. The suspension was change from white to pale yellow after calcined at 400 °C for 5 h at a heating rate of 10 °C min⁻¹ under a static air atmosphere to remove the remaining impurities. For Mg-modified ceria support, the level of MgO was varied from 5-20 wt% of total support. Mg(NO₃)₂·6H₂O were mixed Ce(NO₃)₃·6H₂O at the designed CeO₂: MgO weight ratios: 100:0, 95:5 and 80:20, respectively before dissolved by NaOH solution.

- Supported catalysts preparation

CuO/CeO₂ catalysts were obtained by conventional impregnation method. Copper solution were impregnated on ceria support with the CuO level varied from 2.5-10 wt%. The catalysts were dried at 110 °C overnight and then calcined at 500 °C for 5 h at a heating rate of 10 °C min⁻¹ under a static air atmosphere to remove the remaining impurities. The catalyst was designated as xwt%CuO/Ce_yMg_z, where x is the loading levels (wt%) of CuO, while y and z are the level of CeO₂ and MgO in support, respectively. For example, the 5wt%CuO/Ce_{0.95}Mg_{0.05} catalyst was composed of 5 wt% CuO on the support which has 95 wt% CeO₂ and 5 wt% MgO.

3.3.2.2 Catalysts characterization

- *Field Emission Scanning Electron Microscopy (FESEM)*: the particle morphology of catalysts was carried out in a JSM-7610F instrument, an ultra-high resolution Schottky Field Emission Scanning Electron Microscope, equipped with an energy dispersive X-ray analyzer (EDX). The FESEM with 2 Secondary electrons (upper and lower) and 1 backscattered electrons detectors provide high resolution at 15 kV

and high magnification x20,000 to x100,000. The catalysts were dried overnight and coated with gold before analyze.

- *X-ray diffraction (XRD)*: The XRD patterns of the samples were taken with a Bruker D8 Advance X-Ray diffractometer, operated at 40 kV and 40 mA using monochromatic Cu K_{α} radiation with a wavelength of 0.154 nm. The XRD patterns were recorded over a scanning angle (2θ) range from 5–80° at a rate of 5° min⁻¹. The analysis was performed to examine the crystalline structure and average copper particle size. The particle sizes were calculated by the Debye-Scherrer equation at the diffraction peak of Cu (111).

- *Brunauer-Emmett-Teller (BET)*: the BET method was used to determine the specific surface area, pore volume and pore diameter of the catalysts. Nitrogen (N₂) adsorption-desorption isotherms were measured at -196 °C using Micromeritics ASAP 2020 equipment. Prior to analysis, the samples were degassed at 250 °C for 1 h and increased to 300 °C for 1 h. The specific surface area of the samples was determined according to the BET method.

- *Temperature-programmed reduction (TPR)*: The reduction temperature of the catalysts was evaluated by H₂-TPR analysis. The catalysts were pretreated in a U-shaped quartz reactor under an argon (Ar) flow rate of 40 mL min⁻¹ at 500 °C for 1 h at a heating rate of 10 °C min⁻¹. After this pretreatment, the catalysts were cooled to room temperature. A reducing gas of 10% (v/v) H₂ in Ar was then switched to the reactor at a flow rate of 40 mL min⁻¹ and the catalysts were heated

up to 500 °C at a rate of 10 °C min⁻¹. A thermal conductivity detector (TCD) was employed to determine the amount of H₂ uptake.

3.3.2.3 Catalytic activity measurement

Catalytic tests were performed by sandwich-packing 0.1 g of sample between two layers of quartz wool in a 6-mm internal diameter U shaped tube reactor. The catalyst was pretreated in situ with 40 mL min⁻¹ of pure He at 300 °C for 1 h to remove remaining impurities before measure the catalytic performance. The water was fed into the vaporizer by a syringe pump while He was used as a carrier gas. H₂, CO, CO₂, O₂ and H₂O were pre-mixed at a given ratio with He balanced in a mixing chamber and then feed into a reactor at a rate of 100 mL min⁻¹. The composition of H₂, CO₂ and H₂O were fixed at 40%v/v, 20%v/v and 15%v/v, respectively while CO and O₂ were varied with different oxygen excess factor from 0.75 to 2. The gas mixture was then directed into reactor at reaction temperatures between 40–300 °C. The reaction temperature was controlled by a temperature controller and was measured by a thermocouple placed in the center of the catalyst bed. The gaseous influent and effluent were passed through a water-trapping unit and then analyzed by on-line gas chromatography (GC-2014; Shimadzu Scientific Instruments) equipped with a TCD and using He as the carrier gas.

The catalytic performances were expressed in terms of the CO conversion level (%) and CO₂ selectivity (%), respectively, calculated from Eqs. (3.4) –

(3.5), respectively:

$$\text{CO conversion (\%)} = \{([\text{CO}]_{\text{in}} - [\text{CO}]_{\text{out}}) \times 100 / [\text{CO}]_{\text{in}}\} \quad (3.4)$$

$$\text{CO}_2 \text{ selectivity (\%)} = \{0.5 \times ([\text{CO}]_{\text{in}} - [\text{CO}]_{\text{out}}) \times 100 / ([\text{O}_2]_{\text{in}} - [\text{O}_2]_{\text{out}})\} \quad (3.5)$$

where $[\text{CO}]_{\text{in}}$ and $[\text{O}_2]_{\text{in}}$ is the molar flow rate of CO and O₂ in the feed stream (mol min⁻¹), and $[\text{CO}]_{\text{out}}$ and $[\text{O}_2]_{\text{out}}$ are the molar flow rate of CO and O₂ in the effluent, respectively.

To study the catalyst stability, the catalyst that expressed the highest performance at the optimal condition was selected to test its stability over a 48-h reaction period in a presence of CO₂ and H₂O.

3.3.2.4 Statistical design of experiments for optimization

Since univariate analysis informs only a behavior of the catalytic performance when changing one factor at a time, neither any crucial factors on the performance nor optimal conditions are identified. Therefore, a full 2⁴ factorial design with complete randomization was adopted in order to optimize the conditions for complete CO conversion to yield a H₂-rich stream with high selectivity to CO oxidation. The four main factors chosen were the operating temperature (°C), level of CO (%v/v), level of O₂ (%v/v) and amount of catalysts (g), noted as factors *A*, *B*, *C* and *D*, respectively. Two responses, in terms of the CO conversion level and CO selectivity,

respectively, were considered to optimize the condition for the PROX catalytic performance. A matrix of the four factors was then fabricated by varying each factor within the level of the other factors (Table 3.3). The natural measurements were encoded in dimensionless co-ordinates as -1, 0 and +1 for the minimum, median and maximum level, respectively. Other factors that might affect the responses, such as the volume flow rate and the reactor volume, were kept constant throughout the experiments. All tests were run in triplicate and the data is shown as the mean value. The experiments were run completely in random mode in order to minimize any errors. The Design-Expert 7.0 software package (Stat Ease Inc. Minneapolis, USA) was used to analyze the results at a 95% confidence interval, using analysis of variance (ANOVA) and percentage of contribution of each important factor to the responses. Statistical significance of the differences in means was accepted at the $p < 0.05$ level.

After screening the 4 factors for any significant effect upon each response with the factorial design, a Box–Behnken design was design as shown in Table 3.4. This model was adopted in order to optimize the conditions for CO conversion with a highest CO selectivity in PROX unit. To elucidate the adequacy of the PROX results, normal probability plots of residues and the residues with estimated responses were then employed. To verify the models, four more experiments were randomly run, reporting the concurrence between the experimental data and the estimated one in terms of the error percentage. Additionally, to test the sensitivity of the models, two more experiments, which were outside the given level range, were performed.

Table 3.3 Experimental variable over 5wt%CuO/Ce_{0.95}Mg_{0.05} in coded and actual unit for a full 2⁴ design with five central points in the standard order from 1 to 21

Factors	Variables	Unit	Low (-1)	Medium (0)	High (1)
A	Temperature	°C	160	180	200
B	Level of CO	%	0.50	1.00	1.50
C	Level of O ₂	%	0.50	0.75	1.00
D	Catalyst wt.	g	0.10	0.15	0.20

Standard order	Run order	A	B	C	D
1	5	-1	-1	-1	-1
2	12	+1	-1	-1	-1
3	9	-1	+1	-1	-1
4	7	+1	+1	-1	-1
5	1	-1	-1	+1	-1
6	6	+1	-1	+1	-1
7	2	-1	+1	+1	-1
8	21	+1	+1	+1	-1
9	11	-1	-1	-1	+1
10	17	+1	-1	-1	+1
11	3	-1	+1	-1	+1
12	18	+1	+1	-1	+1
13	19	-1	-1	+1	+1
14	13	+1	-1	+1	+1
15	14	-1	+1	+1	+1
16	16	+1	+1	+1	+1
17	10	0	0	0	0
18	8	0	0	0	0
19	15	0	0	0	0
20	4	0	0	0	0
21	20	0	0	0	0

Table 3.4 Experimental variable for Box–Behnken design

Factors	Variables	Unit	Low (-1)	Medium (0)	High (1)
A	Temperature	°C	160	180	200
B	Level of CO	%	0.50	1.00	1.50
C	Level of O ₂	%	0.50	0.75	1.00
D	Catalyst wt.	g	0.10	0.15	0.20

Standard order	Run order	A	B	C	D
1	16	-1	-1	-1	-1
2	7	+1	-1	-1	-1
3	12	-1	+1	-1	-1
4	4	+1	+1	-1	-1
5	15	-1	-1	+1	-1
6	6	+1	-1	+1	-1
7	8	-1	+1	+1	-1
8	10	+1	+1	+1	-1
9	11	-1	-1	-1	+1
10	18	+1	-1	-1	+1
11	9	-1	+1	-1	+1
12	26	+1	+1	-1	+1
13	21	-1	-1	+1	+1
14	19	+1	-1	+1	+1
15	27	-1	+1	+1	+1
16	20	+1	+1	+1	+1
17	1	-1	0	0	0
18	2	+1	0	0	0
19	22	0	-1	0	0
20	25	0	+1	0	0
21	14	0	0	-1	0
22	13	0	0	+1	0

Table 3.4 (cont.)

Standard order	Run order	A	B	C	D
23	3	0	0	0	-1
24	24	0	0	0	+1
25	17	0	0	0	0
26	29	0	0	0	0
27	5	0	0	0	0
28	23	0	0	0	0
29	28	0	0	0	0

3.3.3 Integration of MSR unit and PROX unit

The effective catalysts in each unit were carried out for hydrogen production via integration of MSR unit and PROX unit. The MSR unit was operated at the optimum condition from section 3.3.1 while PROX unit was used to achieve pure hydrogen-rich stream by performed the optimum condition which obtained from section 3.3.2.

CHAPTER IV

METHANOL STEAM REFORMING UNIT

4.1 Catalyst characterization

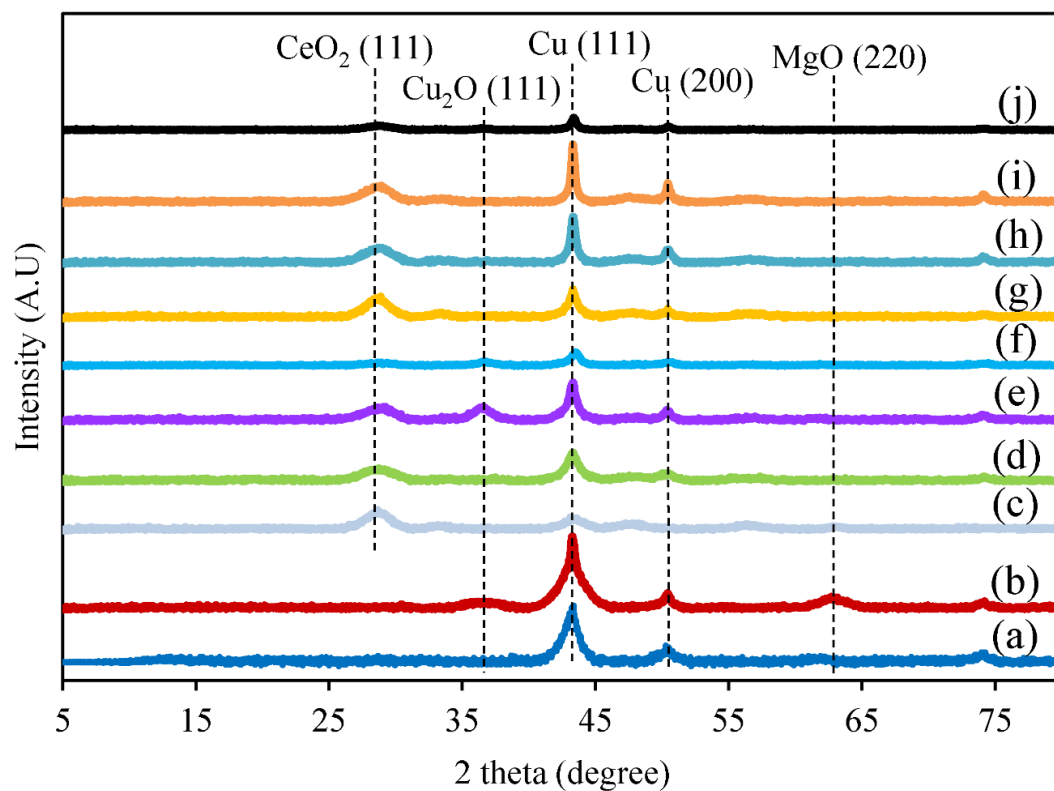


Figure 4.1 Representative (of 10 samples) XRD patterns of the copper-based catalysts after H₂ pretreatment at 300 °C for 1 h. Shown are the fresh (a) Cu_{0.3}/Al, (b) Cu_{0.3}Mg_{0.3}/Al, (c) Cu_{0.2}Ce_{0.15}Mg_{0.15}/Al, (d) Cu_{0.3}Ce_{0.15}Mg_{0.15}/Al, (e) Cu_{0.4}Ce_{0.15}Mg_{0.15}/Al, (f) Cu_{0.5}Ce_{0.15}Mg_{0.15}/Al, (g) Cu_{0.3}Ce_{0.2}Mg_{0.1}/Al, (h) Cu_{0.3}Ce_{0.25}Mg_{0.05}/Al and (i) Cu_{0.3}Ce_{0.3}/Al catalysts, plus (j) the spent Cu_{0.5}Ce_{0.25}Mg_{0.05}/Al catalyst after MSR at 250 °C for 72 h.

The XRD patterns for the freshly synthesized Cu-based catalysts are shown in Fig. 4.1a–i, while the pattern for the spent $\text{Cu}_{0.5}\text{Ce}_{0.25}\text{Mg}_{0.05}/\text{Al}$ catalyst is shown in Fig. 4.1j. Before measuring the catalytic activities, 10% (v/v) H_2 in He was routed through the oxide sample placed in the reactor at a heating rate of $10\text{ }^\circ\text{C min}^{-1}$. The oxygen in the sample reacted with the H_2 to form water which was removed from the system. Simultaneously CuO was reduced to an intermediate or suboxide (Cu_2O) and became metallic Cu^0 . This was a sequential pathway for a change in oxidation state of copper from “+2” to “0” [48]. Each pattern in Fig. 4.1 revealed the Cu species diffraction peaks at 43.1° and 50.3° , which corresponded to the crystalline planes of (111) and (200), respectively, in agreement with JCPDS File No. 04-0836. The Cu intensity peaks at the (111) and (200) planes were higher with increasing Cu loading levels from 20 wt% for $\text{Cu}_{0.2}\text{Ce}_{0.15}\text{Mg}_{0.15}/\text{Al}$ to 30 wt% for $\text{Cu}_{0.3}\text{Ce}_{0.15}\text{Mg}_{0.15}/\text{Al}$ and 40 wt% for $\text{Cu}_{0.4}\text{Ce}_{0.15}\text{Mg}_{0.15}/\text{Al}$, respectively (Fig. 4.1c–e). No peaks of Cu_2O were observed in the pattern of fresh catalysts with a Cu content of < 40 wt% (Fig. 4.1c,d), indicating that the copper species was reduced completely after the H_2 pretreatment [49] at $300\text{ }^\circ\text{C}$ for 1 h. When the relative fraction of Cu became dominant (> 40 wt%), the surface of oxide sample was coated by metallic copper. Probably some H_2 could not penetrate the lattice of the oxide. Once the removal of O was difficult due to the reduced Cu film coating on the sample, the diffraction peaks of metallic Cu and intermediate became weaker, as shown in Fig. 4.1f. There was no peak that represented any other metal form, revealing that the other metal component was still in the metal oxide form. Even though each

catalyst contained Al_2O_3 , the peaks that corresponded to aluminium oxide (JCPDS File No. 29-0063) were not observed due to its amorphous phase [36, 50, 51]. When adding MgO to obtain a mono- (Fig. 4.1b) or bi-promoter (Fig. 4.1c–h) on the copper-based catalysts, the peak of MgO at 62.3° (JCPDS File No. 89-7746), which represented the crystalline planes of (220), was observed only in the XRD pattern of catalysts with a magnesium content of 30 wt% and 15 wt%. When the magnesium content was less than 15 wt%, no peak of MgO was noticed, which is probably due to the MgO being highly dispersed on the catalysts. In addition, the pattern of the ceria mono-promoter catalyst ($\text{Cu}_{0.3}\text{Ce}_{0.3}/\text{Al}$) (Fig. 4.1i) showed the peaks of ceria at 28.5° (JCPDS File No. 34-0394), which corresponded to the crystalline planes of (111). For Ce-Mg bi-promoter catalysts, the peak of ceria was shifted to the right due to the distortion of the ceria matrix structure by the Mg^{2+} ions. The CeO_2 intensity peaks at the (111) planes were higher when increasing the cerium loading from 15–30 wt%. From Fig. 1j, the XRD patterns of the spent $\text{Cu}_{0.5}\text{Ce}_{0.25}\text{Mg}_{0.05}/\text{Al}$ catalyst after MSR at 250°C for 72 h revealed copper peaks at 43.1° and 50.3° , which corresponded to the crystalline planes of (111) and (200), respectively, in agreement with JCPDS File No. 04-0836. The copper oxide peak at 35.9° (Cu_2O , JCPDS File No. 05-0667) was observed in the pattern of the spent catalyst.

Table 4.1 Textural properties of the copper-based catalysts.

Sample	Mg/(Ce+Mg) (wt%)	A_{BET} ($\text{m}^2 \text{g}^{-1}$)	V_{pore} ($\text{cm}^3 \text{g}^{-1}$)	D_{pore} (Å)	D_{Cu} (nm)	Lattice parameter of ceria (111) (nm)
$\text{Cu}_{0.3}\text{Ce}_{0.3}/\text{Al}$	0	80.3	0.137	68.39	24	0.5339
$\text{Cu}_{0.3}\text{Ce}_{0.25}\text{Mg}_{0.05}/\text{Al}$	16.67	101.8	0.151	62.02	18	0.5325
$\text{Cu}_{0.3}\text{Ce}_{0.2}\text{Mg}_{0.1}/\text{Al}$	33.33	103.3	0.158	58.44	13	0.5350
$\text{Cu}_{0.3}\text{Ce}_{0.15}\text{Mg}_{0.15}/\text{Al}$	50	113.8	0.162	56.96	8	0.5346
$\text{Cu}_{0.2}\text{Ce}_{0.15}\text{Mg}_{0.15}/\text{Al}$	50	107.6	0.150	55.99	4	0.5346
$\text{Cu}_{0.4}\text{Ce}_{0.15}\text{Mg}_{0.15}/\text{Al}$	50	109.7	0.163	59.68	12	0.5346
$\text{Cu}_{0.5}\text{Ce}_{0.15}\text{Mg}_{0.15}/\text{Al}$	50	102.8	0.173	67.64	10	0.5346
$\text{Cu}_{0.3}\text{Mg}_{0.3}/\text{Al}$	100	101.5	0.161	63.72	9	-
$\text{Cu}_{0.3}/\text{Al}$	-	116.7	0.193	66.12	9	-
Alumina	-	299.4	0.261	34.89	-	-
* $\text{Cu}_{0.5}\text{Ce}_{0.25}\text{Mg}_{0.05}/\text{Al}$	16.67	102.9	0.174	67.37	11	0.5325

Note: *Spent catalyst after MSR at 250 °C for 72 h

Due to the activity of copper in MSR, the Scherrer equation was used to evaluate the copper crystallite size in order to reflect the level of sintering of the copper, and the results are summarized in Table 4.1. The $\text{Cu}_{0.3}/\text{Al}$ catalyst had a copper crystallite size of around 9 nm, while it increased about 2.67-fold in the $\text{Cu}_{0.3}\text{Ce}_{0.3}/\text{Al}$ catalyst but was still the same in the $\text{Cu}_{0.3}\text{Mg}_{0.3}/\text{Al}$ catalyst as in the $\text{Cu}_{0.3}/\text{Al}$ catalyst. This revealed that the two different types of mono-promoters (Ce- or Mg-) in the catalyst had an influence on the copper crystallite size. At a constant copper content of 30 wt% and a given total weight of Ce+Mg of 30 wt%, the copper crystallite size

was decreased from 24 nm to 8 nm when increasing the Mg/(Ce+Mg) from 0 to 50 wt%, which is likely to be because the presence of MgO improved the dispersion of copper [52, 53]. Due to the oxygen storage property of ceria, Ce⁴⁺ ions were surrounded by eight equivalent O²⁻ ions forming the corner of a cube, representing a ceria lattice parameter of 0.541 nm. The Ce⁴⁺ ions with an ionic radius of 0.87 Å in a six-fold coordination were possibly substituted by the smaller ionic radius Cu²⁺/Mg²⁺ ions (ionic radius of 0.57 Å), giving Cu²⁺/Mg²⁺ in the octahedral sites of CeO₂ with a tetragonal distortion [15, 38, 40, 44]. When inducing a distortion of ceria in order to promote the ability to transfer bulk oxygen [54], deflection in the lattice was introduced, as shown in Table 4.1. The CeO₂ unit cell parameter in the catalyst with Mg/(Ce+Mg) at 16.67 wt% (Cu_{0.3}Ce_{0.25}Mg_{0.05}/Al fresh catalyst and Cu_{0.5}Ce_{0.25}Mg_{0.05}/Al spent catalyst) was around 0.5325 nm, which was smaller than in the other samples. This reduction in the lattice parameters could be attributed to oxygen vacancies that enhance its catalytic performance [38]. This was also confirmed by the results of XRD patterns (Fig. 4.1). At 50 wt% Mg/(Ce+Mg), the copper particle size increased from 4 nm to 12 nm when increasing the amount of copper loading from 20 to 40 wt% and overall the copper particle size of copper depended on the copper content and the Mg/(Ce+Mg) wt% (Table 4.1).

The textural properties of the copper-based catalysts are summarized in Table 4.1. The specific BET surface areas (A_{BET}) of all samples were in range of 80–116.7 m²

g^{-1} . The A_{BET} of the $\text{Cu}_{0.3}/\text{Al}$ catalyst was about $116.7 \text{ m}^2 \text{ g}^{-1}$, and for the mono-promoter catalysts this decreased to 101.5 and $80.3 \text{ m}^2 \text{ g}^{-1}$ when adding MgO or ceria, respectively, to the $\text{Cu}_{0.3}/\text{Al}$ catalyst. For the bi-promoter catalysts, at a constant copper content of 30 wt%, the A_{BET} was increased from $101.8 \text{ m}^2 \text{ g}^{-1}$ to $113.8 \text{ m}^2 \text{ g}^{-1}$ when increasing the $\text{Mg}/(\text{Ce}+\text{Mg})$ wt% from 16.67 to 50 wt%. Meanwhile, increasing the $\text{Mg}/(\text{Ce}+\text{Mg})$ wt% caused the pore volume (V_{pore}) to increase from 0.151 to $0.162 \text{ cm}^3 \text{ g}^{-1}$, while the pore diameter (D_{pore}) was decreased from 62.02 to 56.96 \AA . This suggested that the catalyst samples had a larger amount of smaller pores on the surface, presumably since MgO inhibited copper agglomeration and improved the dispersion of copper particles [52]. When increasing the copper content from 20 to 50 wt%, the A_{BET} was decreased from 107.6 to $102.8 \text{ m}^2 \text{ g}^{-1}$, while the D_{pore} increased from 55.99 to 67.64 \AA . Here, some copper might have filled in the minor pores of the support.

The H_2 -TPR profiles of the copper-based catalysts are shown in Fig 4.2, where only the TPR profiles of copper species were detected within $500 \text{ }^\circ\text{C}$. The profile of the $\text{Cu}_{0.3}/\text{Al}$ catalyst had three broad peaks with the center at 164, 187 and $222 \text{ }^\circ\text{C}$, respectively, which represent isolated copper ions (β , $135\text{--}180 \text{ }^\circ\text{C}$), large clusters of copper species (γ , $180\text{--}220 \text{ }^\circ\text{C}$) and bulk copper species (δ , $220\text{--}260 \text{ }^\circ\text{C}$), respectively. For the $\text{Cu}_{0.3}\text{Mg}_{0.3}/\text{Al}$ mono-promoter catalyst, the reduction temperature range was shifted to a lower temperature of $125\text{--}175 \text{ }^\circ\text{C}$ with one major peak at $146 \text{ }^\circ\text{C}$, which was attributed to isolated copper ions, and one minor peak at $178 \text{ }^\circ\text{C}$, which

represented large clusters of copper species. No bulk copper species were observed in the profile of the $\text{Cu}_{0.3}\text{Mg}_{0.3}/\text{Al}$ catalyst, presumably due to the role of MgO in the dispersion of copper. For the $\text{Cu}_{0.3}\text{Ce}_{0.3}/\text{Al}$ mono-promoter catalyst, the copper species were in four forms within the temperature range of 100–260 °C, comprised of two major peaks at around 170 °C and 200 °C, which were isolated copper ions and large clusters of copper species, respectively, and two minor peaks at 130 °C and 235 °C, which were attributed to the reduction of highly dispersed copper species (α , 100 °C–135 °C) and bulk copper species (δ), respectively [36, 49, 55]. For the bi-promoter catalysts at a constant 30 wt% copper loading, a change in the reduction behavior was found when varying the Mg/(Ce+Mg) wt%. The reduction peaks were shifted to a lower temperature range of 100–220 °C. Most copper species were in the form of isolated copper ions and no form of bulk copper species was detected. These profiles also confirmed the role of MgO in the dispersion of copper. Due to the shift in the reduction temperature to a lower level, a higher catalytic activity was achieved [56-58]. Therefore, the performance of the copper-based catalysts was enhanced with the bi-promoter. When increasing copper content from 20 to 40 wt% at constant Mg/(Ce+Mg) wt%, the reduction temperature was shifted to a lower temperature. However, further raising the copper content to 50 wt% shifted the reduction temperature range to a higher temperature. There was not much change in the profiles except for an increase in the H_2 consumption rate.

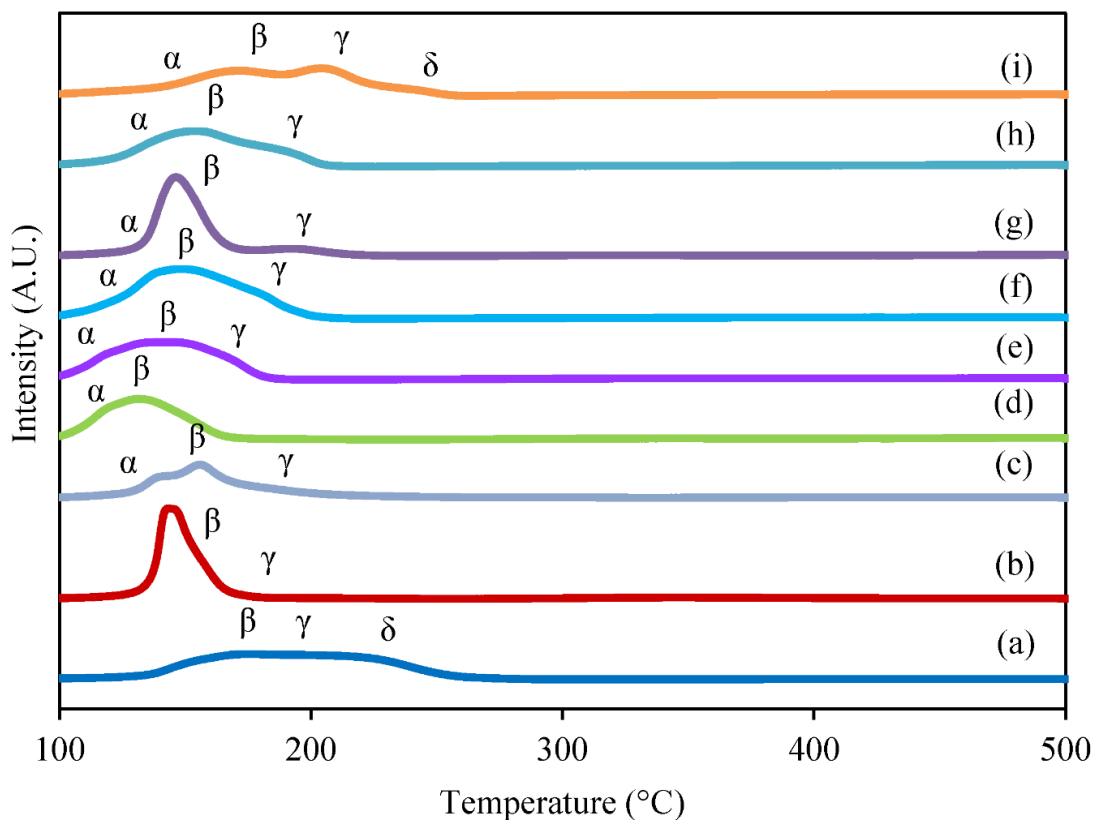


Figure 4.2 Representative (of 9 samples) H_2 -TPR profiles of the copper-based catalysts: (a) $Cu_{0.3}/Al$, (b) $Cu_{0.3}Mg_{0.3}/Al$, (c) $Cu_{0.2}Ce_{0.15}Mg_{0.15}/Al$, (d) $Cu_{0.3}Ce_{0.15}Mg_{0.15}/Al$, (e) $Cu_{0.4}Ce_{0.15}Mg_{0.15}/Al$, (f) $Cu_{0.5}Ce_{0.15}Mg_{0.15}/Al$, (g) $Cu_{0.3}Ce_{0.2}Mg_{0.1}/Al$, (h) $Cu_{0.3}Ce_{0.25}Mg_{0.05}/Al$ and (i) $Cu_{0.3}Ce_{0.3}/Al$.

The morphologies presented in FESEM micrograph of the synthesized copper-based catalysts with various ratios of Ce:Mg promoter at Cu loading of 30 wt% were shown in Fig. 4.3. The $Cu_{0.30}/Al$ catalyst without a promoter (Fig. 4.3a) showed the fractural surface materials. For the $Cu_{0.3}Ce_{0.3}/Al$ mono-promoter catalyst (Fig. 4.3b), it could be observed the surface of the aggregated spherical particles [59, 60] or packed crystallites [61]. Meanwhile FESEM image of the $Cu_{0.3}Mg_{0.3}/Al$ mono-promoter catalyst

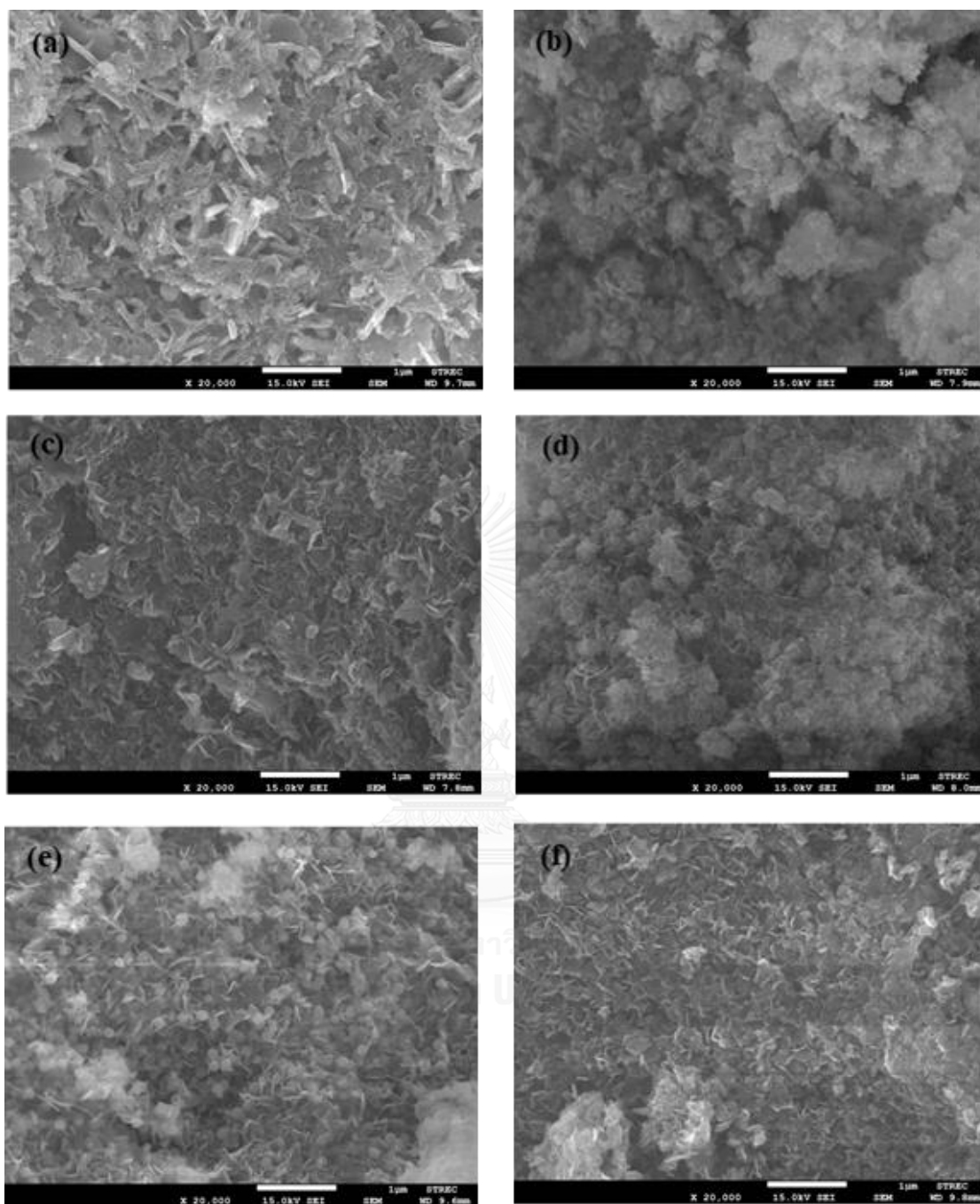


Figure 4.3 Representative FESEM images (20 k magnification; scale bar = 1 μm) of (a) Cu_{0.30}/Al, (b) Cu_{0.30}Ce_{0.30}/Al, (c) Cu_{0.30}Mg_{0.30}/Al, (d) Cu_{0.30}Ce_{0.25}Mg_{0.05}/Al, (e) Cu_{0.30}Ce_{0.20}Mg_{0.10}/Al and (f) Cu_{0.30}Ce_{0.15}Mg_{0.15}/Al catalysts.

(Fig. 4.3c) represented the surface of flakes plate-like materials [62]. FESEM images of the bi-promoter catalysts with various Ce:Mg ratios were shown in Fig. 4.4d-f. When adding 5 wt% Mg to the ceria mono-promoter catalyst to form the $\text{Cu}_{0.30}\text{Ce}_{0.25}\text{Mg}_{0.05}/\text{Al}$ bi-promoter catalysts, the formation of small-sized aggregated spherical particles combined with flakes plate-like structure was observed as shown in Fig. 4.4d. Further adding more amount of magnesium to obtain the $\text{Cu}_{0.30}\text{Ce}_{0.20}\text{Mg}_{0.10}/\text{Al}$ catalysts, it could be noticeable in Fig. 4.4e that the spherical particles combined with flakes plate-like structure was still found. The dispersion of those particles was in random arrangement. Further adding more amount of magnesium to obtain the $\text{Cu}_{0.30}\text{Ce}_{0.15}\text{Mg}_{0.15}/\text{Al}$ catalysts, the spherical particles were not observed in the FESEM image as shown in Fig. 4.4f. It could be observed only the surface of flakes plate-like materials. Any separated CeO_2 fragment particles can be hardly seen. This indicates that CeO_2 phase disperses well on MgO particles [63].

4.2 Catalytic activities test

4.2.1 Level of copper content

The reaction effluent mainly contained H_2 , CO and CO_2 , with no methane being detected. The catalytic activities for MSR over the series of copper based-catalysts were evaluated in terms of the methanol conversion level (%), CO selectivity (%) and

H₂ yield (%). The performance of copper-based catalysts with increasing copper loading levels at 50 wt% Mg/(Ce+Mg) is shown in Fig. 4.4a–c. When increasing the temperature, the methanol conversion level increased to a complete conversion, while the CO selectivity decreased to a minimal level. With further increases in the temperature, the CO selectivity increased as did the H₂ yield. It is supposed that overall the MSR is comprised of the sequential reactions of MD and the WGS reaction of CO. From the stoichiometry, one mole of methanol is decomposed to one mole of CO and two moles of H₂. The CO then reacts with H₂O via the WGS reaction of CO to produce CO₂ and H₂. Raising the temperature drives forward the MD and WGS of CO reactions, resulting in the complete methanol conversion and higher H₂ yield. The CO selectivity was initially decreased to a minimal value with increasing temperatures, but then increased significantly at higher temperatures, which likely reflects that the rate of the WGS reaction was lower than that of the MD. At temperatures above 350 °C, the reverse WGS reaction occurred and resulted in a lower H₂ yield with a higher CO selectivity [54, 64].

At temperatures of < 275 °C, increasing the level of copper from 20 to 40 wt% (Cu_{0.2}Ce_{0.15}Mg_{0.15}/Al, Cu_{0.3}Ce_{0.15}Mg_{0.15}/Al and Cu_{0.4}Ce_{0.15}Mg_{0.15}/Al, respectively) increased the methanol conversion level and H₂ yield and decreased the CO selectivity. At 300 °C, the Cu_{0.3}Ce_{0.15}Mg_{0.15}/Al catalyst expressed a lower CO selectivity and higher H₂ yield than the other catalysts, although complete methanol conversion was still achieved

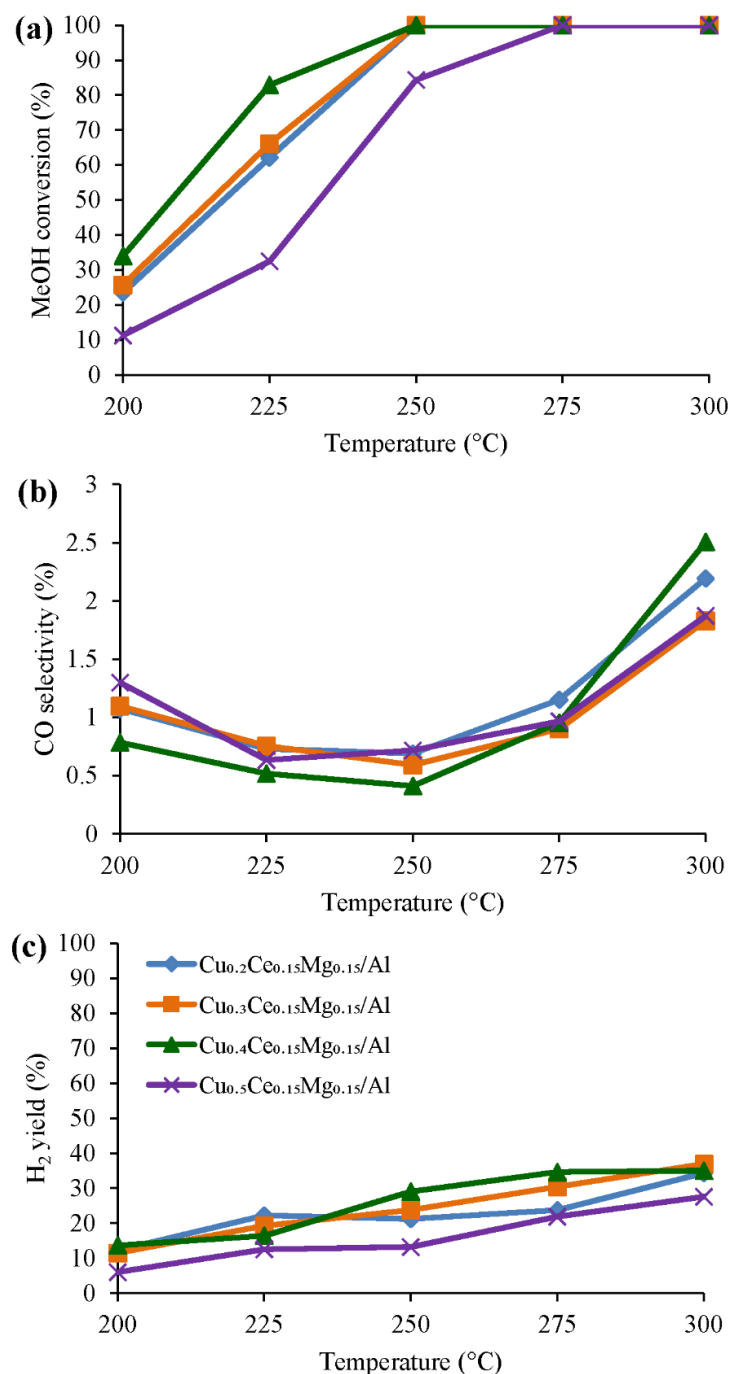


Figure 4.4 The MSR catalytic performances in terms of the (a) methanol conversion level, (b) CO selectivity and (c) H_2 yield for the copper based catalysts with different copper loading levels; $\text{Cu}_{0.2}\text{Ce}_{0.15}\text{Mg}_{0.15}/\text{Al}$ (\blacklozenge), $\text{Cu}_{0.3}\text{Ce}_{0.15}\text{Mg}_{0.15}/\text{Al}$ (\blacksquare), $\text{Cu}_{0.4}\text{Ce}_{0.15}\text{Mg}_{0.15}/\text{Al}$ (\blacktriangle) and $\text{Cu}_{0.5}\text{Ce}_{0.15}\text{Mg}_{0.15}/\text{Al}$ (\blackcross). All reactions had an S/C of 1.5, feed rate of 1 mL h^{-1} and 0.1 g of catalyst. Data are shown as the mean, derived from three replicates.

at 250 °C. Further increasing the copper content to 50 wt% decreased the methanol conversion level and H₂ yield and increased the CO selectivity, with the complete methanol conversion shifted up to 275 °C for this catalyst. From the H₂-TPR analysis (Fig. 4.2), catalysts with a copper content of 40 wt% and Mg/(Ce+Mg) of 50 wt% expressed a lower reduction temperature, giving a higher catalytic performance. Moreover, it could be seen from the XRD results that the copper species was completely reduced to metallic Cu⁰ when the Cu content was less than 40 wt%. The suboxide intermediate was found with a Cu loading level of up to 50 wt%. However, the Cu⁰ content of the 50 wt% Cu catalysts was less than that of the 20, 30 and 40 wt% ones (Fig. 4.1). The performance of the Cu_{0.4}Ce_{0.15}Mg_{0.15}/Al catalyst was higher than that of the other three (Cu_{0.3}Ce_{0.15}Mg_{0.15}/Al, Cu_{0.2}Ce_{0.15}Mg_{0.15}/Al and Cu_{0.5}Ce_{0.15}Mg_{0.15}/Al). Since the target of this work was to obtain a high yield of H₂ with a low CO content via MSR, the potential catalyst to approach this milestone should express a high methanol conversion level and H₂ yield with a low CO selectivity in the operating temperature range. This was best fitted by the Cu_{0.3}Ce_{0.15}Mg_{0.15}/Al catalyst that exhibited a complete methanol conversion and higher H₂ production and lower CO content when operating at 200–300 °C. Accordingly, a copper content of 30 wt% was chosen to investigate the effect of the Mg/(Ce+Mg) wt% on the catalytic performance in MSR.

4.2.2 Mono- and bi-promoter catalysts with various Mg/(Ce+Mg) wt%

At a 50 wt% Mg/(Ce+Mg), increasing the level of copper from 20 to 50 wt% increased the catalytic performance, due to the higher level of active sites. For a fixed copper content of 30 wt%, changing the Ce: Mg weight ratio also changed the catalytic performance. Overall, the $\text{Cu}_{0.3}\text{Ce}_{0.25}\text{Mg}_{0.05}/\text{Al}$ catalyst was a potential catalyst for H_2 production with a low CO selectivity via MSR, since it had a higher methanol conversion level and H_2 yield than the other catalysts over the whole range of operating temperatures. This is due to the synergistic action of ceria and MgO for producing a H_2 -rich stream with a low CO content. Accordingly, this bi-promoter catalyst is suggested for use in MSR.

The performances of each catalyst without and with promoters when holding the copper content at 30 wt% are shown in Fig. 4.5a–c. For the $\text{Cu}_{0.3}/\text{Al}$ catalysts, the methanol conversion level increased with increasing operating temperatures from 4.9% at 200 °C to 92.5% at 300 °C, while there was no trace of CO at 200–250 °C. However, CO was then increasingly formed at higher temperatures (0.52% at 275 °C and 0.98% at 300 °C). The low methanol conversion level at a lower temperature implied that the MD rate was quite low at lower temperatures. All the CO produced from the MD reacted with H_2O via the WGS reaction of CO to produce CO_2 and H_2 . Therefore, no CO was detected in the effluent gas. When increasing the temperature above 250 °C, more methanol was decomposed, resulting in a higher methanol

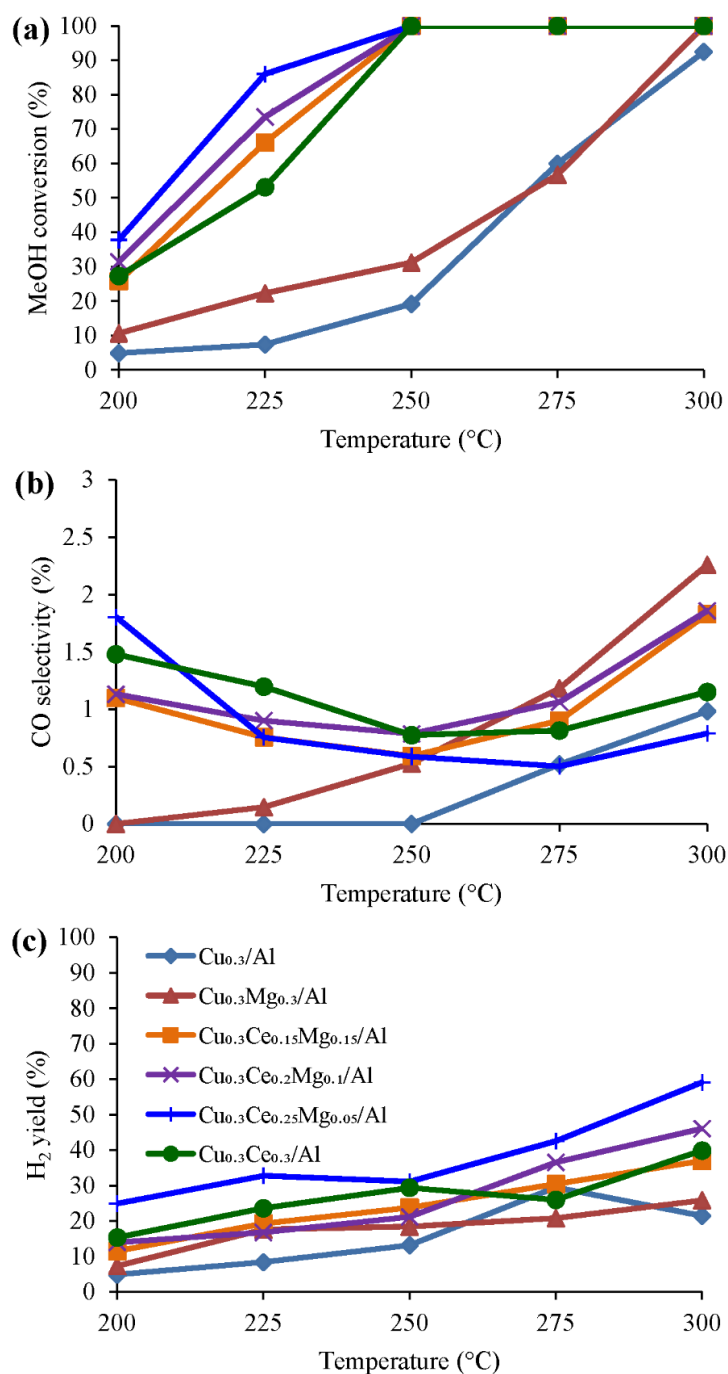


Figure 4.5 The MSR catalytic performances in terms of the (a) methanol conversion level, (b) CO selectivity and (c) H₂ yield for the copper based catalysts with different promoter ratios; Cu_{0.3}/Al (♦), Cu_{0.3}Mg_{0.3}/Al (▲), Cu_{0.3}Ce_{0.15}Mg_{0.15}/Al (■), Cu_{0.3}Ce_{0.2}Mg_{0.1}/Al (×), Cu_{0.3}Ce_{0.25}Mg_{0.05}/Al (+) and Cu_{0.3}Ce_{0.3}/Al (●). All reactions had an S/C of 1.5, feed rate of 1 mL h⁻¹ and 0.1 g of catalyst. Data are shown as the mean, derived from three replicates.

conversion level and H₂ yield. Some CO remained in the stream, as evidenced by the higher CO selectivity at higher temperatures.

The methanol conversion level and H₂ yield over the mono-promoter catalysts (Cu_{0.3}Mg_{0.3}/Al and Cu_{0.3}Ce_{0.3}/Al) was higher than that of the catalyst without a promoter (Cu_{0.3}/Al), and they increased with temperature. This is probably due to the higher dispersion level of copper species on the Cu_{0.3}Mg_{0.3}/Al catalyst (Table 4.1) and the strong interaction between copper and ceria [49, 52] for the Cu_{0.3}Ce_{0.3}/Al catalyst that led to lower reduction temperature (Fig. 4.2) and so to the enhanced catalytic activities. A complete methanol conversion level was achieved at temperatures above 250 and 300 °C for the Cu_{0.3}Ce_{0.3}/Al and Cu_{0.3}Mg_{0.3}/Al catalysts, respectively, with a higher H₂ yield being obtained with the Cu_{0.3}Ce_{0.3}/Al catalyst. The CO selectivity of the Cu_{0.3}Mg_{0.3}/Al catalyst was similar to that for the Cu_{0.3}/Al one. For the Cu_{0.3}Ce_{0.3}/Al catalyst, increasing the temperature decreased the CO selectivity to a minimum at 250 °C and then it increased at higher temperatures, presumably because the MgO enhanced the WGS reaction of CO, while ceria with its oxygen storage, enhanced the MD reaction. This resulted in a lower CO selectivity for the Cu_{0.3}Mg_{0.3}/Al catalyst and a higher methanol conversion level for the Cu_{0.3}Ce_{0.3}/Al catalyst. It is interesting to utilize their action for the MSR.

Thus, the performance of the Ce-Mg bi-promoter catalysts with various bi-promoter wt% were investigated, and the results are shown in Fig. 4.5 After adding

MgO to $\text{Cu}_{0.3}\text{Ce}_{0.3}/\text{Al}$ to obtain the bi-promoter catalyst, a higher methanol conversion level and H_2 yield was obtained than with the mono-promoter catalysts. Meanwhile, the CO selectivity over the bi-promoter catalysts was lower than that over the mono-promoter catalysts in the temperature range of 225–250 °C. This is possibly due to the lower size of the copper crystallites (Table 4.1), which were active in the MSR reaction. Increasing the temperature to 250 °C gave a complete methanol conversion with the Ce-Mg bi-promoter catalysts due to their lower reduction temperature (Fig. 4.2) and the oxygen storage property of ceria. The H_2 yield over each catalyst was increased with temperature, while the CO selectivity at first declined and then increased at temperatures above 250 °C. Adding 5 wt% of magnesium to the Ce mono-promoter catalyst to obtain the $\text{Cu}_{0.3}\text{Ce}_{0.25}\text{Mg}_{0.05}/\text{Al}$ catalyst resulted in a higher methanol conversion level and H_2 yield with a lower CO selectivity, but increasing the magnesium level to 10 or 15 wt% ($\text{Cu}_{0.3}\text{Ce}_{0.2}\text{Mg}_{0.1}/\text{Al}$ and $\text{Cu}_{0.3}\text{Ce}_{0.15}\text{Mg}_{0.15}/\text{Al}$, respectively) decreased the methanol conversion level and H_2 yield. Meanwhile, the CO selectivity over the $\text{Cu}_{0.3}\text{Ce}_{0.2}\text{Mg}_{0.1}/\text{Al}$ catalysts was higher than that over the $\text{Cu}_{0.3}\text{Ce}_{0.15}\text{Mg}_{0.15}/\text{Al}$ and $\text{Cu}_{0.3}\text{Ce}_{0.25}\text{Mg}_{0.05}/\text{Al}$ ones, respectively.

The size of the copper particles was reduced by around 0.75-, 0.54- and 0.33-fold when adding 5, 10 and 15 wt%, respectively, of magnesium to the Ce mono-promoter catalyst (Table 4.1). The increased catalytic performance by the addition of MgO to the catalysts was due to the improved copper dispersion, strong interaction

between copper and the support [55, 58, 65] and the lower reduction temperature. Moreover, the lattice parameter of ceria was decreased when adding an optimum amount of magnesium, which encouraged the ability of bulk oxygen transfer and then enhanced the catalytic performance. From the experimental results, the order of catalytic performance was similar to that of the lattice parameter of ceria. The Ce-Mg bi-promoter catalysts with an optimum $\text{Mg}/(\text{Ce}+\text{Mg})$ of 16.67 wt% could best promote the MSR.

4.2.3 S/C ratio

From the experimental results, $\text{Cu}_{0.3}\text{Ce}_{0.25}\text{Mg}_{0.05}/\text{Al}$ gave the highest methanol conversion level and H_2 yield with a lower CO selectivity at an operating temperature of 225–300 °C, and so was chosen to investigate the effect of the S/C ratio. The MSR is comprised of the sequential MD and WGS of CO reactions. The catalyst used here had a high MD catalysis, resulting in the complete methanol conversion, but the H_2 yield was not high enough, which might due to a low WGS reaction rate. The stoichiometry of the WGS of CO has an S/C ratio of 1, and so to drive the reaction forward, the S/C ratio was investigated at a constant 1.5, 2 and 2.5, with the results, in terms of the catalytic performance, shown in Fig. 4.6. The other parameters that might affect the performance were kept constant, such as feed rate at 1 mL h^{-1} . When

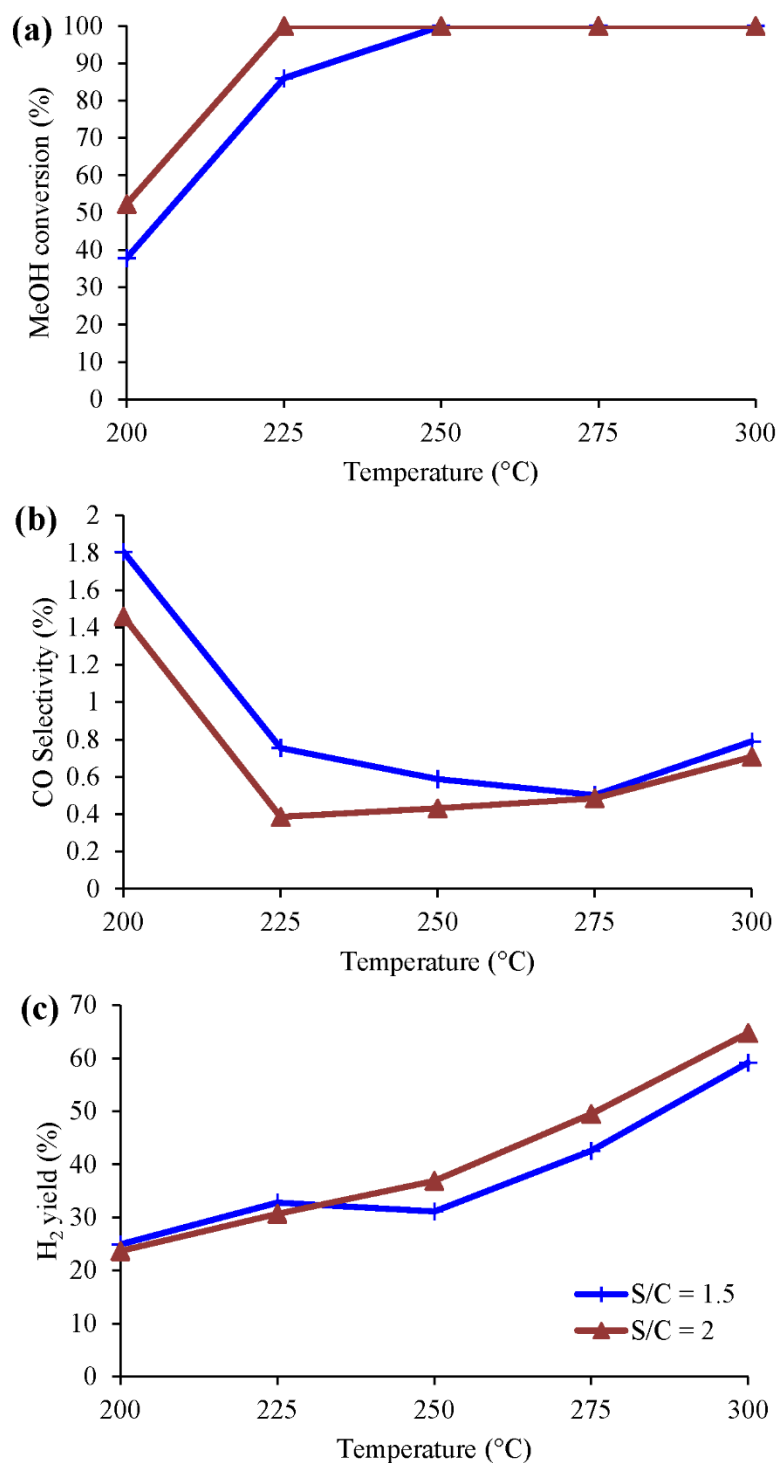


Figure 4.6 The MSR catalytic performances in terms of the (a) methanol conversion level, (b) CO selectivity and (c) H₂ yield of Cu_{0.3}Ce_{0.25}Mg_{0.05}/Al with S/C ratios of 1.5 (+) and S/C = 2 (▲) at a feed rate of 1 mL h⁻¹ and 0.1 g of catalyst. Data are shown as the mean, derived from three replicates.

increasing S/C ratio from 1.5 to 2, a higher methanol conversion level and H₂ yield with a lower CO content was achieved. However, complete methanol conversion was achieved at 250 and 225 °C when the S/C ratio was at 1.5 and 2, respectively. The lower CO selectivity at higher S/C ratios inferred that the increased proportion of steam could drive the WGS reaction forward and so promote the catalytic performance. Further increasing the S/C ratio to 2.5 decreased the catalytic performance (data not shown), as the excess steam adsorbed on the active copper species and inhibited the reaction. Thus, an improved catalytic performance, in terms of a higher H₂ yield with a lower CO content, can be achieved when using an optimal S/C ratio.

4.3 Statistical designs for optimization

The catalytic activity, in terms of the methanol conversion level, CO selectivity and H₂ yield, were observed to depend on the reaction temperature, S/C ratio, Mg/(Ce+Mg) wt% and Cu content. However, the interaction between these factors and the effect of each factor on the activities accompanied with the level of the other factors were not determined, preventing the more optimal condition for MSR catalysis from being ascertained. An experimental matrix of FCCCD-RSM with five central points was then fabricated as shown in Table 4.2, and statistical analysis at a 95% confidence interval was employed to evaluate the data using ANOVA to identify which factors and

interactions had a significant effect on each response, as shown in Table 4.3. If the *P*-value of any effect was less than 0.05, the effect had a significant influence on the response. Some factors with a *P*-value of > 0.05 were included in the model as well because sometimes a main factor does not have any influence on the response but its interaction or its transformation (i.e. quadratic form) is significant and so should be taken into account. From Table 4.3, the sole main factor was the Mg/(Ce+Mg) wt% for the methanol conversion and H₂ yield, whereas it was the Mg/(Ce+Mg) wt% and copper content for the CO selectivity.

Table 4.2 Independent factors and the FCCCD-RSM experimental design.

Factors	Variable	Unit	Low	Medium	High
A	Temperature	°C	200	225	250
B	S/C ratio	-	1.50	1.75	2.00
C	Mg/ (Ce+Mg)	wt%	0.00	16.67	33.33
D	Cu content	wt%	30	40	50

Standard order	Factor				MeOH conversion ^e (%)	CO selectivity ^e (%)	H ₂ yield ^e (%)
	A ^a	B ^b	C ^c	D ^d			
1	-1	-1	-1	-1	27.3	1.48	15.4
2	+1	-1	-1	-1	100.0	0.77	29.4
3	-1	+1	-1	-1	54.7	0.86	31.1
4	+1	+1	-1	-1	100.0	0.51	28.6
5	-1	-1	+1	-1	31.5	1.47	13.9
6	+1	-1	+1	-1	100.0	0.79	21.2
7	-1	+1	+1	-1	48.1	0.31	20.9
8	+1	+1	+1	-1	100.0	0.40	43.1
9	-1	-1	-1	+1	34.5	1.03	23.3

Table 4.2 (cont.)

Standard order	Factor				MeOH conversion ^e (%)	CO selectivity ^e (%)	H ₂ yield ^e (%)
	A ^a	B ^b	C ^c	D ^d			
10	+1	-1	-1	+1	100.0	0.48	33.7
11	-1	+1	-1	+1	55.0	0.80	29.7
12	+1	+1	-1	+1	100.0	0.38	23.3
13	-1	-1	+1	+1	42.9	0.49	19.4
14	+1	-1	+1	+1	100.0	0.52	20.3
15	-1	+1	+1	+1	78.6	0.36	28.6
16	+1	+1	+1	+1	100.0	0.51	47.6
17	-1	0	0	0	49.2	0.39	23.6
18	+1	0	0	0	100.0	0.29	29.1
19	0	-1	0	0	100.0	0.37	35.3
20	0	+1	0	0	100.0	0.28	38.5
21	0	0	-1	0	45.7	1.05	24.8
22	0	0	+1	0	92.7	1.12	24.8
23	0	0	0	-1	74.6	0.49	27.9
24	0	0	0	+1	100.0	0.71	29.5
25	0	0	0	0	78.6	0.38	22.5
26	0	0	0	0	83.2	0.24	21.0
27	0	0	0	0	81.7	0.25	21.5
28	0	0	0	0	81.3	0.25	21.6
29	0	0	0	0	79.3	0.24	22.3

^a Coded values of (-1), (0) and (+1) refer to the actual values of 200, 225 and 250 °C, respectively.

^b Coded values of (-1), (0) and (+1) refer to the actual values of 1.50, 1.75 and 2.00, respectively.

^c Coded values of (-1), (0) and (+1) refer to the actual values of 0.00, 16.67 and 33.33%, respectively.

^d Coded values of (-1), (0) and (+1) refer to the actual values of 30, 40 and 50%, respectively.

^e The catalyst weight, aqueous methanol solution feed rate and He feed rate were constant at 0.1 g, 1 mL h⁻¹ and 40 mL min⁻¹, respectively.

The contribution percentage, which is related to the total sum of squares, was used to rank the relative importance of these factors and interaction, revealing a ranked order (from the highest to the lowest) of temperature (71.49%) >>> Mg/(Ce+Mg) wt% in quadratic form (5.10%) > temperature-S/C ratio interaction (3.53%) \cong S/C ratio (3.14%) > Mg/(Ce+Mg) (1.84%) for the methanol conversion response, and Mg/(Ce+Mg) wt% in quadratic form (28.98%) > S/C ratio (14.20) > temperature (10.23%) > S/C ratio-copper content interaction (6.82%) > copper content (5.11%) > Mg/(Ce+Mg) (3.13%) for the CO selectivity response, and S/C ratio (21.47%) > temperature (16.80%) > S/C ratio-Mg/(Ce+Mg) interaction (11.35%) >>>> Mg/(Ce+Mg) wt% (0.0014%) for the H₂ yield (values in parentheses correspond to the percentage of their contribution). This evidenced that not only the main effects but also their interactions should be taken into account to determine an optimal condition. The model *F*-value of 26.27 for the methanol conversion response, 7.96 for CO selectivity response and 5.91 for H₂ yield response, respectively, implies that the models were significant. The response surface equations in terms of coded factors could be expressed by Eqs. (4.1)-(4.3) for the methanol conversion, CO selectivity and H₂ yield, respectively:

$$\text{MeOH conversion (\%)} = 84.35 + 26.56A + 5.57B + 4.26C - 6.26AB - 11.52C^2, \quad (4.1)$$

$$\text{CO Selectivity (\%)} = 0.35 - 0.14A - 0.17B - 0.077C - 0.10D + 0.12BD + 0.39C^2, \quad (4.2)$$

$$\text{H}_2 \text{ yield (\%)} = 26.62 + 3.91A + 4.42B + 0.036C + 3.41BC. \quad (4.3)$$

Table 4.3 ANOVA results for the methanol conversion level, CO selectivity and H₂ yield from FCCCD-RSM

Source	Sum of squares	DF	Mean square	F-value	P-value ^d	Estimated coefficient	Percentage contribution
MeOH conversion							
Model	15120.60	5	3024.12	26.27	< 0.0001		
A ^a	12702.59	1	12702.59	110.35	< 0.0001	26.56	71.49
B ^a	558.11	1	558.11	4.85	0.0380	5.57	3.14
C ^a	326.32	1	326.32	2.83	0.1058	4.26	1.84
AB ^b	627.88	1	627.88	5.45	0.0286	-6.26	3.53
C ^{2c}	905.71	1	905.71	7.87	0.0101	-11.52	5.10
Residual	2647.65	23	115.12				
Pure error	13.74	4	3.44				
Cor total	17768.26	28					
$r =$	0.9225	C.V. % =	13.90	Adeq Precision =			16.544
CO selectivity							
Model	2.41	6	0.40	7.96	0.0001		
A ^a	0.36	1	0.36	7.12	0.0140	-0.14	10.23
B ^a	0.50	1	0.50	9.87	0.0047	-0.17	14.20
C ^a	0.11	1	0.11	2.13	0.1583	-0.077	3.13
D ^a	0.18	1	0.18	3.58	0.0719	-0.10	5.11
BD ^b	0.24	1	0.24	4.77	0.0399	0.12	6.82
C ^{2c}	1.02	1	1.02	20.31	0.0002	0.57	28.98
Residual	1.11	22	0.050				
Pure error	0.015	4	0.004				
Cor total	3.52	28					
$r =$	0.8275	C.V. % =	37.78	Adeq Precision =			10.523

H ₂ yield							
Model	812.75	4	203.19	5.91	0.0019		
A ^a	275.26	1	275.26	8.00	0.0093	3.91	16.80
B ^a	351.48	1	351.48	10.22	0.0039	4.42	21.47
C ^a	0.023	1	0.023	0.0007	0.9794	0.036	0.0014
BC ^b	185.98	1	185.98	5.41	0.0288	3.41	11.35
Residual	825.33	24	34.39				
Pure error	1.52	4	0.38				
Cor total	1638.08	28					
$r =$	0.8044	C.V. % =	22.03	Adeq Precision =		9.642	

^a Factors A, B, C and D are the main factors.

^b Factors AB, AC, AD, BC, BD and CD are the interactions between the main factors.

^c Factors A², B², C² and D² are the quadratic terms of the main factors.

^d P-value is based on the 95% confidence intervals.

The positive sign of the coefficient infers a synergistic effect on the response, where the response increased with an increasing level of synergistic factors. The negative sign of the coefficient estimate inferred an antagonistic effect on the response, where the magnitude of the response decreases with increasing levels of antagonistic factors.

For the methanol conversion response, all the main factors except for the copper loading were significant, even though the copper species were active for MSR. It was observed in section 4.2.1 that, at each level of copper content in the catalysts, complete methanol conversion was achieved when the operating temperature was higher than 250 °C. This explains the importance of the copper content and operating

temperature on the conversion response, as revealed in Table 4.3. However, the methanol conversion level decreased with increasing levels of the temperature-S/C ratio interaction and the $Mg/(Ce+Mg)$ wt% in quadratic form, which could not be observed in the univariate experiments.

For the CO selectivity response, all the main factors were antagonistic, while the S/C ratio-copper content interaction and $Mg/(Ce+Mg)$ in quadratic form were synergistic. For the H_2 yield response, the S/C ratio- $Mg/(Ce+Mg)$ interaction and all the main factors except for the copper content were significant. To obtain a higher H_2 yield with a lower CO content in the MSR, the catalysts need to have a high activity in the MD and WGS of CO reactions. Accordingly, the Ce-Mg bi-promoter catalyst was suggested due to the synergistic action of ceria and MgO. Ceria, with its oxygen storage, enhanced the MD reaction, while MgO enhanced the WGS reaction of CO and improved the copper dispersion. Additionally, the WGS reaction was promoted by increasing the S/C ratio, resulting in a lower CO selectivity. However, an excess S/C ratio could inhibit the reaction due to the excess steam blocking the catalyst surface. These results were in accordance with the measured catalytic activities (Section 4.2), and so the models appeared satisfactory.

The correlation coefficient (r) for each model was higher than 0.8, indicating a strong relationship between the response and these factors. Meanwhile, the coefficient of variation revealed that only 13.90%, 37.78% and 22.03% of the data points for the

methanol conversion level, CO selectivity and H₂ yield, respectively, were dispersed around the mean. Moreover, the adequate precision signal to noise ratio for each model was greater than 0.4, revealing that each RSM can be used to navigate the design space. To maximize the methanol conversion level and increase the H₂ yield, the Ce-Mg bi-promoter copper-based catalysts seem suitable when operated at a high temperature and S/C ratio. However, the interaction of temperature-S/C ratio and Mg/(Ce+Mg) in the quadratic form should be considered since they caused a reduction in the methanol conversion level. The use of Ce-Mg bi-promoter copper-based catalysts with a high copper content and Mg/(Ce+Mg) at a high temperature and S/C ratio would achieve a minimal CO selectivity due to the endothermic nature of the MSR reaction. The addition of MgO and ceria to the catalyst improved the copper dispersion and oxygen vacancy defects, respectively, as discussed in section 4.2, while increasing the S/C ratio invigorated the WGS reaction and so led to an improved overall MSR reaction.

To evaluate the adequacy of the models, a normal plot of the residues and the residues with estimated responses were analyzed. From the residues plot (Fig. 4.7a-c), all the plotted points fell along an imaginary straight line, indicating the model fitted sufficiently the experimental data. This also reflects that all requisite terms were taken into account in the models. From the plot between residues and estimated responses (Fig. 4.7d-f), no distribution pattern in the plotted points was observed,

suggesting that the model is acceptable. To optimize the conditions, the contour of 3D response surface curve was constructed by connecting a constant estimated response (Fig. 4.8). The optimal operating region for a maximal methanol conversion level (100%) to give a high H₂ yield (28.9–29.4%) with a low CO selectivity (0.16–0.18%) was at the shaded portion, representing a copper level of 46–50 wt%, Mg/(Ce+Mg) of 16.2–18.0 wt%, temperature of 245–250 °C and S/C ratio of 1.74–1.80. To verify the RSM models, four more experiments were randomly run, as shown in Table 4.4. The estimated responses were close to the experimental results with an error range of $\pm 3.0\%$. This implied the potential of the RSM model to evaluate the optimization capacity and provide the feasible operating regions for catalytic performance. Additionally, two more experiments, in which the level of one factor was outside of the given range, were performed in order to test the sensitivity of the models. The obtained error range was $\pm 3.0\%$, suggesting that the RSM models were acceptable within this range.

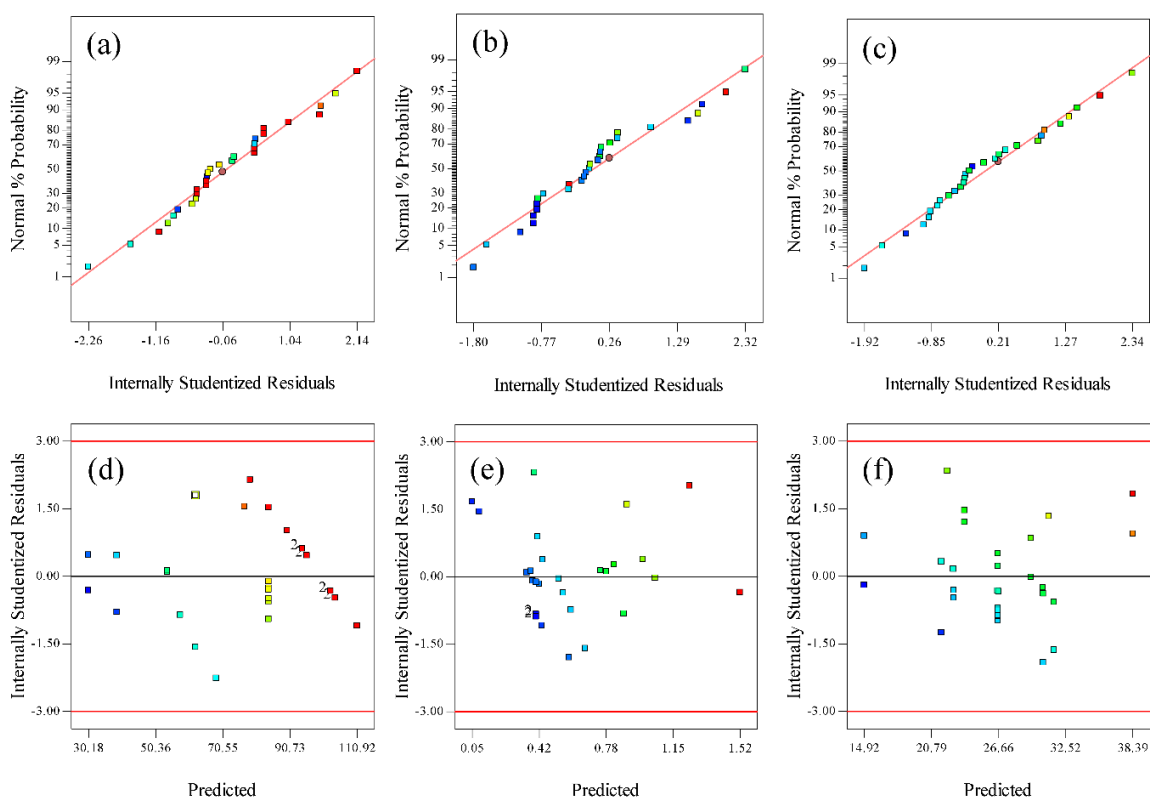


Figure 4.7 Normal probability plots of the residues for each response (a–c) and plots of residues and each evaluated response (d–f): (a and d) MeOH conversion; (b and e) CO selectivity; and (c and f) H₂ yield.

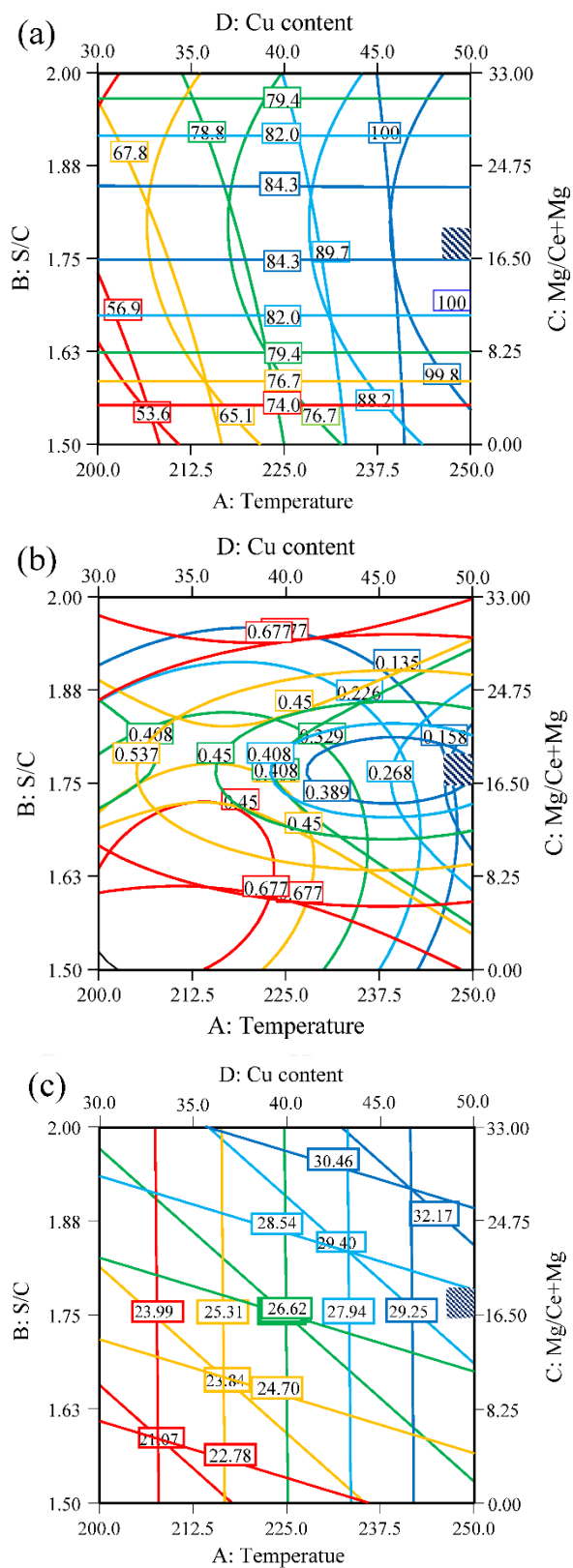


Figure 4.8 Contour plots for the optimal conditions for the (a) methanol conversion level; (b) CO selectivity; and (c) H₂ yield.

Table 4.4 Validation of the RSM

Number	A	B	C	D	MeOH conversion			CO selectivity			H ₂ yield		
					Exp	Est	% Err	Exp	Est	% Err	Exp	Est	% E
1	215.0	1.75	18.64	40.0	75.52	74.08	1.91	0.42	0.43	-2.38	24.95	25.06	-0.4
2	235.0	1.85	16.50	45.0	95.46	96.20	-0.78	0.25	0.245	2.00	30.62	29.95	2.1
3	190.0	2.00	33.00	41.4	55.33	54.24	1.97	0.12	0.117	2.50	28.87	29.01	-0.4
4	225.0	1.50	16.50	40.0	79.62	78.78	1.06	0.33	0.321	2.73	22.65	22.20	1.9
5	240.0	1.50	22.00	35.0	97.34	98.62	-1.31	0.36	0.37	-2.78	24.06	23.42	2.6
6	225.0	1.75	25.43	55.0	82.85	83.61	-0.92	0.58	0.57	1.72	26.58	27.00	-1.5

Note: Catalyst weight was maintained at 0.1 g, aqueous methanol solution feed rate was constant at 1 mL h⁻¹, and He feed rate was 40 mL min⁻¹.

4.4 Stability test

In practice, a good catalyst should express a high performance and durability. Therefore, the optimal $\text{Cu}_{0.5}\text{Ce}_{0.25}\text{Mg}_{0.05}/\text{Al}$ catalyst, suggested by the 3D-RSM evaluation, was fabricated and tested for its MSR catalytic activity and stability in the optimal operating region. Prior to use 0.1 g of $\text{Cu}_{0.5}\text{Ce}_{0.25}\text{Mg}_{0.05}/\text{Al}$ catalyst was reduced in situ with 40 mL min^{-1} of H_2 in Ar balance at $300 \text{ }^\circ\text{C}$ for 1 h. After cooling down in He carrier gas to $250 \text{ }^\circ\text{C}$, the influent was then switched to the water/methanol mixture with an S/C ratio of 1.75 in He balance at a total flow rate of 40 mL min^{-1} . The reaction temperature was controlled by a temperature controller and the test was run for 72 h, with the results shown in Fig. 4.9.

The catalyst expressed a constant complete methanol conversion level and CO selectivity of 0.14–0.16% throughout the 72 h study period. The H_2 yield was in the range of 28–29% within the first 32 h and then decreased by around 2–3% within the next 16 h. After that the H_2 yield remained constant at 24–25% until the end of the 72 h study period. There were no signs of catalyst deactivation during the 72 h study period. The catalyst was still active even though some Cu_2O was observed in the XRD pattern of the spent $\text{Cu}_{0.5}\text{Ce}_{0.25}\text{Mg}_{0.05}/\text{Al}$ catalyst (Fig. 4.1j). As described above, adding some MgO improved the dispersion of active copper species and encouraged a stronger interaction between copper and the support, resulting in the enhanced catalytic performance. Meanwhile, the reduction in the ceria lattice parameter

encouraged the ability of bulk oxygen transfer, resulting in a higher catalytic activity. Simultaneously some active copper species might transform to copper oxide during the reaction, while some of the H₂ product could reduce the copper oxide to suboxide and metallic Cu, as evidenced in Fig. 4.1j. This is a possible reason to explain the slight decrease in the H₂ yield. This result indicated that addition of ceria/MgO bi-promoter could improve the thermal stability of the copper particles and prevent them from sintering during the reaction. Accordingly, the Cu_{0.5}Ce_{0.25}Mg_{0.05}/Al catalyst is a good candidate for MSR.

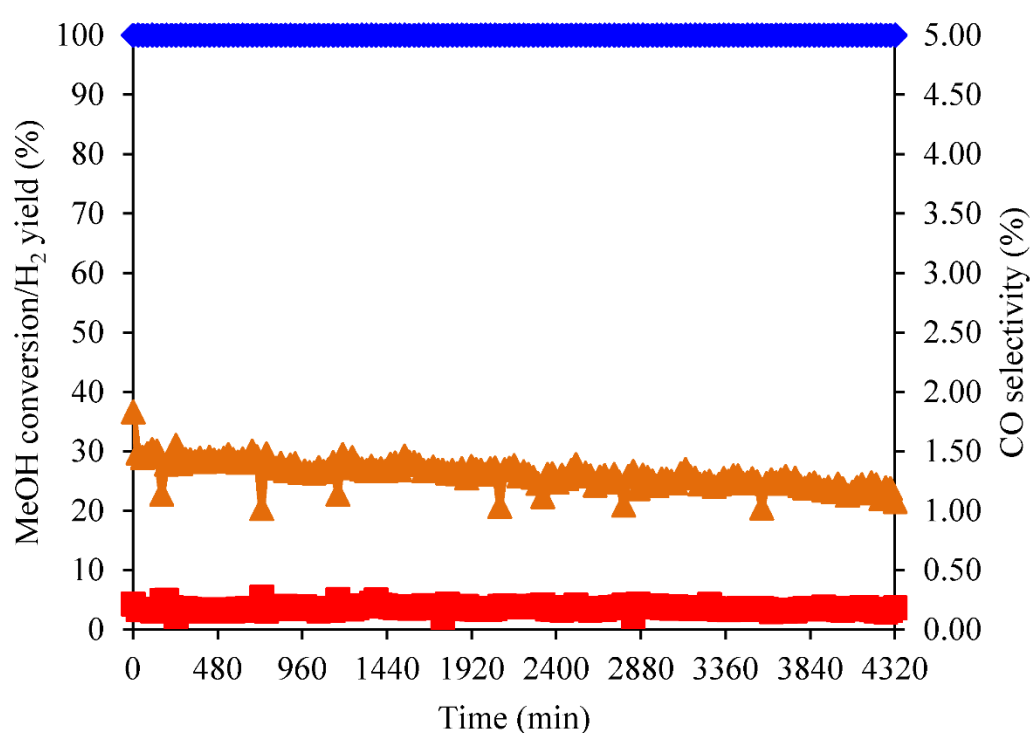


Figure 4.9 Catalyst stability test in the MSR reaction in terms of the methanol conversion level (◆), CO selectivity (■) and H₂ yield (▲) over 0.1 g of Cu_{0.5}Ce_{0.25}Mg_{0.05}/Al catalyst at 250 °C and a S/C ratio of 1.75.

CHAPTER V

PREFERENTIAL OXIDATION OF CO UNIT

5.1 Catalyst characterization

FESEM images were used as a magnifier-glass to identify the shape of ceria support. The morphology from FESEM for the commercial ceria at 20,000x was shown in Fig. 5.1a, while the fresh synthesized ceria supports at 100,000x were shown in Fig. 5.1b-e. Before taking the images, all the samples were dried overnight at 110 °C and then coated with gold particle to improve conductivity on the support's surface, avoiding charge build-up on the support under the electron beam at the high voltage needed to obtain high magnification [66]. The FESEM images expressed that commercial ceria (Fig. 5.1a) had large particles with very smooth surface while synthesized ceria support had rod-like shape morphology with much rougher surface and this was corresponded with BET results. It could be seen that the particles of synthesized ceria support were long and thin shape. In case of CeO₂ support which prepared with 5M NaOH, the formation of nanorods with average diameter 13.8 nm (80-130nm length) was observed coexist with plate shape. There was significant change in support morphology when increased NaOH concentration to 15 M (Fig. 5.1b),

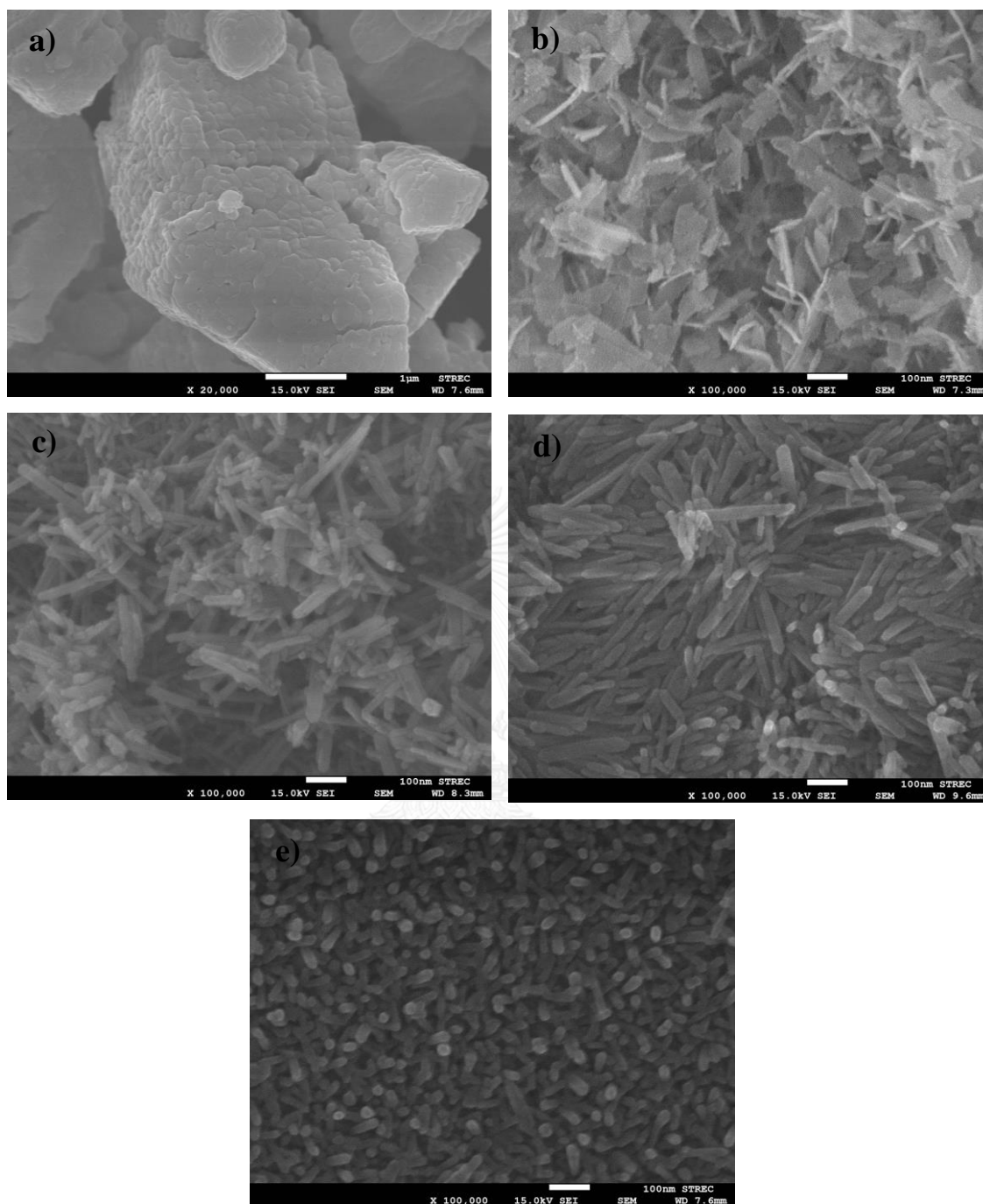


Figure 5.1 FESEM images of ceria support shown are the fresh (a) commercial CeO_2 , (b) synthesized CeO_2 prepared with 5M NaOH, (c) synthesized CeO_2 prepared with 15M NaOH, (d) synthesized $\text{Ce}_{0.95}\text{Mg}_{0.05}$ and (e) synthesized $\text{Ce}_{0.80}\text{Mg}_{0.20}$

the particles of synthesized ceria support were mainly rod shape without plate shape could be detected. It should be noted that average diameters of nanorods were also increased to 23.4 nm (80-180nm length). The diameter of the nanorods increased as the NaOH concentration used during hydrothermal treatment increased due to higher chemical potential to drive the anisotropic growth (growth rate is not equal in all directions) of the $\text{Ce}(\text{OH})_3$ nuclei which then oxidized to ceria [67-69].

Fig. 5.1c-e showed FESEM images of three ceria support with different ratios of MgO (CeO_2 , $\text{Ce}_{0.95}\text{Mg}_{0.05}$ and $\text{Ce}_{0.80}\text{Mg}_{0.20}$). Addition of MgO to 5 wt% and 20 wt% on synthesized ceria support slightly increased rods diameter from 23.4 nm to 25.3 nm (100 – 200 nm length) and 27.2 nm (60-120 nm length), respectively. It's well known that nanostructure ceria formed with the dissolution/recrystallization mechanism [70, 71]. It's suggested that NO_3^- ions acted as an oxidizer simultaneously and oxidize $\text{Ce}(\text{OH})_3$ to CeO_2 . NO_3^- ions which could selective adsorb on CeO_2 nuclei and kinetically control the locatable deposition of CeO_2 species, resulted that the additional of NO_3^- which came along with magnesium source promote the growth of ceria nanostructure. Synthesized ceria support with variation of magnesium results not only increased diameter of nanorods but also improved rods arrangement. From these results, it's suggest that the controllable synthesis of CeO_2 nanorods is relevant to the magnesium ions in the hydrothermal reaction.

The textural properties of the ceria support and CuO/CeO₂ catalysts were summarized in Table 5.1. The specific BET surface areas (A_{BET}) of commercial CeO₂ was 13.67 m² g⁻¹ while all the synthesized ceria supports were in range of 83–129 m² g⁻¹. As seen that synthesized samples expressed 6 times higher A_{BET} when compare to commercial ceria, these results were due to synthesized ceria had formed in nanostructure as observed in FESEM results (Fig. 1). Addition of CuO on commercial CeO₂ reduced A_{BET} to 3.06 m² g⁻¹ with the reduction of average pore volume (V_{pore}) and average pore diameter (D_{pore}) from 0.0128 to 0.0005 cm³ g⁻¹ and 37.44 Å to 6.99 Å, respectively. This result was suggested that copper could not diffuse into the pore and cloak on the surface of ceria support. The A_{BET} of synthesized ceria support was decreased from 128.43 to 83.41 m² g⁻¹ when increased NaOH concentration used during hydrothermal treatment from 5 to 15 M due to the increment in the diameter size of nanostructure ceria from 13.8 to 23.4 nm [68]. In case of ceria support with 5 M NaOH treatment, it expressed significant decline in A_{BET} which reduced to 89.92 m² g⁻¹ when adding CuO to 5 wt%. While ceria support with 15 M NaOH treatment exhibit slightly decreased A_{BET} to 81.03 m² g⁻¹. This result implied that ceria nanostructure could improve copper dispersion. Thus, ceria support with 15 M NaOH treatment seem to be more promised for study further effect.

Table 5.1 Textural properties of ceria support and CuO/CeO₂ catalysts

Sample	A _{BET} (m ² g ⁻¹)	V _{pore} (cm ³ g ⁻¹)	D _{pore} (Å)	Crystallite size of Cu (nm)
com-CeO ₂ ^a	13.67	0.0128	37.44	-
5%CuO/com-CeO ₂ ^a	3.06	0.0005	6.99	30.6
CeO ₂ ^b	128.43	0.4800	149.50	-
5%CuO/CeO ₂ ^b	89.92	0.3908	173.85	31.1
CeO ₂ ^c	83.41	0.1347	64.61	-
5.0%CuO/CeO ₂ ^c	81.03	0.1310	65.66	-
Ce _{0.95} Mg _{0.05} ^c	83.33	0.1398	67.11	-
2.5%CuO/ Ce _{0.95} Mg _{0.05} ^c	76.72	0.1265	65.96	-
5.0%CuO/Ce _{0.95} Mg _{0.05} ^c	75.18	0.1245	66.26	26.4
7.5%CuO/ Ce _{0.95} Mg _{0.05} ^c	67.62	0.1168	67.09	26.4
10.0%CuO/ Ce _{0.95} Mg _{0.05} ^c	59.41	0.0998	67.24	26.4
Ce _{0.80} Mg _{0.20} ^c	83.77	0.1322	63.15	-
5.0%CuO/Ce _{0.80} Mg _{0.20} ^c	74.86	0.1211	64.73	27.9

^a commercial CeO₂

^b ceria support prepared in 5 M NaOH

^c ceria support prepared in 15 M NaOH

Adding 5wt% of MgO to ceria support during hydrothermal treatment slightly decreased A_{BET} from 83.41 to 83.33 m² g⁻¹ with the increment in the diameter size of nanostructure ceria from 23.4 to 25.3 nm. Further increased MgO to 20 wt% improved rods arrangement and caused the A_{BET} to increase to 83.77 m² g⁻¹. For the Mg-promoted support at a constant copper content of 5 wt%, the A_{BET} was around 75 m² g⁻¹ for both case. Meanwhile, addition of CuO caused the pore volume (V_{pore}) to decrease, while the pore diameter (D_{pore}) was increased. This suggested that MgO inhibited copper

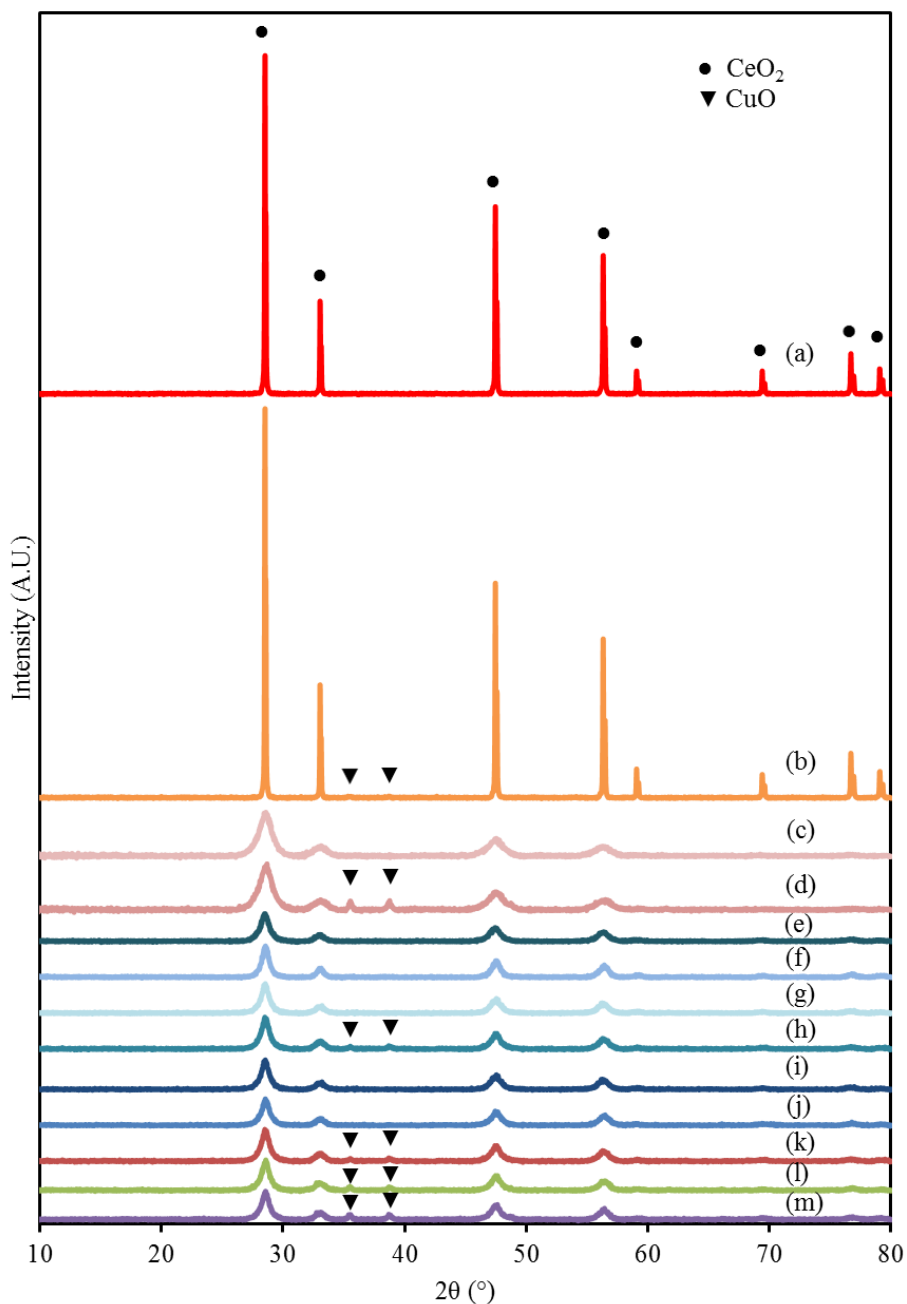


Figure 5.2 Representative (of 13 samples) XRD patterns of the ceria support and CuO/CeO₂ catalysts: (a) com-CeO₂^a, (b) 5.0wt%CuO/com-CeO₂^a, (c) CeO₂^b, (d) 5.0wt% CuO/CeO₂^b, (e) CeO₂^c (f) 5.0wt% CuO/CeO₂^c, (g) Ce_{0.80}Mg_{0.20}^c, (h) 5.0wt% CuO/Ce_{0.80}Mg_{0.20}^c, (i) Ce_{0.95}Mg_{0.05}^c, (j) 2.5wt% CuO/Ce_{0.95}Mg_{0.05}^c, (k) 5.0wt% CuO/Ce_{0.95}Mg_{0.05}^c, (l) 7.5wt% CuO/Ce_{0.95}Mg_{0.05}^c and (m) 10.0wt% CuO/Ce_{0.95}Mg_{0.05}^c; ^a commercial CeO₂, ^b ceria support prepared in NaOH 5M and ^c ceria support prepared in NaOH 15M.

agglomeration and improved the dispersion of copper particles [52]. When increasing the copper content from 2.5 to 10.0 wt% on $\text{Ce}_{0.95}\text{Mg}_{0.05}$ support, the A_{BET} was decreased from 76.72 to 59.41 $\text{m}^2 \text{g}^{-1}$, while the D_{pore} increased from 65.96 to 67.24 Å with the reduction of (V_{pore}) from 0.1265 to 0.0998 $\text{cm}^3 \text{g}^{-1}$. Here, some copper might have filled in the minor pores of the support.

The XRD patterns for ceria support and CuO/CeO_2 catalysts were shown in Fig. 5.2. Each pattern in Fig. 5.2 revealed the ceria diffraction at 28.5°, 33.0°, 47.5°, 56.3°, 59.2°, 69.6°, 76.7° and 79.1°, which corresponded to the crystalline planes of (111), (200), (220), (311), (222), (400), (331) and (420), respectively, in agreement with JCPDS No.34-0394 [40, 42, 69, 72]. The XRD peaks of commercial ceria as shown in Fig. 5.2a-b were higher than synthesized ceria support (Fig. 5.2c-m). This result suggested that commercial ceria has higher ceria crystallinity as seen in Fig. 5.1 that commercial ceria structure arranged in high degree of order. When increased NaOH concentration used during hydrothermal treatment from 5M (Fig. 5.2c-d) to 15M (Fig. 5.2e-f), peaks intensity was decreased due to the disorder of nanorods. While introduced MgO on synthesized ceria support could increase peaks intensity, revealing that addition on MgO could promote ceria crystallinity. Even though each catalyst contained MgO, the peaks that corresponded to magnesium oxide (JCPDS No.89-7746) were not observed which was probably due to the MgO being highly dispersed on the catalysts.

5wt%CuO/com-CeO₂ (Fig. 5.2b) expressed 2 diffraction peaks of CuO at 35.5° and 38.7° (JCDPS No. 41-0254) which represented the crystalline planes of (002) and (111), respectively. Peaks of CuO were also observed on 5wt%CuO/CeO₂ catalysts which prepared in 5M NaOH (Fig. 5.2d) but could not be detected on 5wt%CuO/CeO₂ catalysts which increased NaOH concentration to 15 M (Fig. 5.2f). This result indicated that copper has highly dispersion, revealing that nanorods in synthesized ceria support could improve copper dispersion [43]. The Cu intensity peaks at the (111) and (200) planes were higher with increasing Cu loading levels from 2.5 to 10.0 wt% on Ce_{0.95}Mg_{0.05} support. This is typically for catalysts prepared by impregnation and then calcination which could lead to partial segregation of copper [73]. Due to the activity of copper in PROX, the Debye-Scherrer equation was used to evaluate the copper crystallite size in order to reflect the level of sintering of the copper, and the results are summarized in Table 5.1. The 5wt%CuO/com-CeO₂ catalyst had a copper crystallite size of around 30.6 nm, while it slightly increased in the 5wt%CuO/5M-CeO₂ catalyst but could not evaluate in the 5wt%CuO/15M-CeO₂ catalyst. This revealed that the different morphology of ceria support had an influence on the copper crystallite size. At a constant copper content of 5 wt% on synthesized ceria support, the copper crystallite size was decreased from 30.6 nm to 26.4 nm when adding MgO to 5 wt%, which is likely to be because the presence of MgO improved the dispersion of copper.

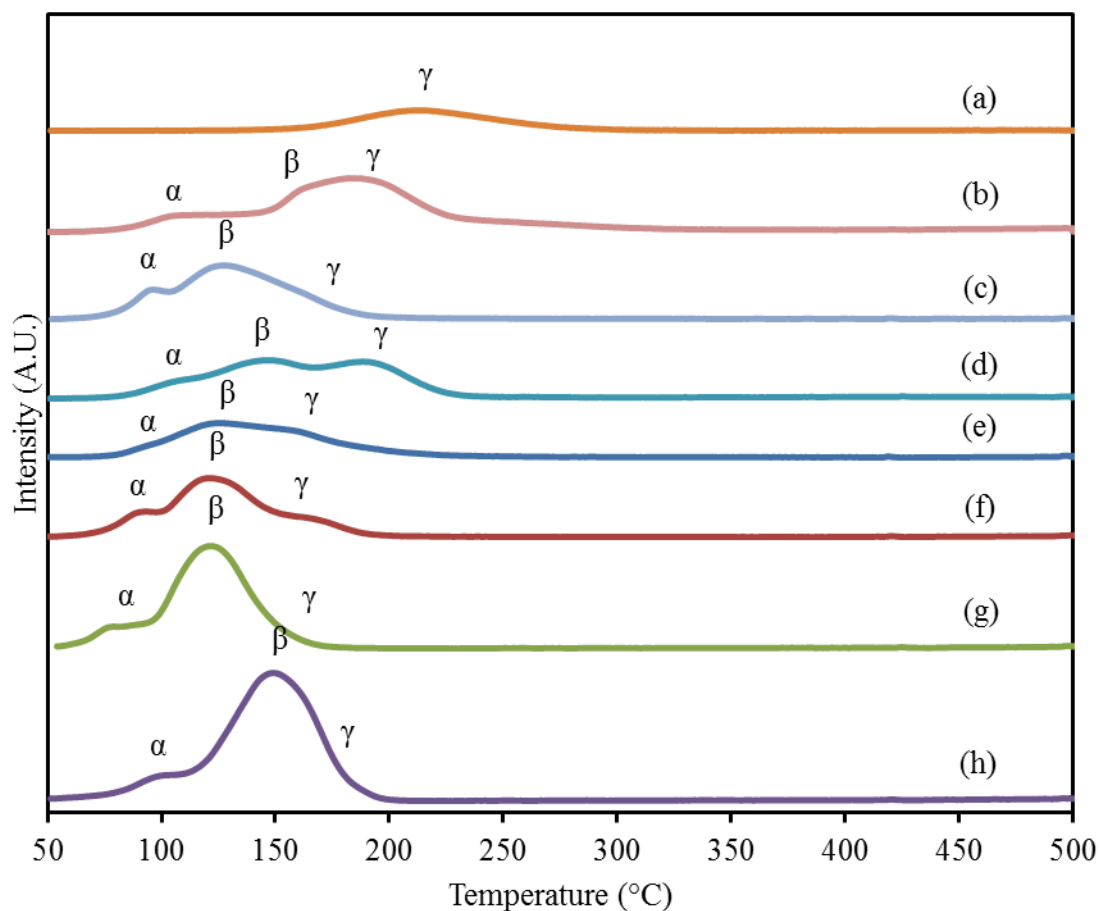


Figure 5.3 Representative (of 8 samples) H_2 -TPR profiles of the CuO/CeO_2 catalysts: (a) 5.0wt% $CuO/com-CeO_2$ ^a, (b) 5.0wt% CuO/CeO_2 ^b, (c) 5.0wt% CuO/CeO_2 ^c, (d) 5.0wt% $CuO/Ce_{0.80}Mg_{0.20}$ ^c, (e) 2.5wt% $CuO/Ce_{0.95}Mg_{0.05}$ ^c, (f) 5.0wt% $CuO/Ce_{0.95}Mg_{0.05}$ ^c, (g) 7.5wt% $CuO/Ce_{0.95}Mg_{0.05}$ ^c and (h) 10.0wt% $CuO/Ce_{0.95}Mg_{0.05}$ ^c; ^a commercial CeO_2 , ^b ceria support prepared in NaOH 5M and ^c ceria support prepared in NaOH 15M.

The H_2 -TPR profiles of the CuO/CeO_2 catalysts were shown in Fig 5.3, where only the TPR profiles of copper species could be detected within the study temperature range from 50 to 500 °C. The profile of the 5wt% $CuO/com-CeO_2$ catalyst

(Fig. 5.3a) had only one broad peaks with the center at 215 °C which represent bulk copper species (γ , 160–260 °C) [74-76]. For the 5wt%CuO/CeO₂ catalyst prepared in 5 M NaOH (Fig. 5.3b), the reduction temperature range was shifted to a lower temperature of 80-250 °C with three major peak at 106, 158 and 194 °C, which was attributed to highly dispersed copper species (α , 50 °C–110 °C), copper species which incorporated into ceria lattice (β , 110–160 °C) and bulk copper species (γ), respectively. The change in reduction temperature range presumably due to the morphology of ceria support which formed into nanostructure. While the 5wt%CuO/CeO₂ catalyst prepared in 15 M NaOH shown in Fig. 5.3c also expressed three reduction peaks at 93, 129 and 164 °C within reduction temperature range from 60 to 200 °C. Further increased NaOH concentration could decreased reduction temperature range due to higher nanorods ratio on ceria support as seen in Fig. 5.1. Addition of MgO to 5wt% on ceria support didn't show significant change in reduction temperature as seen that 5wt%CuO/Ce_{0.95}Mg_{0.05} (Fig. 5.3f) also expressed three reduction peaks at 91, 125 and 162 °C within the same reduction temperature range of 5wt%CuO/CeO₂. For the 5wt%CuO/Ce_{0.80}Mg_{0.20} catalyst shown in Fig. 5.3d, the copper species were in three forms within the temperature range of 83–234 °C, comprised of three peaks at around 108, 147 °C and 192 °C, which were highly dispersed copper species (α), copper species which incorporated into ceria lattice (β) and bulk copper species (γ), respectively. Further increased MgO to 20wt% of ceria support shifted the reduction temperature to the higher range due to interaction between magnesium and copper species [38,

52, 65]. When increasing copper content from 2.5 to 7.5 wt% on $\text{Ce}_{0.95}\text{Mg}_{0.05}$, the reduction temperature was shifted to a lower temperature. However, further raising the copper content to 10 wt% shifted the reduction temperature range to a higher temperature. There was not much change in the profiles except for an increase in the H_2 consumption rate.

5.2 Catalytic activity test

5.2.1 type of ceria support

The catalytic activities for PROX over a series of CuO on ceria support catalysts were evaluated in terms of CO conversion (%) and CO_2 selectivity (%). Since the effluent contained only H_2 , O_2 , CO and CO_2 without other hydrocarbons could be detected, the catalytic activities would be calculated by eq. (3.4) - (3.4) as mentioned in chapter 3. The catalytic performance of copper based catalysts over different type of ceria support were shown in Fig. 5.4A-B. When increasing the temperature, the CO conversion increased to the maximum value and then gradually drop at higher temperature range. While the CO_2 selectivity start from maximum value at low temperature and then decreased after achieved maximum CO conversion. It's supposed that overall PROX was comprised of 2 competitive reaction; H_2 oxidation and CO oxidation. From stoichiometry, one mole of CO was reacted with 0.5 mole of O_2 and converted to CO_2 . The excess O_2 could react with H_2 via H_2 oxidation to produce

H₂O. It's well known that hydrogen molecules could form into hydroxyl group which could promote CO oxidation, resulting that mainly CO oxidation occurred at low temperature due to its high heat of adsorption than hydrogen [73, 77, 78]. Raising the temperature drove forward the H₂ oxidation, resulting in lower both CO conversion and CO₂ selectivity at high temperature.

5wt%CuO/com-CeO₂ catalysts didn't exhibit any catalytic activities at temperature lower than 160 °C. Then, CO conversion and CO₂ selectivity gradually increased when further increased reaction temperature and achieved maximum value of 36.3% at 260°C and 50.2% at 220 °C, respectively. From the H₂-TPR analysis (Fig. 5.3a), 5wt%CuO/com-CeO₂ catalysts expressed a high reduction temperature over 160 °C and found only bulk copper species, which followed by lower catalytic performance. Moreover, it could be seen from BET results (Table 5.1) that both A_{BET} and V_{pore} were almost completely reduced after loading copper over commercial ceria support. In case of synthesized ceria support, increasing the level of NaOH concentration used during hydrothermal treatment from 5 M to 15 M (5wt%CuO/CeO₂ 5M NaOH and 5wt%CuO/CeO₂ 15M NaOH) improved CO conversion but decreased CO₂ selectivity. 5wt%CuO/CeO₂ 5M NaOH catalysts reached maximum CO conversion of 97.1% at 180 °C and maintained high CO₂ selectivity to 160 °C. While 5wt%CuO/CeO₂ 15M NaOH catalysts achieved complete CO conversion at lower temperature 140 °C and maintained high CO₂ selectivity to 120 °C. From the H₂-TPR analysis shown in Fig. 5.3b-c,

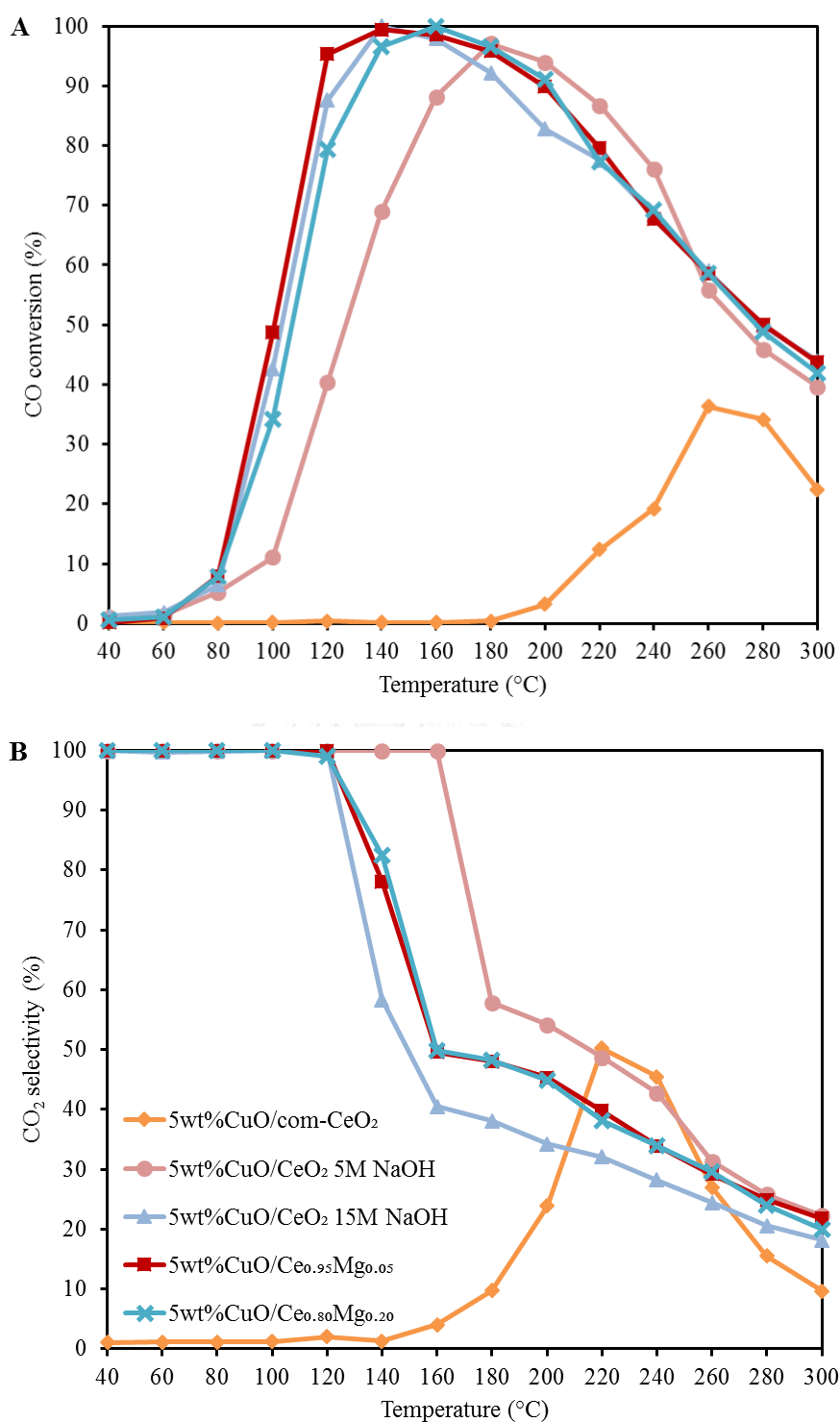


Figure 5.4 The PROX catalytic performances in terms of the (A) CO conversion level and (B) CO₂ selectivity for the 5wt%CuO/CeO₂ catalysts with different supports. All reactions had oxygen excess factor of 2, feed rate of 100 mL h⁻¹ and 0.1 g of catalyst. Data are shown as the mean, derived from three replicates.

the reduction temperature range was shifted to a lower temperature of 60-200 °C when increased NaOH concentration, giving a higher catalytic performance at low temperature. Furthermore, CeO₂ 5M NaOH support expressed significant change in A_{BET} when loading copper to 5wt%, indicated that copper had low dispersion on the support. For ceria support prepared in 15M NaOH with fixed copper content of 5 wt%, addition on MgO to 5 wt% on the support slightly increased the catalytic performance, due to reduction temperature shifted to lower range. 5wt%CuO/Ce_{0.95}Mg_{0.05} catalysts expressed maximum CO conversion of 99.4% at 140 °C and kept CO₂ selectivity higher than 5wt%CuO/CeO₂ 15M NaOH catalysts after achieved maximum CO conversion. This result reveal that the presence of MgO could promote CO₂ selectivity by inducing water-gas shift reaction. Further increasing MgO content to 20 wt% shifted the temperature to achieved maximum CO conversion to higher range at 160 °C but still gave higher CO₂ selectivity when compare with 5wt%CuO/CeO₂ 15M NaOH catalysts. This result suggested that the catalytic performance decreased due to strong interaction between Cu and Mg [52], resulted that reduction temperature shifted to higher range. Since the target of this work was to obtain high purity hydrogen stream with via PROX for PEMFC, the potential ceria support to approach these results should express high CO conversion to eliminate impurities and high CO₂ selectivity to reduce hydrogen loss within the operating temperature range. 5wt%CuO/Ce_{0.95}Mg_{0.05} catalyst was the best candidate which gave almost complete CO conversion with high CO₂ selectivity. Thus, Ce_{0.95}Mg_{0.05} support was chosen to investigate the effect of copper content on the catalytic performance in PROX.

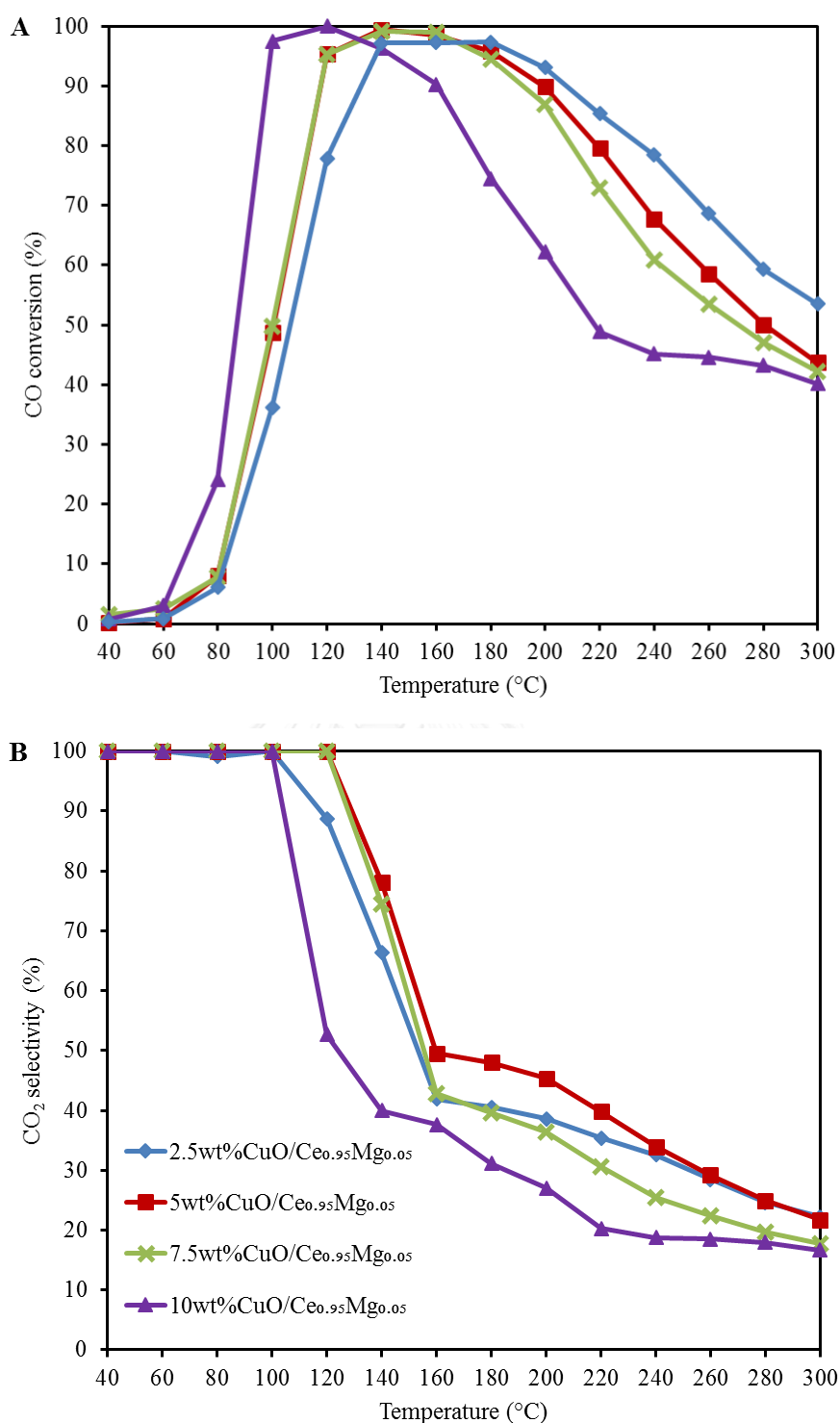


Figure 5.5 The PROX catalytic performances in terms of the (A) CO conversion level and (B) CO₂ selectivity for the CuO/Ce_{0.95}Mg_{0.05} catalysts with different level of copper oxide. All reactions had oxygen excess factor of 2, feed rate of 100 mL h⁻¹ and 0.1 g of catalyst. Data are shown as the mean, derived from three replicates.

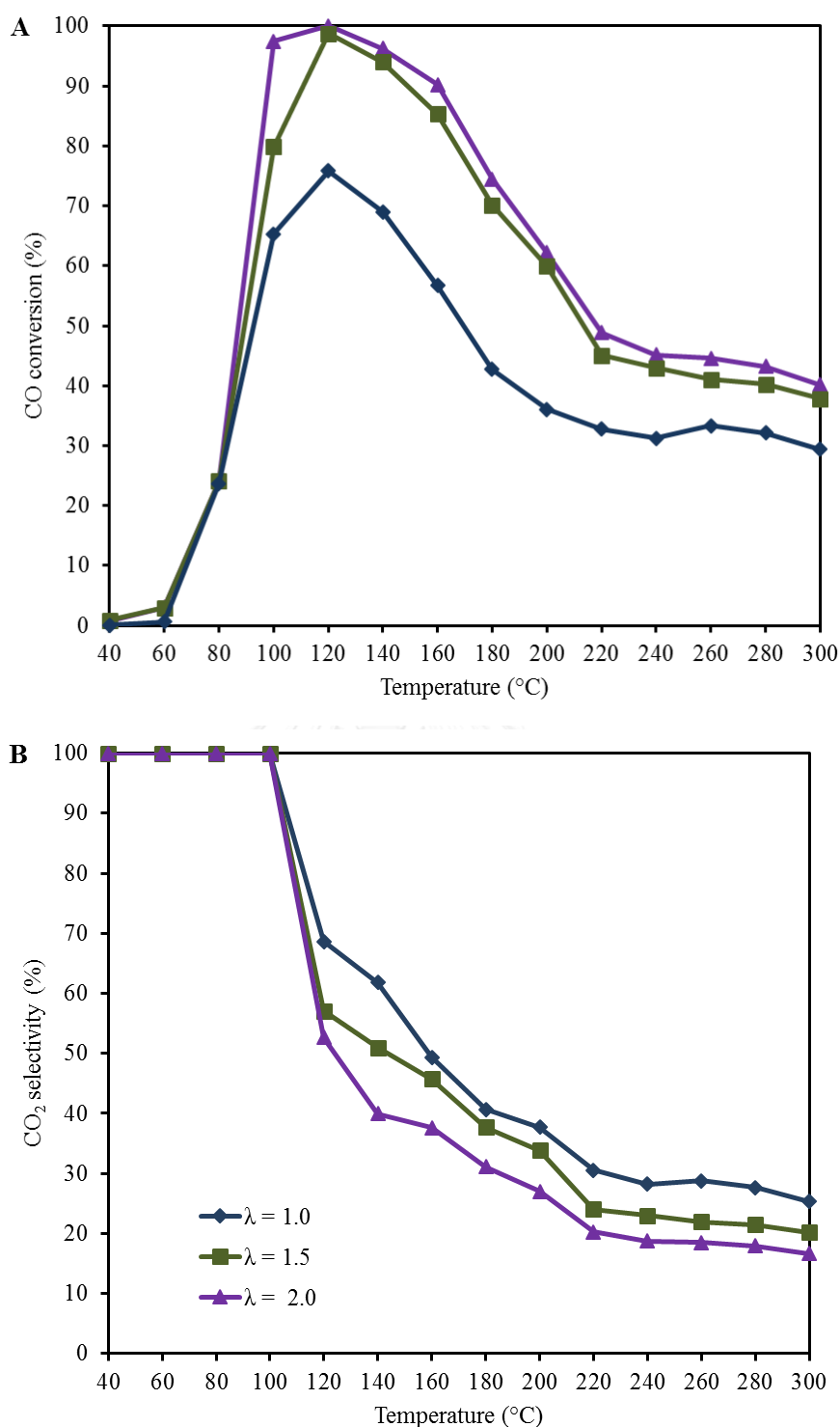


Figure 5.6 The PROX catalytic performances in terms of the (A) CO conversion level and (B) CO₂ selectivity for the 10wt%CuO/Ce_{0.95}Mg_{0.05} catalysts with different level of oxygen excess factor. All reactions had feed rate of 100 mL h⁻¹ and 0.1 g of catalyst. Data are shown as the mean, derived from three replicates.

5.2.2 Level of copper content

The catalytic performance of copper based catalysts over $\text{Ce}_{0.95}\text{Mg}_{0.05}$ support was shown in Fig. 5.5A-B. At a 5 wt% MgO on ceria support, increasing the level of copper from 2.5 to 5.0 wt% ($2.5\text{wt}\%\text{CuO}/\text{Ce}_{0.95}\text{Mg}_{0.05}$ and $5.0\text{wt}\%\text{CuO}/\text{Ce}_{0.95}\text{Mg}_{0.05}$, respectively) improved the catalytic performance, due to higher level of active sites as seen in H_2 -TPR analysis that the amount of copper species which incorporated into ceria lattice (β) increased with the copper level, suggested that monomeric Cu^{2+} on the CeO_2 surface was responsible for the improvement of CO oxidation [72]. Further increased copper content level to 7.5 wt% and 10wt% ($7.5\text{wt}\%\text{CuO}/\text{Ce}_{0.95}\text{Mg}_{0.05}$ and $10.0\text{wt}\%\text{CuO}/\text{Ce}_{0.95}\text{Mg}_{0.05}$, respectively) also increased CO conversion but the level of CO_2 selectivity after achieved maximum conversion decreased. Cu crystalline size was increased with the level of copper as shown in Table 5.1, revealed that CO_2 selectivity may relevant to Cu crystalline size. The $10.0\text{wt}\%\text{CuO}/\text{Ce}_{0.95}\text{Mg}_{0.05}$ catalyst expressed the lowest temperature to achieved complete CO conversion at 120 °C although the CO_2 selectivity was much lower than other catalysts. Since PEMFCs typically operated at 80 °C, the lower temperature different was preferred. The $10.0\text{wt}\%\text{CuO}/\text{Ce}_{0.95}\text{Mg}_{0.05}$ catalyst was best fitted to this criterion and would be chosen to investigate further effects.

5.2.3 O₂/CO molar ratio

From the experimental results, 10.0wt%CuO/Ce_{0.95}Mg_{0.05} catalyst expressed the highest CO conversion at low temperature (120 °C), and was chosen to investigate the effect of O₂/CO level which represented in term of oxygen excess factor (λ). O₂/CO level was an important factor which affect catalytic performance since PROX was comprised of 2 competitive reaction; CO oxidation and H₂ oxidation. The desired catalysts should have a high CO oxidation rate than H₂ oxidation to obtain high purity hydrogen stream with less hydrogen loss. The catalytic performance of 10.0wt%CuO/Ce_{0.95}Mg_{0.05} support with different oxygen excess factor was shown in Fig. 5.6A-B. the result expressed that CO conversion increased with the oxygen excess factor while CO₂ selectivity decreased. At $\lambda=1$ which is stoichiometry ratio for CO oxidation, the catalyst could achieve maximum conversion of 75.8% at 120 °C with 68.6% CO₂ selectivity. At the same temperature, increasing oxygen excess factor to 1.5 promote CO oxidation to 98.7% with 57.0% CO₂ selectivity but could not reach higher conversion and the effluent still has CO concentration higher than 10 ppm. Higher oxygen excess factor was required to reduce CO to less than 10 ppm which complete CO conversion could obtain after increased oxygen excess factor to 2.0 with 52.6% CO₂ selectivity. Further increased oxygen excess factor was not recommended because it could inhibit catalytic performance [79]. The CO₂ selectivity decreased from 68.6% to 52.6% when increased oxygen excess factor from 1 to 2 due to excess oxygen after complete CO oxidation was then used by H₂ oxidation [80, 81]. Thus, optimal O₂/CO

molar ratio was needed to improve catalytic performance in terms of high CO conversion and CO₂ selectivity.

5.3 Statistical design for optimization

The catalytic activity, in terms of the CO conversion and CO₂ selectivity, were observed to depend on the reaction temperature, CO level, O₂ level and amount of catalysts. However, the interaction between these factors and the effect of each factor on the activities accompanied with the level of the other factors were not determined.

Table 5.2 Independent factors and the Box Behnken-RSM experimental design.

Factors	Variable	Unit	Low	Medium	High
A	Temperature	°C	100	120	140
B	CO level	%	0.50	1.00	1.50
C	O ₂ level	%	0.50	0.75	1.00
D	Amount of catalyst	g	0.1	0.15	0.2

Standard order	Factor				CO conversion ^e (%)	CO ₂ selectivity ^e (%)
	A ^a	B ^b	C ^c	D ^d		
1	-1	-1	0	0	71.0	78.7
2	1	-1	0	0	98.2	32.8
3	-1	1	0	0	90.4	100.0
4	1	1	0	0	83.5	85.4
5	0	0	-1	-1	77.3	77.4
6	0	0	1	-1	99.3	100.0
7	0	0	-1	1	79.3	84.1
8	0	0	1	1	100.0	50.0

Table 5.2 (cont.)

Standard order	Factor				CO conversion ^e (%)	CO ₂ selectivity ^e (%)
	A ^a	B ^b	C ^c	D ^d		
9	-1	0	0	-1	77.9	99.9
10	1	0	0	-1	94.7	63.2
11	-1	0	0	1	92.2	100.0
12	1	0	0	1	95.3	63.7
13	0	-1	-1	0	98.7	62.0
14	0	1	-1	0	72.4	100.0
15	0	-1	1	0	97.2	97.5
16	0	1	1	0	99.3	74.5
17	-1	0	-1	0	74.2	97.2
18	1	0	-1	0	77.7	77.8
19	-1	0	1	0	91.5	90.5
20	1	0	1	0	98.0	49.0
21	0	-1	0	-1	98.2	88.7
22	0	1	0	-1	92.8	92.9
23	0	-1	0	1	100.0	95.5
24	0	1	0	1	97.9	97.9
25	0	0	0	0	98.4	65.6
26	0	0	0	0	100.0	82.3
27	0	0	0	0	99.2	74.0
28	0	0	0	0	99.6	78.1
29	0	0	0	0	98.8	72.8

^a Coded values of (-1), (0) and (+1) refer to the actual values of 100, 120 and 140 °C, respectively.

^b Coded values of (-1), (0) and (+1) refer to the actual values of 0.50, 1.00 and 1.50%, respectively.

^c Coded values of (-1), (0) and (+1) refer to the actual values of 0.50, 0.75 and 1.00%, respectively.

^d Coded values of (-1), (0) and (+1) refer to the actual values of 0.10, 0.15 and 0.20g, respectively.

^e The feed rate were constant at 100 mL h⁻¹ over 10wt%CuO/Ce_{0.95}Mg_{0.05} catalyst.

If there were any significant interaction effect between each factor, the optimal condition obtained from univariate experiment would differ from the correct results, preventing the more optimal condition for PROX catalysis from being recognized. An experimental matrix of Box behnken-RSM with five central points was then fabricated as shown in Table 5.2, and statistical analysis at a 95% confidence interval was employed to evaluate the data using ANOVA to identify which factors and interactions had a significant effect on each response, as shown in Table 5.3. Box-Behnken design which base on rotatable second order of three level incomplete factorial designs, had many advantages for response surface methodology, It could give an estimation of the parameters of the quadratic model while demonstrate more efficient with the number of experiments conducted for this is much lesser when compared to a central composite design [82]. Moreover, it did not contain combination which all factors were at highest or lowest value, preventing unsatisfactory results that might occur under extreme conditions. In this analysis, if the P-value of any effect was less than 0.05, the effect had a significant influence on the response. Some factors with a P-value of > 0.05 were included in the model as well because sometimes a main factor does not have any influence on the response but its interaction or its transformation (i.e. quadratic form) is significant and so should be taken into account. From Table 5.3, the 2 main factors were the reaction temperature and O₂ level for CO conversion, whereas it was the reaction temperature and CO level for the CO₂ selectivity.

The relative importance of these factors and interaction were rank by the contribution percentage which evaluated from total sum of square. For CO conversion, the rank was ordered from the highest to the lowest. O₂ level (34.20%) had the highest effect followed by reaction temperature in quadratic form (17.76%), temperature-CO level interaction (10.64%), O₂ level in quadratic form (8.59%), reaction temperature (7.74%) and CO level-O₂ level interaction (7.41%), respectively. The contribution percentage revealed a ranked order for CO₂ selectivity as followed; reaction temperature (35.49%), CO level-amount of catalyst interaction (10.50%) O₂ level-amount of catalyst interaction (9.09%) and CO level (8.58%) (values in parentheses correspond to the percentage of their contribution). This evidenced that not only the main effects but also their interactions should be taken into account to determine an optimal condition. The model F-value of 17.88 for the CO conversion response and 7.07 for CO₂ selectivity response, respectively, indicated that the models were significant.

The response surface equations in terms of coded factors could be expressed by Eqs. (5.1)–(5.2) for the CO conversion and CO₂ selectivity:

$$\text{CO conversion (\%)} = 97.37 + 4.19A - 2.26B + 8.81C - 8.52AB + 7.10BC - 8.37A^2 - 5.82C^2 \quad (5.1)$$

$$\text{CO}_2 \text{ selectivity (\%)} = 80.40 - 16.19A + 7.96B - 3.08C - 2.56D - 15.25BC - 14.19CD \quad (5.2)$$

The positive sign of the coefficient infers a synergistic effect on the response, where the response increased with an increasing level of synergistic factors. The negative sign of the coefficient estimate inferred an antagonistic effect on the response, where the magnitude of the response decreases with increasing levels of antagonistic factors.

For CO conversion response, the main factors which expressed significant effect were reaction temperature and O₂ level while the level of CO was less significant. It was observed in previous section that CO conversion increased with reaction temperature and O₂/CO level where the effect of CO level was obscure by level of O₂

Table 5.3 ANOVA results for the CO conversion level and CO₂ selectivity from Box Behnken-RSM

Source	Sum of squares	DF	Mean square	F-value	P-value ^d	Estimated coefficient	Percentage contribution
CO conversion							
Model	2333.17	7	333.31	17.88	< 0.0001		
A ^a	210.92	1	210.92	11.32	0.0029	4.19	7.74
B ^a	61.20	1	61.20	3.28	0.0843	-2.26	2.25
C ^a	931.75	1	931.75	49.99	< 0.0001	8.81	34.20
AB ^b	290.02	1	290.02	15.56	0.0007	-8.52	10.64
BC ^b	201.78	1	201.78	10.83	0.0035	7.10	7.41
A ^{2c}	483.80	1	483.80	25.96	< 0.0001	-8.37	17.76
C ^{2c}	234.07	1	234.07	12.56	0.0019	-5.82	8.59
Residual	391.40	21	18.64				
Pure error	1.60	4	0.4				
Cor total	2724.57	28					
<i>r</i> =	0.8563	C.V. % =	4.72	Adeq Precision =		15.450	

Table 5.3 (cont.)

CO ₂ selectivity							
Model	5834.69	6	972.45	7.07	0.0003		
A ^a	3145.39	1	3145.39	22.85	< 0.0001	-16.19	35.49
B ^a	760.02	1	760.02	5.52	0.0282	7.96	8.58
C ^a	113.96	1	113.96	0.83	0.3727	-3.08	1.29
D ^a	78.75	1	78.75	0.57	0.4574	-2.56	0.89
BD ^b	930.86	1	930.86	6.76	0.0163	-15.25	10.50
CD ^b	805.71	1	805.71	5.85	0.0243	-14.19	9.09
Residual	3028.07	22	137.64				
Pure error	157.21	4	39.30				
Cor total	8862.75	28					
<i>r</i> =	0.6583		C.V. % =	14.59		Adeq Precision =	8.751

^a Factors A, B, C and D are the main factors.

^b Factors AB, BC, BD and CD are the interactions between the main factors.

^c Factors A² and C² are the quadratic terms of the main factors.

^d *P*-value is based on the 95% confidence intervals.

as seen from the great different percentage contribution. CO conversion decreased, when further increased temperature, could expressed by antagonistic effect of reaction temperature in quadratic form and temperature-CO level interaction. However, the declined of CO conversion when increasing levels of O₂ in quadratic form could not be observed in the univariate experiments. For CO₂ selectivity response, the CO level-amount of catalyst interaction and O₂ level-amount of catalyst were antagonistic while the main factors expressed opposite effect with CO conversion response. Reaction temperature and O₂ level were antagonistic while CO level and amount of catalyst

were synergistic. The CO level-O₂ level interaction did not show significant effect on CO₂ selectivity, even though it was observed in section 5.2.3.

To obtain a high purity H₂ with CO content lower than 10 ppm, the catalysts need to have a high activity in the CO elimination. Thus, the copper based catalyst on modified ceria support was suggested due to the synergistic action of ceria and MgO. Ceria, with its oxygen storage, enhanced the CO oxidation, while MgO enhanced the WGS reaction of CO and improved the copper dispersion. Additionally, the CO oxidation was promoted by increasing the O₂/CO ratio or modified ceria support into nanostructure, resulting in a higher CO conversion. However, overheating inhibits CO oxidation and promote H₂ oxidation, resulted on lower CO conversion nans CO₂ selectivity. These results were in accordance with the measured catalytic activities (Section 5.2), and so the models appeared satisfactory.

The correlation coefficient (*r*) for each model was higher than 0.8, indicating a strong relationship between the response and these factors. Meanwhile, the coefficient of variation revealed that only 4.72% and 14.59% of the data points for the CO conversion and CO₂ selectivity, respectively, were dispersed around the mean. Moreover, the adequate precision signal to noise ratio for each model was greater than 0.4, revealing that each RSM can be used to navigate the design space.

To maximize the CO conversion level and CO₂ selectivity, the 10wt%CuO/Ce_{0.95}Mg_{0.05} catalysts seem suitable when operated at a high temperature and O₂/CO ratio. However, the interaction of temperature-CO level and O₂ level in the

quadratic form should be considered since they caused a reduction in the CO conversion. The addition of MgO on ceria support improved the copper dispersion, as discussed in section 5.2, while increasing the O₂/CO ratio invigorated the CO oxidation and improved overall reaction.

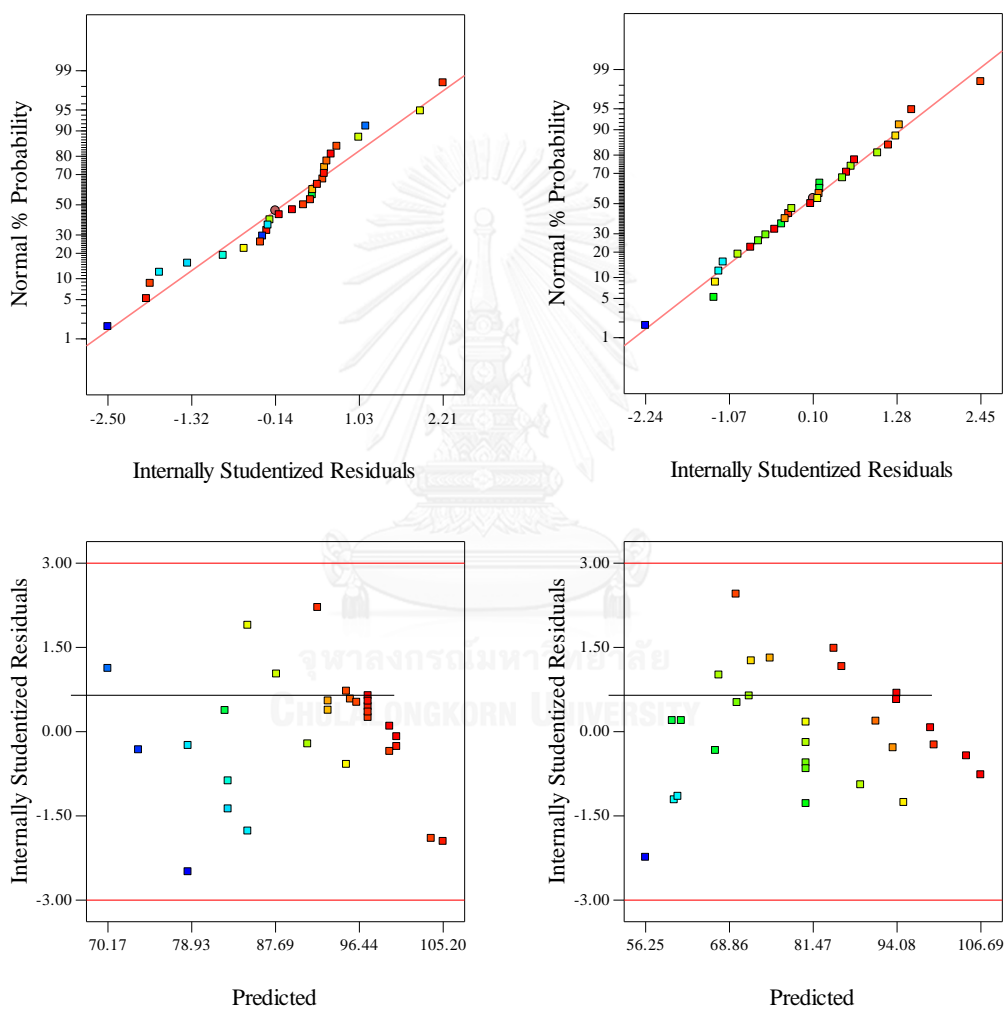


Figure 5.7 Normal probability plots of the residues for each response (a–b) and plots of residues and each evaluated response (c–d): (a and c) CO conversion and (b and d) CO₂ selectivity.

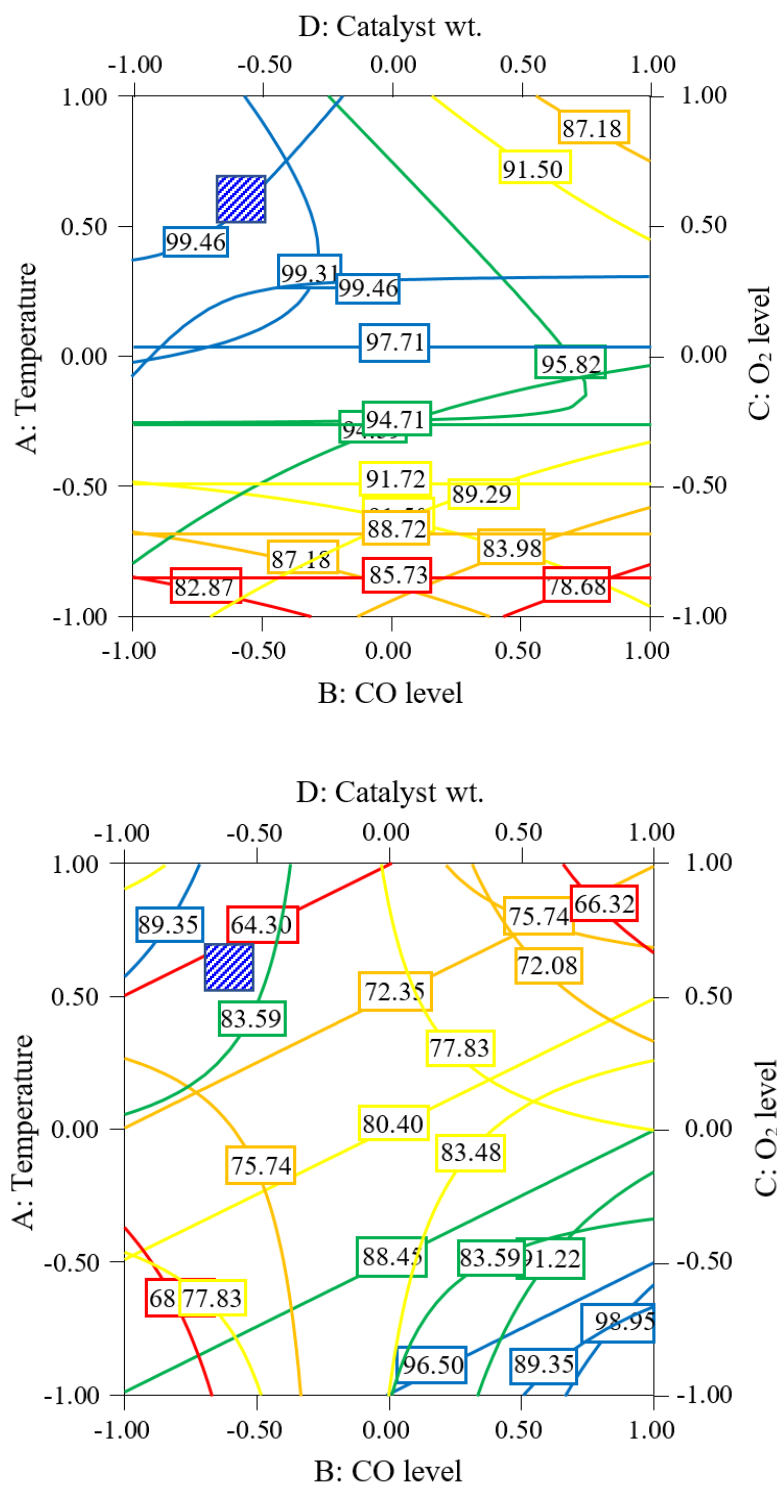


Figure 5.8 Contour plots for the optimal conditions for the 10wt%CuO/Ce_{0.95}Mg_{0.05} catalyst (a) CO conversion level and (b) CO₂ selectivity.

To evaluate the adequacy of the models, a normal plot of the residues and the residues with estimated responses were analyzed. From the residues plot (Fig. 5.7a-b), all the plotted points fell along an imaginary straight line, indicating the model fitted sufficiently the experimental data. This also reflects that all requisite terms were taken into account in the models. From the plot between residues and estimated responses (Fig. 5.7c-d), no distribution pattern in the plotted points was observed, suggesting that the model is acceptable. To optimize the conditions, the contour of 3D response surface curve was constructed by connecting a constant estimated response (Fig. 5.8). The optimal operating region for a maximal CO conversion level (>99%) with a high CO₂ selectivity (80-90%) was at the shaded portion (Fig.5.8), representing a CO level of 0.65–0.75 %, O₂ level of 0.80-0.90% ($\lambda \approx 2$), temperature of 130–140 °C and amount of catalyst of 0.10–0.13 g.

5.4 Stability test

In our study, the stability of 10.0wt%CuO/Ce_{0.95}Mg_{0.05} catalyst was also determined since a good catalyst should express a high performance and durability. Therefore, the optimal 10.0wt%CuO/Ce_{0.95}Mg_{0.05} catalyst, suggested by the univariate evaluation, was fabricated and tested for its PROX catalytic activity and stability in the optimal operating region from RSM design. 0.13 g of 10.0wt%CuO/Ce_{0.95}Mg_{0.05} catalyst

was placed in quartz reactor and the He carrier gas was fed at 130 °C for 1 h, the influent was then switched to the composite gas with oxygen factor ratio of 2.0 in He balance at a total flow rate of 100 mL min⁻¹. The reaction temperature was controlled by a temperature controller and the test was run for 48 h, with the results shown in Fig. 5.9. Four cases chosen to investigate the stability of the catalysts were (A) without the presence of H₂O and CO₂, (B) CO₂ 20%, (C) H₂O 15% and (D) CO₂ 20% and H₂O 15%. The results showed no deactivation during study period with the complete CO conversion and 80-90% CO₂ selectivity in case A (Fig. 5.9A). Addition of 20% CO₂ decreased both CO conversion and CO₂ selectivity to around 95% and 65-70% as shown in Fig. 5.9B, respectively. Even though the catalytic performance was significantly lower but a stable CO conversion and CO₂ selectivity was observed. The drop of catalytic activities in the presence of CO₂ in feed stream was caused from competitive adsorption of CO₂ on the active sites and inhibition of oxygen mobility due to carbonate was formed on the ceria support. The catalytic performance of 10.0wt%CuO/Ce_{0.95}Mg_{0.05} catalyst in the presence of 15% H₂O was expressed in Fig 5.9C. CO conversion was lower to around 95% while CO₂ selectivity was remained at the same level with case A around 80-90%. The negative effect on catalytic performance was due to blocking of water on the active sites, limiting the access of reactant to catalyst surface [39, 45, 73, 83]. When CO₂ 20% and H₂O 15% were present in feed stream, CO conversion dropped to 90% with CO₂ selectivity lower to 65-70%, revealed the diminish of catalytic performance due to water blocking and carbonate

adsorption. It should be noticed that no deactivation was observed in each case, suggested that the optimal catalyst has high performance and durability with the tolerant to CO₂ and H₂O.

After testing the stability of the 10.0wt%CuO/Ce_{0.95}Mg_{0.05} catalyst, the regeneration of the spent catalysts was then studied and shown in Fig. 5.10. To eliminate any impurities species on the catalyst surface and improve the performance of the spent catalysts, thermal treatment under an atmosphere of He, instead of the reactant gas stream, was then carried out for 2 h at 200 °C. After regeneration, the catalytic activities were tested with a reactant gas composition of 40% H₂, 0.75% O₂, and 0.75% CO in helium balance at 130 °C for 24h. The catalytic performance of the fresh catalysts was presented in Zone A in Fig. 5.10 with the regenerated catalysts, with the addition of CO₂ (Zone B), CO₂ and H₂O (Zone C) and without any addition in feed stream (Zone D). The catalytic performance of the regenerated catalysts was increased and approached the performance of the fresh catalysts, revealed that the in situ thermal regeneration could recovered the active sites for PROX reaction [84].

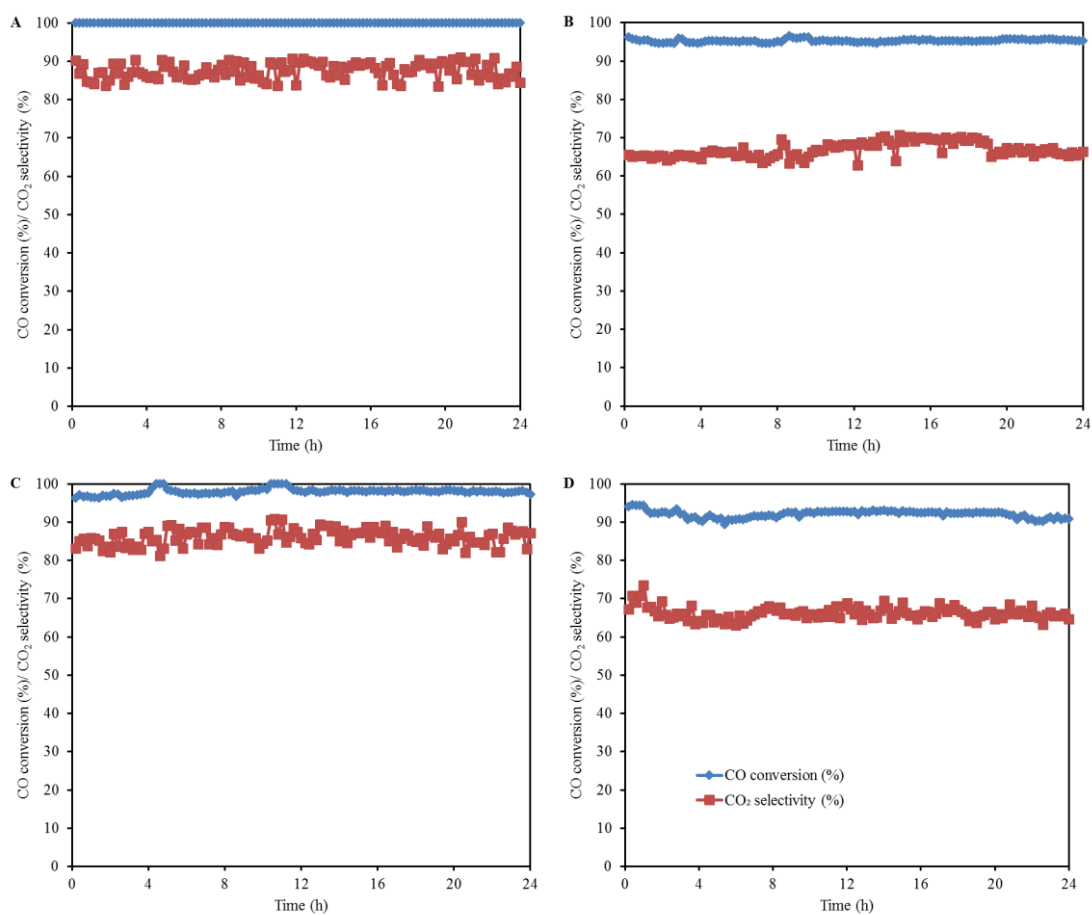


Figure 5.9 Catalyst stability test in the PROX reaction in terms of the CO conversion level (◆) and CO₂ selectivity (■) over 0.13 g of 10wt%CuO/Ce_{0.95}Mg_{0.05} catalyst at 130 °C and oxygen excess factor of 2; (A) without CO₂ and H₂O, (B) CO₂ 20%, (C) H₂O 15% and (D) CO₂ 20% and H₂O 15%

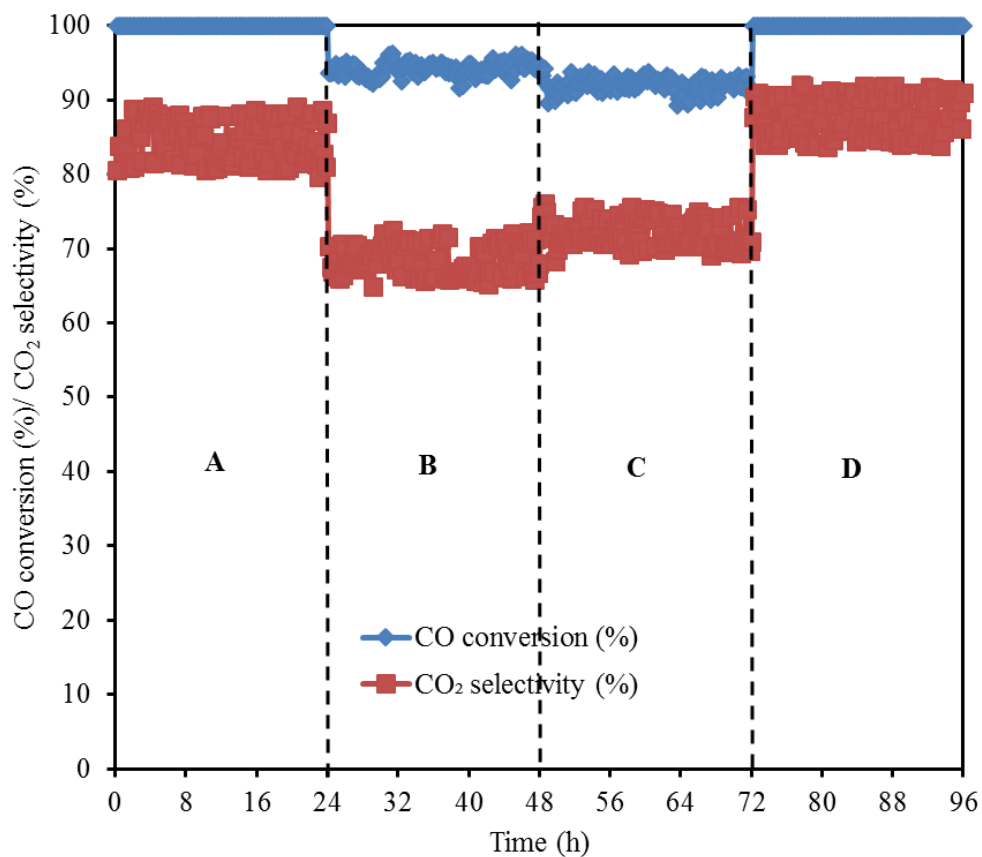


Figure 5.10 Catalyst stability test in sequence via PROX reaction in terms of the CO conversion level (◆) and CO₂ selectivity (■) over 0.13 g of 10wt%CuO/Ce_{0.95}Mg_{0.05} catalyst at 130 °C and oxygen excess factor of 2; (A) without CO₂ and H₂O, (B) CO₂ 20%, (C) CO₂ 20% and H₂O 15% and (D) without CO₂ and H₂O.

CHAPTER VI

INTEGRATION OF MSR AND PROX UNIT

In this chapter, catalytic performance of fuel processor which integrate both methanol steam reformer (MSR) and preferential oxidation (PROX) of CO unit for high purity hydrogen production was investigated. The effective catalyst for each unit was employed in the fuel processor. The methanol steam reformer was operated at optimum conditions over $\text{Cu}_{0.5}\text{Ce}_{0.25}\text{Mg}_{0.05}/\text{Al}$ catalyst which obtained from chapter 4 while the optimum conditions of PROX unit over 10.0wt%CuO/ $\text{Ce}_{0.95}\text{Mg}_{0.05}$ catalyst was achieved from chapter 5. The durability of the effective catalysts at optimum conditions for fuel processor to achieved maximal methanol conversion with CO level less than 100 ppm was studied in this chapter

6.1 Stability test

Durability of the catalysts for fuel processor was tested in period of 48 h, as shown in Fig. 6.1-6.3. The effective catalyst for each unit was employed in the fuel processor; 0.1 g of $\text{Cu}_{0.5}\text{Ce}_{0.25}\text{Mg}_{0.05}/\text{Al}$ catalyst for MSR unit and 0.13 g of 10.0wt%CuO/ $\text{Ce}_{0.95}\text{Mg}_{0.05}$ catalyst for PROX unit. The MSR catalyst was reduced in situ with 40 mL min^{-1} of H_2 in Ar balance at 300 °C for 1 h and then cooling down in He carrier gas to 250 °C. After the catalysts were placed in the fuel processor and the He

carrier gas was fed at 40 mL h^{-1} for 1 h, the influent was then switched to water/methanol mixture with an S/C ratio of 1.75 in He balance at a total flow rate of 40 mL min^{-1} while additional oxygen was mixed with reformat with the oxygen factor ratio of 2.0. The reaction temperature was controlled by a temperature controller at the optimal temperature for each unit; $250 \text{ }^\circ\text{C}$ for MSR and $130 \text{ }^\circ\text{C}$ for PROX. The catalytic performance for fuel processor was reported in terms of methanol conversion level, CO selectivity and H_2 yield as shown in Fig. 6.1. Complete methanol conversion was obtained in the first 30 h and then slightly decreased to around 97% and remained constant throughout the studied period. Hydrogen yield slightly increased from 45% to 47% while no CO could be detected, implied that PROX catalyst was active and stable throughout the studied period. However, Product composition as shown in Fig 6.2 revealed that the effluent gas consisted of $\sim 60\% \text{H}_2$ and $\sim 40\% \text{CO}_2$ (dry basis), suggested that some of H_2 was oxidized to water. The hydrogen production rate was presented in Fig 6.3. The yield of hydrogen was 45-47% with the production rate of $\sim 120 \text{ L d}^{-1} \text{ g.cat}^{-1}$.

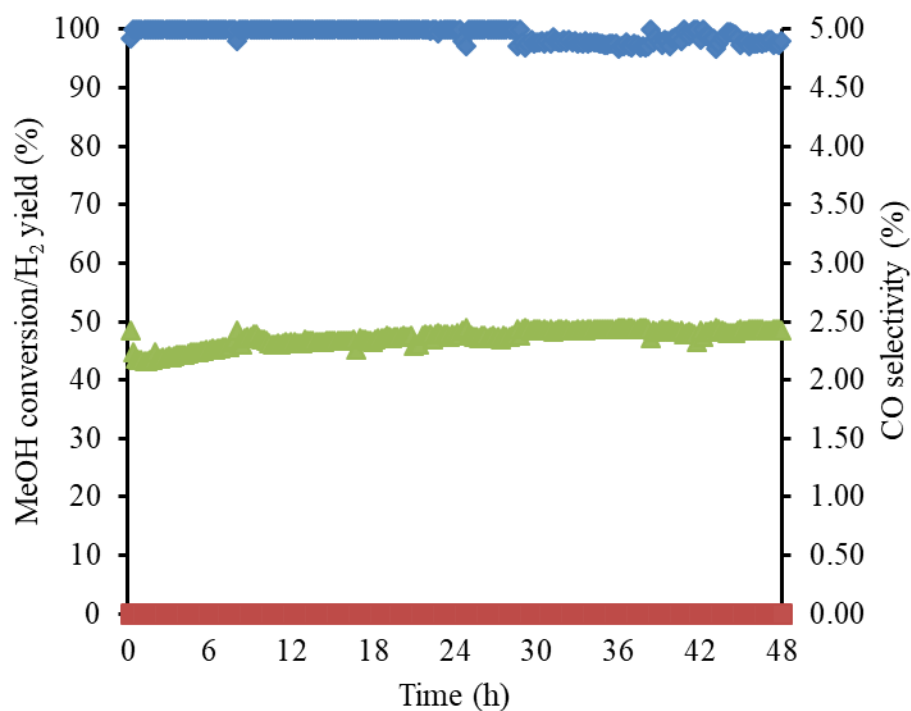


Figure 6.1 Catalyst stability test for fuel processor at the optimum conditions in terms of the methanol conversion level (◆), CO selectivity (■) and H₂ yield (▲) over 0.1 g of Cu_{0.5}Ce_{0.25}Mg_{0.05}/Al catalyst in MSR unit at 250 °C and a S/C ratio of 1.75 and 0.13 g of 10wt%CuO/Ce_{0.95}Mg_{0.05} catalyst in PROX unit at 130 °C and oxygen excess factor=2.

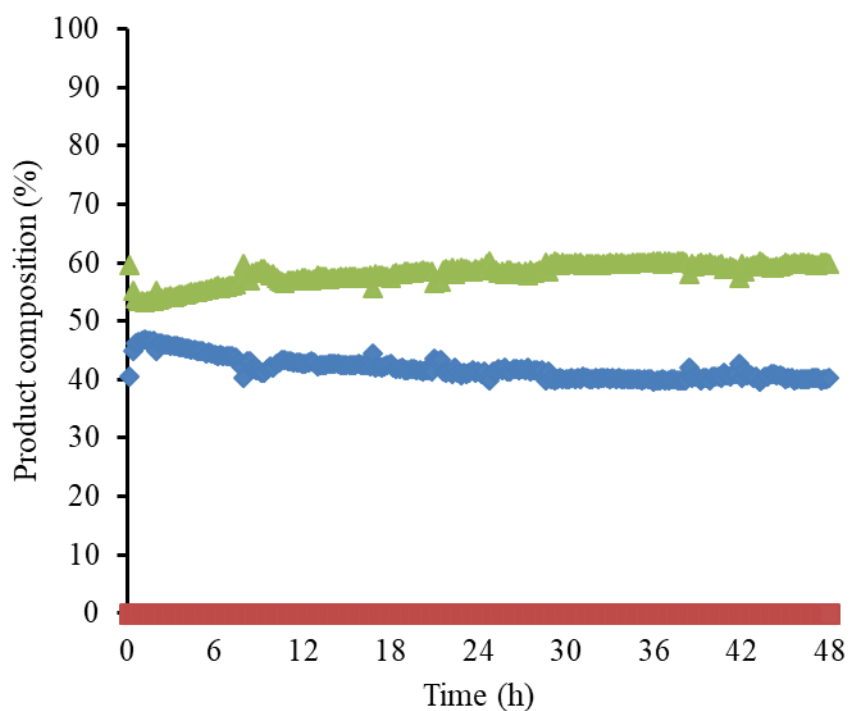


Figure 6.2 Product composition for fuel processor at the optimum conditions over 0.1 g of $\text{Cu}_{0.5}\text{Ce}_{0.25}\text{Mg}_{0.05}/\text{Al}$ catalyst in MSR unit at 250 °C and a S/C ratio of 1.75 and 0.13 g of 10wt% $\text{CuO}/\text{Ce}_{0.95}\text{Mg}_{0.05}$ catalyst in PROX unit at 130 °C and oxygen excess factor=2. H₂ (▲), CO (■) and CO₂ (◆)

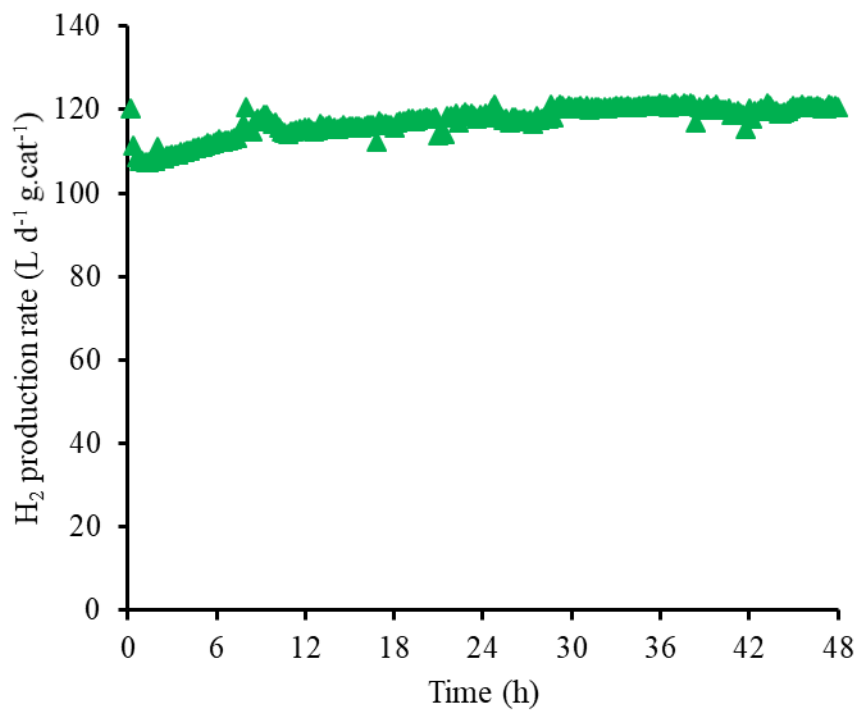


Figure 6.3 Hydrogen production rate for fuel processor at the optimum conditions over 0.1 g of $\text{Cu}_{0.5}\text{Ce}_{0.25}\text{Mg}_{0.05}/\text{Al}$ catalyst in MSR unit at 250 °C and a S/C ratio of 1.75 and 0.13 g of 10wt% $\text{CuO}/\text{Ce}_{0.95}\text{Mg}_{0.05}$ catalyst in PROX unit at 130 °C and oxygen excess factor=2.

CHAPTER VII

CONCLUSIONS

7.1 Methanol steam reformer unit

To attain a high catalyst activity and stability in the MSR reaction to yield a high H₂ yield and low CO selectivity, a series of copper-based catalysts prepared by co-precipitation with ceria or MgO or both were investigated in this work. The catalytic performance was assessed in terms of the methanol conversion level, CO selectivity and H₂ yield. The methanol conversion level and H₂ yield obtained with the two mono-promoter catalysts (Cu_{0.3}Mg_{0.3}/Al and Cu_{0.3}Ce_{0.3}/Al) were higher than that of the catalyst without a promoter (Cu_{0.3}/Al), which is probably due to the higher dispersion level of copper species on the Cu_{0.3}Mg_{0.3}/Al catalyst and the strong interaction between copper and ceria on the Cu_{0.3}Ce_{0.3}/Al catalyst that led to a lower reduction temperature and enhanced the catalytic activity. It is likely that MgO enhanced the WGS reaction of CO while ceria, with its oxygen storage, enhanced the MD reaction, resulting in a lower CO selectivity for the Cu_{0.3}Mg_{0.3}/Al catalyst and a higher methanol conversion level for the Cu_{0.3}Ce_{0.3}/Al catalyst. When adding MgO to Cu_{0.3}Ce_{0.3}/Al to form the bi-promoter catalyst, a higher methanol conversion level and H₂ yield and lower CO selectivity was obtained (at 225–250 °C) than with either mono-promoter catalyst. The increased

catalytic activity by adding MgO was possibly due to the smaller size of copper crystallites, the improved copper dispersion, and the lower reduction temperature. The Mg^{2+} ions penetrated into the cerium structure and caused oxygen vacancy defects in the ceria, which enhanced the catalytic performance. That a lower CO selectivity was obtained at a S/C ratio of 2 inferred that an excess of steam drove the WGS reaction forward. An experimental FCCCD-RSM matrix with five central points at a 95% confidence interval was fabricated in order to determine the optimal condition, where the 3D response surface curve contour, constructed by connecting constant estimated responses, revealed the optimal operating region for maximal methanol conversion (100%) and H_2 yield (28.9–29.4%) with a low CO selectivity (0.16–0.18%), to be a copper level of 46–50 wt%, $\text{Mg}/(\text{Ce}+\text{Mg})$ of 16.2–18.0 wt%, temperature of 245–250 °C and S/C ratio of 1.74–1.80. To verify the RSM model, four more experiments were randomly performed, with the estimated responses being close (within $\pm 3\%$) to the experimental results, while two more trials where one factor was outside of the given range, performed in order to test the sensitivity of the model, were also within $\pm 3.0\%$, suggesting that the RSM model was acceptable. In practice, a good catalyst has a high performance and durability. Therefore, the optimal $\text{Cu}_{0.5}\text{Ce}_{0.25}\text{Mg}_{0.05}/\text{Al}$ catalyst (from the 3D-RSM evaluation) was evaluated for its MSR catalytic activity and stability at the optimal operating region over 72 h. The catalyst expressed a constant complete methanol conversion level and CO selectivity level of 0.14–0.16% throughout the

study period, with a H₂ yield of 24–25%. There were no signs of catalyst deactivation during the study period.

7.2 Preferential oxidation of CO unit

10.0wt%CuO/Ce_{0.95}Mg_{0.05} catalyst prepared by impregnate copper on modified ceria support, appeared to be an excellent catalyst for PROX as is performed high catalytic activities with complete CO conversion and high CO₂ selectivity more than 80% at 130°C. Modified ceria support with MgO improved the activity by decreased reduction temperature of copper species and promoted WGS reaction. The statistical design of experiment was used to investigate effect of reaction temperature, CO level, O₂ level and amount of catalysts. It was observed that CO conversion significantly increased with reaction temperature and O₂/CO level while CO₂ selectivity decreased at high temperature. The fitted models from Box behnken-RSM revealed the desired condition were as followed; CO level of 0.65–0.75 %, O₂ level of 0.80-0.90% ($\lambda \approx 2$), temperature of 130–140 °C and amount of catalyst of 0.10–0.13 g. To simulate a real reformat gas, addition of CO₂ and H₂O on feed stream were studied. The presence of CO₂ and H₂O had a negative effect on both response due to blocking of carbonate and water on the active sites. Even though the catalytic performance was significantly lower but a stable CO conversion and CO₂ selectivity was observed

7.3 Integration of MSR and PROX unit

In this part, integration of methanol steam reformer (MSR) and preferential oxidation (PROX) of CO unit for high purity hydrogen production was continuously operated. The effective catalyst for each unit was employed in the fuel processor. Complete methanol conversion was achieved with the effluent composition of $\sim 60\% \text{H}_2$ and $\sim 40\% \text{CO}_2$ (dry basis). Moreover, CO was completely removed from the effluent stream. This revealed the potential of the fuel processor for further development for fuel cell applications. This hydrogen fuel processor could produce hydrogen at a rate of $\sim 120 \text{ L d}^{-1} \text{ g.cat}^{-1}$.

7.4 Recommendation

Although both the MSR catalyst and PROX catalyst exhibited excellent catalytic performance for high purity hydrogen production. Nevertheless, it was still introduced in lab scale. In practice, more parameters were continued for further study before applying to the industrial. Especially, the long start-up time for the MSR catalyst, which needs prior in situ reduction, would limit the applications of the fuel processor. Moreover, the fuel processor should be self-sustained. The introduction of methanol oxidation as a catalytic burner was one of the remarkable milestones to reduce external heat supply.

REFERENCES

- [1] Chen, G. Q. and Wu, X. F. Energy overview for globalized world economy: Source, supply chain and sink. Renewable and Sustainable Energy Reviews 69 (2017): 735-749.
- [2] Quadrelli, R. and Peterson, S. The energy-climate challenge: Recent trends in CO₂ emissions from fuel combustion. Energy Policy 35 (2007): 5938-5952.
- [3] Van Hoa, T. and Limskul, K. Economic impact of CO₂ emissions on Thailand's growth and climate change mitigation policy: A modelling analysis. Economic Modelling 33 (2013): 651-658.
- [4] Bretschger, L. Climate policy and economic growth. Resource and Energy Economics 49 (2017): 1-15.
- [5] Al-Amin, A. Q., Rasiah, R. and Chenayah, S. Prioritizing climate change mitigation: An assessment using Malaysia to reduce carbon emissions in future. Environmental Science & Policy 50 (2015): 24-33.
- [6] Fouquet, R. Lessons from energy history for climate policy: Technological change, demand and economic development. Energy Research & Social Science 22 (2016): 79-93.
- [7] Dincer, I. and Acar, C. Review and evaluation of hydrogen production methods for better sustainability. International Journal of Hydrogen Energy 40 (2015): 11094-11111.
- [8] Ni, M., Leung, D. Y. C., Leung, M. K. H. and Sumathy, K. An overview of hydrogen production from biomass. Fuel Processing Technology 87 (2006): 461-472.
- [9] Holladay, J. D., Hu, J., King, D. L. and Wang, Y. An overview of hydrogen production technologies. Catalysis Today 139 (2009): 244-260.
- [10] Sá, S., Silva, H., Brandão, L., Sousa, J. M. and Mendes, A. Catalysts for methanol steam reforming-A review. Applied Catalysis B: Environmental 99 (2010): 43-57.
- [11] Tanksale, A., Beltramini, J. N. and Lu, G. M. A review of catalytic hydrogen production processes from biomass. Renewable and Sustainable Energy Reviews 14 (2010): 166-182.

- [12] Singh, S., et al. Hydrogen: A sustainable fuel for future of the transport sector. Renewable and Sustainable Energy Reviews 51 (2015): 623-633.
- [13] Mrad, M., Hammoud, D., Gennequin, C., Aboukaïs, A. and Abi-Aad, E. A comparative study on the effect of Zn addition to Cu/Ce and Cu/Ce-Al catalysts in the steam reforming of methanol. Applied Catalysis A: General 471 (2014): 84-90.
- [14] Pongstabodee, S., Monyanon, S. and Luengnaruemitchai, A. Hydrogen production via methanol steam reforming over Au/CuO, Au/CeO₂, and Au/CuO-CeO₂ catalysts prepared by deposition-precipitation. Journal of Industrial and Engineering Chemistry 18 (2012): 1272-1279.
- [15] Das, D., et al. Methanol steam reforming behavior of copper impregnated over CeO₂-ZrO₂ derived from a surfactant assisted coprecipitation route. International Journal of Hydrogen Energy 40 (2015): 10463-10479.
- [16] Mishra, A. and Prasad, R. A Review on Preferential Oxidation of Carbon Monoxide in Hydrogen Rich Gases. Bulletin of Chemical Reaction Engineering & Catalysis 6 (2011): 1-14.
- [17] Liu, K., Wang, A. and Zhang, T. Recent Advances in Preferential Oxidation of CO Reaction over Platinum Group Metal Catalysts. ACS Catalysis 2 (2012): 1165-1178.
- [18] IEA. World Energy Outlook 2016. France: International Energy Agency, 2016.
- [19] BP. BP Statistical Review of World Energy June 2016. London, UK: BP 2016.
- [20] กรมพัฒนาพลังงานทดแทนและอนุรักษ์พลังงาน. สถานการณ์พลังงานของประเทศไทย มกราคม-ธันวาคม 2558. กรุงเทพมหานคร: กรมพัฒนาพลังงานทดแทนและอนุรักษ์พลังงาน กระทรวงพลังงาน, 2016.
- [21] กรมพัฒนาพลังงานทดแทนและอนุรักษ์พลังงาน. แผนพัฒนาพลังงานทดแทนและพลังงานทางเลือก พ.ศ.2558-2579. กรุงเทพมหานคร: กรมพัฒนาพลังงานทดแทนและอนุรักษ์พลังงาน กระทรวงพลังงาน, 2016.
- [22] Wang, Y., Chen, K. S., Mishler, J., Cho, S. C. and Adroher, X. C. A review of polymer electrolyte membrane fuel cells: Technology, applications, and needs on fundamental research. Applied Energy 88 (2011): 981-1007.

- [23] Zhao, T., Kruer, K. and Nguyen, T. Advances in Fuel Cells. Oxford, UK: Elsevier Ltd, 2007.
- [24] Liu, K., Song, C. and Subramani, V. Hydrogen and syngas production and purification technologies. Hoboken, New Jersey: John Wiley & Sons, Inc., 2009.
- [25] Kalamaras, C. M. and Efstathiou, A. M. Hydrogen Production Technologies: Current State and Future Developments. Conference Papers in Energy 2013 (2013): 1-9.
- [26] Sperle, T., Chen, D., Lødeng, R. and Holmen, A. Pre-reforming of natural gas on a Ni catalyst. Applied Catalysis A: General 282 (2005): 195-204.
- [27] Olah, G. A., Goeppert, A. and Prakash, G. K. S. Beyond Oil and Gas: The Methanol Economy. Germany: WILEY-VCH, 2009.
- [28] Yang, M., Jiao, F., Li, S., Li, H. and Chen, G. A self-sustained, complete and miniaturized methanol fuel processor for proton exchange membrane fuel cell. Journal of Power Sources 287 (2015): 100-107.
- [29] Perego, C. and Villa, P. Catalyst preparation methods. Catalysis Today 34 (1997): 281-305.
- [30] Schwarz, J. A., Contescu, C. and Contescu, A. Methods for Preparation of Catalytic Materials. Chemical Reviews 95 (1995): 477-510.
- [31] Copéret, C. Synthesis of Solid Catalysts. Edited by Krijn P. de Jong. ChemCatChem 2 (2010): 706-706.
- [32] Nguyen, T.-D. and Do, T.-O. Size- and Shape-Controlled Synthesis of Monodisperse Metal Oxide and Mixed Oxide Nanocrystals. Quebec, Canada: Department of Chemical Engineering, Laval University, 2011.
- [33] Einarsrud, M. A. and Grande, T. 1D oxide nanostructures from chemical solutions. Chem Soc Rev 43 (2014): 2187-99.
- [34] Leofanti, G., et al. Catalyst characterization: characterization techniques. Catalysis Today 34 (1997): 307-327.
- [35] Pechenkin, A. A., Badmaev, S. D., Belyaev, V. D. and Sobyenin, V. A. Performance of bifunctional CuO-CeO₂/γ-Al₂O₃ catalyst in dimethoxymethane steam reforming to hydrogen-rich gas for fuel cell feeding. Applied Catalysis B: Environmental 166-167 (2015): 535-543.

- [36] Wang, X., et al. Steam reforming of dimethyl ether over Cu-Ni/ γ -Al₂O₃ bifunctional catalyst prepared by deposition-precipitation method. International Journal of Hydrogen Energy 35 (2010): 4060-4068.
- [37] Zhang, R., Wang, H. and Hou, X. Catalytic reforming of toluene as tar model compound: effect of Ce and Ce-Mg promoter using Ni/olivine catalyst. Chemosphere 97 (2014): 40-6.
- [38] Mallesham, B., Sudarsanam, P., Reddy, B. V. S. and Reddy, B. M. Development of cerium promoted copper-magnesium catalysts for biomass valorization: Selective hydrogenolysis of bioglycerol. Applied Catalysis B: Environmental 181 (2016): 47-57.
- [39] Mariño, F., Descorme, C. and Duprez, D. Supported base metal catalysts for the preferential oxidation of carbon monoxide in the presence of excess hydrogen (PROX). Applied Catalysis B: Environmental 58 (2005): 175-183.
- [40] Li, J., Han, Y., Zhu, Y. and Zhou, R. Purification of hydrogen from carbon monoxide for fuel cell application over modified mesoporous CuO-CeO₂ catalysts. Applied Catalysis B: Environmental (2011): 72-80.
- [41] Li, J., Zhu, P. and Zhou, R. Effect of the preparation method on the performance of CuO-MnO_x-CeO₂ catalysts for selective oxidation of CO in H₂-rich streams. Journal of Power Sources 196 (2011): 9590-9598.
- [42] Maciel, C. G., Silva, T. d. F., Hirooka, M. I., Belgacem, M. N. and Assaf, J. M. Effect of nature of ceria support in CuO/CeO₂ catalyst for PROX-CO reaction. Fuel 97 (2012): 245-252.
- [43] Araiza, D. G., Gómez-Cortés, A. and Díaz, G. Partial oxidation of methanol over copper supported on nanoshaped ceria for hydrogen production. Catalysis Today 282 (2017): 185-194.
- [44] Yan, L., et al. Synthesis of Pr-doped ceria nanorods with a high specific surface area. Scripta Materialia 56 (2007): 301-304.
- [45] Gamarra, D. and Martínez-Arias, A. Preferential oxidation of CO in rich H₂ over CuO/CeO₂: Operando-DRIFTS analysis of deactivating effect of CO₂ and H₂O. Journal of Catalysis 263 (2009): 189-195.

- [46] Park, G.-G., et al. Hydrogen production with integrated microchannel fuel processor using methanol for portable fuel cell systems. Catalysis Today 110 (2005): 108-113.
- [47] Wang, H. H. F., Chen, S. C., Yang, S. Y., Yeh, G. T. and Rei, M. H. Design of compact methanol reformer for hydrogen with low CO for the fuel cell power generation. International Journal of Hydrogen Energy 37 (2012): 7487-7496.
- [48] Svintsitskiy, D. A., et al. In Situ XRD, XPS, TEM, and TPR Study of Highly Active in CO Oxidation CuO Nanopowders. The Journal of Physical Chemistry C 117 (2013): 14588-14599.
- [49] Zhang, L., et al. Effects of precipitation aging time on the performance of CuO/ZnO/CeO₂-ZrO₂ for methanol steam reforming. Journal of Fuel Chemistry and Technology 41 (2013): 883-888.
- [50] Zhou, X., Meng, M., Sun, Z., Li, Q. and Jiang, Z. Prominent enhancement of Mn or Co addition on the performance of Cu-Ce-O catalyst used for H₂ production via dimethyl ether steam reforming. Chemical Engineering Journal 174 (2011): 400-407.
- [51] Al-Musa, A. A., et al. Steam reforming of iso-octane toward hydrogen production over mono- and bi-metallic Cu-Co/CeO₂ catalysts: Structure-activity correlations. International Journal of Hydrogen Energy 39 (2014): 19541-19554.
- [52] Villaverde, M. M., Garetto, T. F. and Marchi, A. J. Liquid-phase transfer hydrogenation of furfural to furfuryl alcohol on Cu-Mg-Al catalysts. Catalysis Communications 58 (2015): 6-10.
- [53] Chen, L., Liu, Z., Sun, P. and Huo, W. Formulation of a fuel spray SMD model at atmospheric pressure using Design of Experiments (DoE). Fuel 153 (2015): 355-360.
- [54] Monyanon, S., Luengnaruemitchai, A. and Pongstabodee, S. Optimization of methanol steam reforming over a Au/CuO-CeO₂ catalyst by statistically designed experiments. Fuel Processing Technology 96 (2012): 160-168.
- [55] Perezhernandez, R., Gutierrezmartinez, A. and Gutierrezwing, C. Effect of Cu loading on CeO₂ for hydrogen production by oxidative steam reforming of methanol. International Journal of Hydrogen Energy 32 (2007): 2888-2894.

- [56] Wu, Y., Gu, F., Xu, G., Zhong, Z. and Su, F. Hydrogenolysis of cellulose to C4-C7 alcohols over bi-functional CuO-MO/Al₂O₃ (M=Ce, Mg, Mn, Ni, Zn) catalysts coupled with methanol reforming reaction. Bioresour Technol 137 (2013): 311-317.
- [57] Wang, J., Chernavskii, P. A., Wang, Y. and Khodakov, A. Y. Influence of the support and promotion on the structure and catalytic performance of copper-cobalt catalysts for carbon monoxide hydrogenation. Fuel 103 (2013): 1111-1122.
- [58] Nolan, M., Parker, S. C. and Watson, G. W. The electronic structure of oxygen vacancy defects at the low index surfaces of ceria. Surface Science 595 (2005): 223-232.
- [59] Li, Y., et al. Catalytic activity for CO oxidation of Cu-CeO₂ composite nanoparticles synthesized by a hydrothermal method. Anal. Methods 7 (2015): 3238-3245.
- [60] Shukla, A., Singha, R. K., Konathala, L. N. S., Sasaki, T. and Bal, R. Catalytic oxidation of aromatic amines to azoxy compounds over a Cu-CeO₂ catalyst using H₂O₂ as an oxidant. RSC Adv. 6 (2016): 22812-22820.
- [61] Chen, J., et al. Characterization and catalytic performance of Cu/CeO₂ and Cu/MgO-CeO₂ catalysts for NO reduction by CO. Applied Catalysis A: General 363 (2009): 208-215.
- [62] Dhal, J. P., Sethi, M., Mishra, B. G. and Hota, G. MgO nanomaterials with different morphologies and their sorption capacity for removal of toxic dyes. Materials Letters 141 (2015): 267-271.
- [63] Osaka, M., Miwa, S. and Tachi, Y. Simple fabrication process for CeO₂-MgO composite as surrogate for actinide-containing target for use in nuclear fuel. Ceramics International 32 (2006): 659-663.
- [64] Thouchprasitchai, N., Luengnaruemitchai, A. and Pongstabodee, S. The activities of Cu-based Mg-Al layered double oxide catalysts in the water gas shift reaction. International Journal of Hydrogen Energy 41 (2016): 14147-14159.

- [65] Qin, H., Guo, C., Sun, C. and Zhang, J. Influence of the support composition on the hydrogenation of methyl acetate over Cu/MgO-SiO₂ catalysts. Journal of Molecular Catalysis A: Chemical 409 (2015): 79-84.
- [66] Clausell, J. V., Bastida, J., Serrano, F. J., Pardo, P. and Huertas, F. J. A new FESEM procedure for assessment of XRD microstructural data of kaolinites. Applied Clay Science 37 (2007): 127-132.
- [67] Torrente-Murciano, L., et al. Shape-dependency activity of nanostructured CeO₂ in the total oxidation of polycyclic aromatic hydrocarbons. Applied Catalysis B: Environmental 132-133 (2013): 116-122.
- [68] López, J. M., et al. The prevalence of surface oxygen vacancies over the mobility of bulk oxygen in nanostructured ceria for the total toluene oxidation. Applied Catalysis B: Environmental 174-175 (2015): 403-412.
- [69] Huang, Y., Cai, Y., Qiao, D. and Liu, H. Morphology-controllable synthesis and characterization of CeO₂ nanocrystals. Particuology 9 (2011): 170-173.
- [70] Hirano, M. and Kato, E. Hydrothermal Synthesis of Cerium(IV) Oxide. Journal of the American Ceramic Society 79 (2005): 777-780.
- [71] Wu, Q., et al. Great Influence of Anions for Controllable Synthesis of CeO₂ Nanostructures: From Nanorods to Nanocubes. The Journal of Physical Chemistry C 112 (2008): 17076-17080.
- [72] Araújo, V. D., Bellido, J. D. A., Bernardi, M. I. B., Assaf, J. M. and Assaf, E. M. CuO-CeO₂ catalysts synthesized in one-step: Characterization and PROX performance. International Journal of Hydrogen Energy 37 (2012): 5498-5507.
- [73] Arango-Díaz, A., et al. Preferential CO oxidation (CO-PROX) catalyzed by CuO supported on nanocrystalline CeO₂ prepared by a freeze-drying method. Applied Catalysis A: General 477 (2014): 54-63.
- [74] Zeng, S., Zhang, W., Śliwa, M. and Su, H. Comparative study of CeO₂/CuO and CuO/CeO₂ catalysts on catalytic performance for preferential CO oxidation. International Journal of Hydrogen Energy 38 (2013): 3597-3605.
- [75] Maciel, C. G., Silva, T. d. F., Profeti, L. P. R., Assaf, E. M. and Assaf, J. M. Study of CuO/CeO₂ catalyst with for preferential CO oxidation reaction in hydrogen-rich feed (PROX-CO). Applied Catalysis A: General 431-432 (2012): 25-32.

- [76] Qi, L., et al. Influence of cerium precursors on the structure and reducibility of mesoporous CuO-CeO₂ catalysts for CO oxidation. Applied Catalysis B: Environmental 119-120 (2012): 308-320.
- [77] Laguna, O. H., et al. Preferential oxidation of CO (CO-PROX) over CuO_x/CeO₂ coated microchannel reactor. Catalysis Today 180 (2012): 105-110.
- [78] Di Benedetto, A., Landi, G. and Lisi, L. CO reactive adsorption at low temperature over CuO/CeO₂ structured catalytic monolith. International Journal of Hydrogen Energy 42 (2017): 12262-12275.
- [79] Laguna, O. H., et al. Influence of the O₂/CO ratio and the presence of H₂O and CO₂ in the feed-stream during the preferential oxidation of CO (PROX) over a CuO_x/CeO₂-coated microchannel reactor. Catalysis Today 203 (2013): 182-187.
- [80] Zhang, Q., Shore, L. and Farrauto, R. J. Selective CO oxidation over a commercial PROX monolith catalyst for hydrogen fuel cell applications. International Journal of Hydrogen Energy 37 (2012): 10874-10880.
- [81] Laguna, O. H., González Castaño, M., Centeno, M. A. and Odriozola, J. A. Microreactors technology for hydrogen purification: Effect of the catalytic layer thickness on CuO_x/CeO₂-coated microchannel reactors for the PROX reaction. Chemical Engineering Journal 275 (2015): 45-52.
- [82] Ferreira, S. L., et al. Box-Behnken design: an alternative for the optimization of analytical methods. Anal Chim Acta 597 (2007): 179-86.
- [83] Di Benedetto, A., Landi, G., Lisi, L. and Russo, G. Role of CO₂ on CO preferential oxidation over CuO/CeO₂ catalyst. Applied Catalysis B: Environmental 142-143 (2013): 169-177.
- [84] Sakwarathorn, T., Luengnaruemitchai, A. and Pongstabodee, S. Preferential CO oxidation in H₂-rich stream over Au/CeO₂ catalysts prepared via modified deposition-precipitation. Journal of Industrial and Engineering Chemistry 17 (2011): 747-754.



APPENDIX

จุฬาลงกรณ์มหาวิทยาลัย
CHULALONGKORN UNIVERSITY

APPENDIX A

CATALYST PREPARATION

A.1 Co-precipitation method

Example: Preparation of $\text{Cu}_{0.50}\text{Ce}_{0.25}\text{Mg}_{0.05}/\text{Al}$ 1000 mg

1. Preparation of mixed nitrate solution 50 mL

Composition	wt%	wt (mg)	M.W.	mole (mmol)	M.W. of nitrate salt	wt of nitrate salt (mg)
Cu	50	500	63.55	7.87	241.60	1,898.50
CeO ₂	25	250	172.11	1.45	434.23	630.74
MgO	5	50	40.30	1.24	256.40	318.11
Al ₂ O ₃	20	200	101.96	1.96	375.13	735.83
Total	100	1000		12.52		3,583.18

2. Preparation of 1.0 M Na₂CO₃ aqueous solution 1000 mL

Sodium carbonate anhydrous (Na₂CO₃) = 1.0 M

M.W. of Na₂CO₃ = 105.99 g mol⁻¹

So, the amount of Na₂CO₃ required = 105.99 g

A.2 Hydrothermal method

Example: Preparation of $\text{Ce}_{0.95}\text{Mg}_{0.05}$ in NaOH 15 M

1. Preparation of mixed nitrate salt

Basis 1,200 mg of $\text{Ce}(\text{NO}_3)_3 \cdot 6\text{H}_2\text{O}$

Composition	wt%	wt (mg)	M.W.	mole (mmol)	M.W. of nitrate salt	wt of nitrate salt (mg)
CeO_2	95	475.63	172.11	2.76	434.23	1,200.0
MgO	5	25.03	40.30	0.62	256.40	159.2
Total	100	500.66		3.38		1,359.2

2. Preparation of 15.0 M NaOH aqueous solution 80 mL

Sodium hydroxide anhydrous (Na_2CO_3) = 15.0 M

M.W. of NaOH = 40.0 g mol^{-1}

the amount of NaOH required = $15/1,000 \times 80 = 1.2$ mol

So, the amount of NaOH required = $1.2 \times 40 = 48.0$ g

A.3 Impregnation method

Example: Preparation of 10% $\text{CuO}/\text{Ce}_{0.95}\text{Mg}_{0.05}$ in NaOH 15 M 1000 mg

1. Preparation of mixed stock solution 100 mL

M.W. of $\text{Cu}(\text{NO}_3)_2 \cdot 3\text{H}_2\text{O} = 241.60 \text{ g mol}^{-1}$

$\text{Cu}(\text{NO}_3)_2 \cdot 3\text{H}_2\text{O}$ solution = 1.0 M

So, the amount of $\text{Cu}(\text{NO}_3)_2 \cdot 3\text{H}_2\text{O}$ required = 24.16 g

M.W. of CuO = 79.55 g mol^{-1}

1000 mg of 10%CuO/Ce_{0.95}Mg_{0.05} catalyst consists of 100 mg CuO

100 mg of CuO = $100/79.55 = 0.00126$ mol

CuO 0.00126 mmol used 1.0 M $\text{Cu}(\text{NO}_3)_2 \cdot 3\text{H}_2\text{O}$ solution

= $1,000/1.0 \times 0.00126 = 1.26$ mL



APPENDIX B

CATALYST CHARACTERIZATION

B.1 X-ray diffraction (XRD)

XRD calculation for crystallite size from Debye Scherrer's equation;

$$D_b = \frac{K \times \lambda}{\beta \times \cos \theta}$$

where

D_b	=	crystallite diameter (Å)	
K	=	Scherrer constant	= 0.9
λ	=	X-ray wavelength	= 1.54 Å
β	=	angular width of peak in term of 2θ at FWHM	
θ	=	Bragg's angle of reflection (degree)	

Example: $\text{Cu}_{0.50}\text{Ce}_{0.25}\text{Mg}_{0.05}/\text{Al}$ spent catalyst

To calculate Cu crystallite size from the XRD pattern of $\text{Cu}_{0.50}\text{Ce}_{0.25}\text{Mg}_{0.05}/\text{Al}$ spent catalyst and given data

At center of major peak (111) plane;

$$2\theta = 43.50^\circ \quad ; \text{ data from XRD pattern}$$

$$\theta = 43.50/2 = 21.75^\circ$$

$$= 21.75 \times \pi / 180 = 0.3796$$

$$\beta = 0.8095^\circ \quad ; \text{ data from XRD pattern}$$

$$= 0.8095 \times \pi / 180 = 0.0141$$

Therefore,

$$\text{CuO crystallite size } (D_p) = (0.9 \times 1.54) / (0.0141 \times \cos(0.3796))$$

$$= 105.62 \text{ \AA} = 10.6 \text{ nm}$$

XRD calculation for lattice parameter cubic ceria from Bragg's law;

$$n\lambda = 2d \sin\theta$$

$$\frac{1}{d_{hkl}^2} = (h^2 + k^2 + l^2) \frac{1}{a^2}$$

where

$$d_{hkl} = \text{spacing between layers of atoms at } (hkl) \text{ plane } (\text{\AA})$$

$$a = \text{lattice parameter}$$

$$\lambda = \text{X-ray wavelength} = 1.54 \text{ \AA}$$

$$d = \text{spacing between layers of atoms } (\text{\AA})$$

$$\theta = \text{Bragg's angle of reflection (degree)}$$

$$n = \text{integer} = 1$$

Example: $\text{Cu}_{0.30}\text{Ce}_{0.25}\text{Mg}_{0.05}/\text{Al}$ catalyst

To calculate CeO_2 lattice parameter from the XRD pattern of $\text{Cu}_{0.30}\text{Ce}_{0.25}\text{Mg}_{0.05}/\text{Al}$ catalyst and given data

At center of major peak (111) plane;

$$2\theta = 29.01^\circ \quad ; \text{ data from XRD pattern}$$

$$\theta = 29.01/2 = 14.50^\circ$$

$$= 14.50 \times \pi / 180 = 0.2531$$

Therefore,

$$d = (1 \times 1.54) / (2 \times \sin(0.2531))$$

$$= 3.075 \text{ \AA}$$

$$a = [(1^2 + 1^2 + 1^2) \times 3.075^2]^{0.5}$$

$$= 5.325 \text{ \AA}$$

$$= 0.5325 \text{ nm}$$

จุฬาลงกรณ์มหาวิทยาลัย
CHULALONGKORN UNIVERSITY

APPENDIX C

CATALYTIC ACTIVITY

C.1 Methanol solution preparation

Example: Preparation of Methanol solution with S/C = 1.75 50 mL

Given Methanol concentration = 24.63 mol L^{-1}

$$\begin{aligned} 50 \text{ mL of methanol solution consists of methanol} &= x \text{ mole} \\ &= 1000x/24.63 = 40.6x \text{ mL} \end{aligned}$$

$$\begin{aligned} 50 \text{ mL of methanol solution consists of water} &= y \text{ mole} \\ &= 18y \text{ mL} \end{aligned}$$

$$\text{Therefore, } 40.6x + 18y = 50 \quad (\text{C1})$$

$$\text{From } S/C=1.75; \text{ Therefore, } 1.75x = y \quad (\text{C2})$$

$$\text{Substitute (C2) in (C1); } x = 0.693 \text{ mol}$$

$$y = 1.213 \text{ mol}$$

$$\text{So, the amount of methanol required} = 40.6(0.693) = 28.15 \text{ mL}$$

$$\text{the amount of water required} = 18(1.213) = 21.85 \text{ mL}$$

C.2 Methanol steam reforming

$$\text{Methanol conversion (\%)} = \{([\text{CO}]_{\text{out}} + [\text{CO}_2]_{\text{out}}) \times 100 / [\text{CH}_3\text{OH}]_{\text{in}}\}$$

$$\text{CO selectivity (\%)} = ([\text{CO}]_{\text{out}} \times 100) / ([\text{H}_2]_{\text{out}} + [\text{CO}]_{\text{out}} + [\text{CO}_2]_{\text{out}})$$

$$\text{H}_2 \text{ yield (\%)} = ([\text{H}_2]_{\text{out}} \times 100) / (3 \times [\text{CH}_3\text{OH}]_{\text{in}})$$

where

$$[\text{CH}_3\text{OH}]_{\text{in}} = \text{molar flow rate of methanol in the feed stream (mol min}^{-1}\text{)}$$

$$[\text{H}_2]_{\text{out}} = \text{molar flow rate of H}_2 \text{ in the effluent (mol min}^{-1}\text{)}$$

$$[\text{CO}]_{\text{out}} = \text{molar flow rate of CO in the effluent (mol min}^{-1}\text{)}$$

$$[\text{CO}_2]_{\text{out}} = \text{molar flow rate of CO}_2 \text{ in the effluent (mol min}^{-1}\text{)}$$

Example: Catalytic activity of $\text{Cu}_{0.50}\text{Ce}_{0.25}\text{Mg}_{0.05}/\text{Al}$ catalyst in fuel processor at 48 h

Given Methanol solution with S/C = 1.75 was fed at 1.0 mL h^{-1}

$$P_{\text{out}} = 1 \text{ atm}$$

$$T_{\text{out}} = 30 \text{ }^\circ\text{C}$$

$$\text{Effluent flow rate} = 54 \text{ mL h}^{-1}$$

$$\text{He flow rate} = 40 \text{ mL h}^{-1}$$

$$\begin{aligned} [\text{CH}_3\text{OH}]_{\text{in}} &= (1 \text{ mL}_{\text{sol}} \text{ h}^{-1}) / (60 \text{ min h}^{-1}) (28.15 \text{ mL}_{\text{MeOH}}) / (50 \text{ mL}_{\text{sol}}) \\ &= (9.383 \times 10^{-3} \text{ mL}_{\text{MeOH}} \text{ min}^{-1}) (24.63 \text{ mol}_{\text{MeOH}} / 1,000 \text{ mL}_{\text{MeOH}}) \\ &= 2.311 \times 10^{-4} \text{ mol min}^{-1} \end{aligned}$$

Component	Peak area	Purity (%)	Composition (%)
H ₂ (Standard)	97,744	99.99	-
CO (Standard)	20,012	1.00	-
CO ₂ (Standard)	828,963	30.00	-
H ₂	3,001	3.07	59.77
CO	0	0.00	0.00
CO ₂	57,095	2.07	40.23
total			100

$$\begin{aligned}
 [\text{H}_2]_{\text{out}} &= \text{composition}(\%)/100 \times (\text{effluent flow}) \\
 &= 59.77/100 \times (54.0-40) \\
 &= (8.37 \text{ mL min}^{-1})(1 \text{ atm})/(303 \text{ K})/(82.05 \text{ mL atm K}^{-1} \text{ mol}^{-1}) \\
 &= 3.366 \times 10^{-4} \text{ mol min}^{-1}
 \end{aligned}$$

$$\begin{aligned}
 [\text{CO}]_{\text{out}} &= \text{composition}(\%)/100 \times (\text{effluent flow}) \\
 &= 0.00/100 \times (54.0-40) \\
 &= 0.00 \text{ mL min}^{-1} = 0.00 \text{ mol min}^{-1}
 \end{aligned}$$

$$\begin{aligned}
 [\text{CO}_2]_{\text{out}} &= \text{composition}(\%)/100 \times (\text{effluent flow}) \\
 &= 40.23/100 \times (54.0-40) \\
 &= (5.63 \text{ mL min}^{-1})(1 \text{ atm})/(303 \text{ K})/(82.05 \text{ mL atm K}^{-1} \text{ mol}^{-1}) \\
 &= 2.265 \times 10^{-4} \text{ mol min}^{-1}
 \end{aligned}$$

Therefore,

$$\begin{aligned}
 \text{Methanol conversion (\%)} &= (0.00 + 2.265 \times 10^{-4}) \times 100 / 2.311 \times 10^{-4} \\
 &= 97.99 \%
 \end{aligned}$$

$$\begin{aligned}
 \text{CO selectivity (\%)} &= (0.00 \times 100) / (3.366 \times 10^{-4} + 0.00 + 2.265 \times 10^{-4}) \\
 &= 0.00 \% \\
 \text{H}_2 \text{ yield (\%)} &= 3.366 \times 10^{-4} \times 100 / (3 \times 2.311 \times 10^{-4}) \\
 &= 48.53 \% \\
 \text{H}_2 \text{ production rate} &= [\text{H}_2]_{\text{out}} / \text{g.cat} \\
 &= (8.37 \text{ mL min}^{-1})(1,440 \text{ min day}^{-1}) / (0.1 \text{ g. cat}) \\
 &= 120.5 \text{ L day}^{-1} \text{ g. cat}^{-1}
 \end{aligned}$$

C.3 Preferential oxidation of CO (%)

$$\text{CO conversion (\%)} = \{([\text{CO}]_{\text{in}} - [\text{CO}]_{\text{out}}) \times 100 / [\text{CO}]_{\text{in}}\}$$

$$\text{CO}_2 \text{ selectivity (\%)} = \{0.5 \times ([\text{CO}]_{\text{in}} - [\text{CO}]_{\text{out}}) \times 100 / ([\text{O}_2]_{\text{in}} - [\text{O}_2]_{\text{out}})\}$$

where

$$[\text{CO}]_{\text{in}} = \text{molar flow rate of CO in the feed stream (mol min}^{-1}\text{)}$$

$$[\text{O}_2]_{\text{in}} = \text{molar flow rate of O}_2 \text{ in the feed stream (mol min}^{-1}\text{)}$$

$$[\text{CO}]_{\text{out}} = \text{molar flow rate of CO in the effluent (mol min}^{-1}\text{)}$$

$$[\text{O}_2]_{\text{out}} = \text{molar flow rate of O}_2 \text{ in the effluent (mol min}^{-1}\text{)}$$

Example: Catalytic activity of 10%CuO/Ce_{0.95}Mg_{0.05} catalyst at 24 h in a presence of

CO₂

Given The composition of mixed gases was H₂ 40%, CO 1% and CO₂ 20% in He balanced and fed at 100 mL min⁻¹

Component	Peak area	composition (%)
CO in	18,516	0.92
O ₂ in	59,368	1.13
CO out	858	0.04
O ₂ out	24,167	0.46

$$\begin{aligned}
 \text{oxygen excess factor } (\lambda) &= 2 \times [\text{O}_2]_{\text{in}} / [\text{CO}]_{\text{in}} \\
 &= 2 \times 1.13 / 0.92 \\
 &= 2.45
 \end{aligned}$$

Therefore,

$$\begin{aligned}
 \text{CO conversion } (\%) &= (0.92 - 0.04) / 0.92 \times 100 \\
 &= 95.65 \%
 \end{aligned}$$

$$\begin{aligned}
 \text{CO}_2 \text{ selectivity } (\%) &= \{0.5 \times (0.92 - 0.04) \times 100 / (1.13 - 0.46)\} \\
 &= 65.67 \%
 \end{aligned}$$

VITA

Name: Mr. Yuththaphan Phongboonchoo

Date of Birth: March 21st, 1987 Nationality: Thai

University Education:

2006-2009 Bachelor degree of Science in Fuel Technology, Department of Chemical Technology, Faculty of Science, Chulalongkorn University. Senior project title “Effect of catalyst preparation on hydrogen production from photochemical oxidation in alcohol waste solution” GPA: 3.42

2010-2011 Master degree of Science in Chemical Technology, Department of Chemical Technology, Faculty of Science, Chulalongkorn University. Thesis title “Hydrogen production from methanol steam reforming over silica-supported copper catalyst” GPA: 3.93

2012-2016 Doctoral degree of Science in Chemical Technology, Department of Chemical Technology, Faculty of Science, Chulalongkorn University. Thesis title “Fuel processor for hydrogen production via methanol steam reforming over copper-based catalysts” GPA: 4.00

Publication:

Phongboonchoo, Y., Thouchprasitchai, N., and Pongstabodee, S. Hydrogen production with a low carbon monoxide content via methanol steam reforming over $Cu_{x}Ce_{y}Mg_{z}/Al_{2}O_{3}$ catalysts: Optimization and stability. International journal of hydrogen energy 42 (2017): 12220-12235.

Phongboonchoo, Y., and Pongstabodee, S. Effect of Ce, Mg mono- and Ce-Mg bi-promoter on performance of Cu-based catalysts for hydrogen production via methanol steam reforming. Proceeding of Pre-symposium of 16th International Congress on Catalysis and 2nd International Symposium of Institute for Catalysis, Sapporo, Japan (2016, June 30 – July 1).